

**Microphysical Processes in Two Stably Stratified Orographic
Cloud Systems**

by
Robert M. Rauber

Department of Atmospheric Science
Colorado State University
Fort Collins, Colorado

**Colorado
State
University**

**Department of
Atmospheric Science**

Paper No. 337

MICROPHYSICAL PROCESSES IN TWO STABLY STRATIFIED
OROGRAPHIC CLOUD SYSTEMS

By

Robert M. Rauber

This report was prepared with support provided by
National Science Foundation Grant ATM 78-19261
Principal Investigator, Lewis O. Grant

Department of Atmospheric Science
Colorado State University
Fort Collins, Colorado

August 1981

Atmospheric Science Paper No. 337

THE UNIVERSITY OF CHICAGO

PHYSICS DEPARTMENT

BY

ALBERT EINSTEIN

THE UNIVERSITY OF CHICAGO
PHYSICS DEPARTMENT
CHICAGO, ILLINOIS

THE UNIVERSITY OF CHICAGO
PHYSICS DEPARTMENT
CHICAGO, ILLINOIS

1917

THE UNIVERSITY OF CHICAGO

ABSTRACT OF THESIS

MICROPHYSICAL PROCESSES IN TWO STABLY STRATIFIED OROGRAPHIC CLOUD SYSTEMS

The microphysical processes associated with the growth of cloud and precipitation particles during two stable orographic storms are identified in this thesis. A two dimensional steady-state model of airflow over an ideal mountain barrier is developed and used to define the location and rate of production of condensate available for liquid water and ice particle growth in these two storms. A crystal trajectory model is also developed to determine origin levels and upwind location of crystals which impact on the mountain barrier.

The major conclusions in this thesis concerning stably stratified storms in the northern Rockies are the following:

a. The majority of cloud liquid water in stably stratified orographic storms exists in a narrow zone over the windward slopes of the primary barrier. Model results indicate that this zone extends vertically over the slope with maximum liquid water contents near the surface. On both days the model predicted location of the zone was in excellent agreement with aircraft observations.

b. Droplet spectra in stable orographic cloud systems vary substantially depending on the air mass source region. On November 24, the overrunning air mass had modified maritime characteristics. Mean droplet sizes were near $15 \mu\text{m}$, droplet concentrations were $60/\text{cm}^3$ and maximum liquid water contents near $.43 \text{ g}/\text{m}^3$. On November 26, the air mass behind the cold front had continental characteristics. Mean droplet sizes were $6-9 \mu\text{m}$, droplet concentrations $200/\text{cm}^3$ and maximum liquid water contents $.13 \text{ g}/\text{m}^3$.

c. Secondary zones of liquid water exist upwind of the primary barrier in regions of enhanced upward motion generated by smaller upwind

topography. The utilization of upwind zones such as these in the northern Rockies may be the best strategy for seeding this type of storm.

d. Model results indicate that single crystals in storms with moderate or strong wind speeds normal to the mountain have essentially horizontal trajectories due to a near equilibrium between increasing fall velocities and air mass lifting. This result was supported by aircraft observations within the dendritic growth zone. The exception was aggregated crystals, which appear at all levels below the initial level of aggregation due to their higher fall velocities.

e. The aggregation process was significantly enhanced in regions where some liquid water was present, particularly at temperatures above -12°C .

f. Trajectory model results indicate that the only single crystals produced within 60 km of the ridge which reach the ground in the November 24 storm were those produced above -12°C . 2-D images indicate that aggregates of crystals from higher levels also have fall velocities large enough that they could reach the ground. The difference in precipitation values between mountain and valley stations seems largely the result of increased condensate supply and the enhancement of the riming and aggregation processes over the windward slopes.

g. Significant ($> 1/\text{liter}$) quantities of crystals smaller than 300 μm were present at temperatures between -6 and -10°C in both cloud systems. The total concentration of crystals showed little dependence on cloud temperature.

Robert M. Rauber
Atmospheric Science Department
Colorado State University
Fort Collins, Colorado 80523
Summer, 1981

ACKNOWLEDGEMENTS

I would like to express my appreciation to Lewis O. Grant, William R. Cotton and Paul W. Mielke for their helpful suggestions and guidance in preparation of this thesis. I would also like to express special thanks to the following people for their help and support: Lucy McCall, drafting; Verne Levenson, map analysis; Patricia Walsh, cloud physics instrumentation and data reduction; Dudley Friday, data reduction and Ruta Radziunas, typing. I also wish to express a special word of thanks to Jan Davis for her support during this research.

This research was supported by the National Science Foundation Grant No. ATM-78-19261.

TABLE OF CONTENTS

<u>Section</u>	<u>Page</u>
Chapter I Introduction	1
1.1 Objectives	2
1.2 Literature Review	3
1.3 Data Sources	10
Chapter II Instrumentation	14
2.1 The Two Dimensional Optical Array Spectrometers	17
2.2 Liquid Water Content Measurements	25
2.2.1 The Forward Scattering Spectrometer Probe	25
2.2.2 The Johnson-Williams Liquid Water Detector	25
2.2.3 Comparison of the JW and FSSP	26
2.3 Ground Based Instrumentation	27
Chapter III Theoretical Considerations	31
3.1 Vertical Velocity	31
3.2 Airflow and Condensate Production	36
3.3 Crystal Trajectories	37
Chapter IV November 24, 1979 Case Study	42
4.1 Major Synoptic Features	42
4.2 Flight Track Descriptions	50
4.3 Cloud Physical and Microphysical Characteristics	54
4.3.1 Cloud Liquid Water and Droplet Spectra	65
4.3.2 Ice Crystal Structure and Crystal Size Spectra	66
4.4 Condensate Production and Production Rates in the November 24 Cloud	79
4.5 Crystal Trajectories	83
4.6 Summary of the November 24 Case Study	91

Chapter V	November 26, 1979 Case Study	93
5.1	Major Synoptic Features	93
5.2	Flight Track Descriptions	100
5.3	Cloud Physical and Microphysical Characteristics	103
5.31	Cloud Liquid Water and Droplet Spectra	114
5.32	Ice Crystal Structure and Crystal Size Spectra	115
5.4	Condensate Production and Production Rates in the November 26 Cloud	125
5.5	Doppler Radar Observations	128
5.6	Summary of the November 26 Case Study	133
Chapter VI	Summary and Conclusions	135
6.1	Summary and Conclusions	135
6.2	Implications of the Results for Weather Modification	140
6.3	Implications of the Results for Flight Operations	142
6.4	Recommendations for Future Research	143
Chapter VII	References	146

LIST OF TABLES

<u>Number</u>		<u>Page</u>
1.	Queen Air Instrumentation	15
2.	Lear Instrumentation	16
3.	FSSP Calibration Data	24
4.	Ground Instrumentation Network	30
5.	Growth Equations Used In Trajectory Model	40

LIST OF FIGURES

<u>Number</u>		<u>Page</u>
1.	The state of Colorado and the COSE study area.	11
2.	The COSE study area.	12
3.	Artifacts of the 2-D probe.	19
4.	Shadow-or crystal concentrations vs. concentrations with rejection criteria applied for the November 24, 1979 Queen Air flight.	21
5.	Shadow-or crystal concentrations vs. concentrations with rejection criteria applied for the November 26, 1979 Queen Air flight.	22
6.	Shadow-or crystal concentrations vs. concentrations with rejection criteria applied for the November 24 and November 26, 1979 Lear flights.	23
7.	FSSP vs. JW determined liquid water contents.	28
8.	Actual and simulated mountain profiles used in the airflow model.	35
9.	Major synoptic features at 12Z on November 24, 1979.	43
10.	Evolution of the surface features during the analysis period of November 24, 1979.	45
11.	Detailed surface analyses at times coinciding with the aircraft microphysical analyses on November 24, 1979 over Hayden, Colorado.	47
12.	Aircraft soundings taken during the November 24, 1979 storm.	48
13.	Upper air analyses for November 25, 1979 at 00Z.	51

14.	Vertical cross-section of potential and equivalent potential temperature from Medford, Oregon to Denver, Colorado showing frontal positions.	52
15.	Queen Air and Lear flight tracks for November 24, 1979.	53
16.	Vertical cross-section along line AA' on Figure 15 showing state, wind and microphysical data collected by the Queen Air on November 24, 1979.	55
17.	Vertical cross-section along line BB' on Figure 15 showing state, wind and microphysical data collected by the Queen Air on November 24, 1979.	56
18.	Vertical cross-section along line BB' on Figure 15 showing state, wind and microphysical data collected by the Queen Air on November 24, 1979.	57
19.	Vertical cross-sections along line CC' (left) and AA' (right) on Figure 15 showing state, wind and microphysical data collected by the Queen Air on November 24, 1979.	58
20.	Vertical cross-sections along line AA' on Figure 15 showing state, wind and microphysical data collected by the Queen Air on November 24, 1979.	59
21.	Vertical cross-section along line AA' on Figure 15 showing state, wind and microphysical data collected by the Queen Air on November 24, 1979.	60
22.	Vertical cross-section along line DD' on Figure 15 showing state and microphysical data collected by the Learjet on November 24, 1979.	61

23.	Vertical cross-sections along line DD' on Figure 15 showing state and microphysical data collected by the Learjet on November 24, 1979.	62
24.	Schematic cross-section of the November 24, 1979 cloud system.	64
25.	FSSP droplet spectra, November 24, 1979.	67
26.	2-D probe images from the Queen Air and Learjet flights.	68
27.	2-D probe images from the Queen Air flight on November 24, 1979.	69
28.	2-D probe images from the Queen Air flight on November 24, 1979.	70
29.	2-D crystal size spectra taken during the November 24, 1979 Lear flight.	71
30.	2-D crystal size spectra taken during the November 24, 1979 Queen Air flight.	72
31.	2-D crystal size spectra taken during the November 24, 1979 Queen Air flight.	73
32.	2-D crystal size spectra taken during the November 24, 1979 Queen Air flight.	74
33.	Model determined streamlines for the November 24, 1979 cloud system.	80
34.	Steady-state potential condensate production in the November 24, 1979 cloud system.	81
35.	Potential condensate production rates in the November 24, 1979 cloud system.	82

36.	Trajectories of platelike crystals originating in the liquid water zone generated by the upwind ridge--line east of Hayden.	86
37.	Trajectories of crystals which develop dendritic characteristics and originate in the liquid water zone generated by the upwind ridgeline east of Hayden.	87
38.	Trajectories of crystals which would impact on the barrier as small (2000 microns) and large (6000 microns) dendrites.	89
39.	Trajectories of crystals which would impact on the barrier as small (1000 microns) and large (3000 microns) plates.	90
40.	Major synoptic features at 12Z on November 26, 1979.	94
41.	Evolution of the surface front during the November 26, 1979 storm.	96
42.	Aircraft soundings taken during the November 26, 1979 storm over Hayden, Colorado.	97
43.	Major synoptic features at 00Z on November 27, 1979.	101
44.	Queen Air and Lear flight tracks for November 26, 1979.	102
45.	Vertical cross-section along line MM' on Figure 44 showing state, wind and microphysical data collected by the Queen Air on November 26, 1979.	104
46.	Vertical cross-sections along line LL' on Figure 44 showing state, wind and microphysical data collected by the Queen Air on November 26, 1979.	105

47.	Vertical cross-sections along line LL' on Figure 44 showing state, wind and microphysical data collected by the Queen Air on November 26, 1979.	106
48.	Vertical cross-section along line LL' on Figure 44 showing state, wind and microphysical data collected by the Queen Air on November 26, 1979.	107
49.	Vertical cross-section along line EE' on Figure 44 showing state and microphysical data collected by the Learjet on November 26, 1979.	108
50.	Vertical cross-sections along line HH' on Figure 44 showing state and microphysical data collected by the Learjet on November 26, 1979.	109
51.	Vertical cross-sections along line JJ' on Figure 44 showing state and microphysical data collected by the Learjet on November 26, 1979.	110
52.	Vertical cross-section along line KK' on Figure 44 showing state and microphysical data collected by the Learjet on November 26, 1979.	111
53.	Vertical cross-sections along line EG' on Figure 44 showing state and microphysical data collected by the Learjet on November 26, 1979.	112
54.	Vertical cross-sections along line EF' on Figure 44 showing state and microphysical data collected by the Learjet on November 26, 1979.	113
55.	FSSP droplet spectra, November 26, 1979.	116
56.	2-D probe images from the November 26, 1979 Lear flight.	117

57.	2-D probe images from the November 26, 1979 Queen Air flight.	118
58.	2-D probe images from the November 26, 1979 Queen Air flight.	119
59.	2-D crystal size spectra taken during the November 26, 1979 Lear flight.	120
60.	2-D crystal size spectra taken during the November 26, 1979 Lear flight.	121
61.	2-D crystal size spectra taken during the November 26, 1979 Queen Air flight.	124
62.	2-D crystal size spectra taken during the November 26, 1979 Queen Air flight.	126
63.	Model determined streamlines for the November 26, 1979 cloud system.	127
64.	Steady-state potential condensate production in the November 26, 1979 cloud system.	129
65.	Potential condensate production rates in the November 26, 1979 cloud system. Isopleths are in units of $10^5 \text{ gm}^{-3} \text{ s}^{-1}$.	130
66.	Doppler radar determined vertical velocities (w_D) on November 26, 1979.	131

LIST OF SYMBOLS

A	constant
a	half width of mountain (vertical velocity equation)
a	basal plane crystal axis (crystal growth equation)
B	constant
b	constant
C	capacitance factor
C_p	specific heat of air at constant pressure
C_v	specific heat of air at constant volume
c_s	speed of sound (vertical velocity equation)
c	longitudinal plane crystal axis (crystal growth equation)
D	maximum dimension of crystal
D_v	diffusivity of water vapor in air
e	vapor pressure
e_r	vapor pressure at crystal surface
e_s	saturation vapor pressure
F	ventillation factor
g	gravity
G	thermodynamic function
h	height of topography
h_m	maximum height of mountain
i	square root of -1
K_{HP}	constant
K_i	thermal conductivity of air
k	horizontal wave number
l	scorer parameter
L_s	latent heat of sublimation

m_w	molecular weight of water
N	Brunt Vaisalla frequency
p	perturbation pressure
Q	heat content
R	gas constant for dry air (vertical velocity equation)
R	universal gas constant (crystal growth equation)
RE	Reynolds number
S	saturation ratio (crystal growth equation)
S	vertical density derivative (vertical velocity equation)
T	temperature at a distance from a crystal
T_o	base state temperature
T_r	temperature at crystal surface
t	time
U	base state horizontal wind velocity
u	perturbation horizontal wind velocity
V_T	crystal terminal velocity
w	perturbation vertical wind velocity
w^*	amplitude of perturbation vertical wind velocity
x_i	crystal mass
x	horizontal coordinate
z	vertical coordinate
β	constant
γ	constant equal to C_p/C_v
δ_s	crystal density
θ	potential temperature
ρ	perturbation air density

ρ_0 base state density
 ρ_w vapor density at a distance from crystal
 $\rho_w(x)$ vapor density at crystal surface
 η vertical displacement of a streamline

CHAPTER I INTRODUCTION

Since the development of modern concepts of weather modification in the 1950's, the potential utilization of weather modification as a major source of additional water supplies for arid and semi-arid land such as the western United States has been continuously hypothesized and tested. Much of this effort has concentrated on the enhancement of winter snowpack in mountainous regions by modification of wintertime orographic cloud systems. Until the early 1970's, the technology was not available to systematically probe these cloud systems with aircraft to determine their microphysical structure and physical characteristics. During the late 1950's and the 1960's, weather modification research programs primarily concentrated on combining ground based measurements and statistical techniques to test the physical models which were developed to describe these systems. In the early 1970's advanced cloud physics instrumentation were developed for aircraft capable of penetrating these cloud systems. Since that time, weather modification research programs have included both aircraft and ground based measurements to refine the physical models as well as statistical techniques to determine the overall effect of modification on precipitation.

Many of the potential benefits from increasing total water supplies in the western United States come from enhancement of the snowpack in the mountains of the Colorado River Basin. The Colorado River is supplied with water from several source mountain ranges including the San Juan Mountains in southern Colorado and several northern Colorado ranges. During the 1970's, most physical studies of natural and seeded cloud systems within the Colorado River Basin were done in conjunction with the Colorado River Basin Pilot Project conducted in the San Juan

Mountains. In general, the source air, and therefore the moisture and stability of storms affecting the southern San Juan massif are often uncharacteristic of storms which affect northern Colorado mountains. Although the northern mountains represent a substantial source of total water to the basin, very little effort has been spent to characterize the cloud systems which affect the northern basin. Beginning in 1978, Colorado State University (CSU), with primary support from the National Science Foundation (NSF) and additional support from government organizations such as the Bureau of Reclamation, the National Center for Atmospheric Research (NCAR) and the National Oceanic and Atmospheric Administration (NOAA) and private corporations such as Colorado International Corporation (CIC), has conducted wintertime field programs in the Park Range area of northwest Colorado. One goal of the field programs has been to systematically document the microphysical and dynamic characteristics of Northern Colorado orographic cloud systems. The research results presented in this thesis were obtained by analysis of data taken during the winter field program conducted by CSU during November and December of 1979, and represent a part of the overall effort in achieving that goal.

1.1 Objectives

Lee (1980) describes five types of storm systems associated with wintertime precipitation in the northern Colorado Rockies. These include orographic storms associated with strong moist stable flow normal to the mountain barrier, storms with weak winds aloft generated primarily by synoptic scale lifting mechanisms, orographically induced storms with considerable imbedded convective elements, convective bands, and isolated convective showers. The purpose of this research is to

systematically describe and model the microphysical and dynamic processes associated with the first of these systems, orographically generated storms associated with strong moist stable flow.

The specific objectives of this study are then to:

- 1) Describe the microphysical processes associated with the growth and development of cloud and precipitation particles during two stable orographic storms by utilizing aircraft and ground based measurements taken during the storms.
- 2) Develop a two dimensional steady-state model of airflow over an ideal mountain barrier which is capable of defining the location and rate of production of condensate available for liquid water and ice particle growth and applying it to these two storms.
- 3) Develop a simple crystal trajectory model and use it to determine the origin levels and upwind location of crystals impacting on the barrier. The model is applied to the November 24, 1979 case study because of the complexity of the microphysical processes evident in this system. The model is also used to test the hypothesis that cloud water zones associated with flow over small upwind topography can serve as sources of crystals at the primary barrier (see section 4.5).

1.2 Literature Review

Physical Studies of Orographic Cloud Systems: Simultaneous aircraft and ground based measurements of the microphysical and dynamic structure of orographic cloud systems began in the early 1970's in association with various weather modification research experiments. Between 1969 and 1974, extensive studies of cloud systems over the Cascade Mountains were conducted by the University of Washington in association with the Cas-

cade Atmospheric Water Resources Program (Hobbs,1975a; Hobbs,1975b; Hobbs and Radke,1975). Observations of natural cloud systems during the program indicated that in prefrontal conditions, ice particles dominate over water droplets above the -10°C level. The ratio of ice to water was lower in post frontal conditions. They found that the passage of an occluded or warm front was accompanied by a sharp lowering of the diffusional growth layers. As a consequence, particles reaching the ground were converted from unrimed to rimed crystals. They also found that the maximum ice particle concentrations in the clouds were often several orders of magnitude greater than measurements of ice nuclei. Results of the study also indicated that the growth of precipitation particles by riming and aggregation is particularly rapid in the last kilometer of fall and that snow particles reaching the ground originate 10 to 100 km upwind.

During the five winter seasons ending in 1974-75, the Colorado River Basin Pilot Project was conducted in the San Juan Mountains of Southwest Colorado (Elliott et al., 1978). Physical studies of cloud systems occurring over the San Juan Massif during this period were conducted by the University of Wyoming (Marwitz,1980; Cooper and Saunders,1980; Cooper and Marwitz,1980) and the University of Washington (Hobbs et al., 1975). Results of these studies indicate that most storms in the San Juans evolve through four stages related to thermodynamic instability, a stable stage followed by neutral, unstable and dissipation stages. During the early storm stages, precipitation developed primarily by diffusional growth of ice crystals, but accretional growth became increasingly important during later storm stages. Extensive regions of cloud water appeared only in the later storm

stages; often associated with imbedded convection. As in the Cascade study, observed ice crystal concentrations were frequently far in excess of measured ice nucleus concentrations.

During the late 1970's, the Sierra Cooperative Pilot Project (SCPP) was initiated to study dynamic and microphysical cloud processes over the American River Basin in the Sierra Mountains of California. Results of cloud physics studies during the SCPP were reported by the University of Wyoming for the winters of 1977-78 and 1978-79 (Marwitz et al., 1978; Marwitz et al., 1979). Initial studies have identified the microphysical processes associated with the radar observed bright band near the melting level and have clearly showed that the Hallet-Mossop process of secondary ice crystal multiplication is active in certain cellular clouds. In general, no significant supercooled water was detected during stable orographic stages. The majority of cloud liquid water was observed at temperatures near -5°C in the organized convection associated with the passage of convective bands.

Computer Simulations of Orographic Cloud Processes: Since the late 1960's several investigators have developed models of orographic cloud development and precipitation processes. As part of the Park Range Atmospheric Water Resources Program (Rhea et al., 1969), Willis (1970) adapted an airflow model from the work of Scorer (1949) and combined it with a simple microphysical parameterization of crystal growth to calculate precipitation rates in Colorado's Park Range. In this model, the flow is assumed to be inviscid and the equations are linearized, thus allowing for an analytical solution for the vertical velocity field with an actual vertical sounding profile as input.

A more complicated treatment of the orographic precipitation problem was presented by Fraser et al. (1973) and Hobbs et al. (1973) in a model developed in conjunction with the Cascades Atmospheric Water Resources Program. The airflow portion of the model again was based on the treatment given by Scorer (1949) but also included dynamic effects due to latent heat release. The microphysical treatment of the growth and fallout of precipitation included effects of riming and aggregation. This model was capable of calculating trajectories of cloud and precipitation particles, as well as adiabatic condensate and distribution of precipitation across the barrier.

Middleton (1971) considered a complex set of growth equations for numerous crystal habits and combined these with an airflow model adapted from the model of Lavoie (1968) to determine crystal trajectories for crystals originating in the cap cloud environment characteristic of Wyoming's Elk Mountain. Middleton also compared these growth equations with the crystal growth equations developed by Cotton (1972) for numerical simulation of microphysical processes occurring in supercooled cumuli.

Young (1974a,b) developed a numerical model of orographic precipitation which made use of a continuous bin technique. Young included microphysical collection processes of coalescence, accretion and aggregation, as well as nucleation processes including activation of cloud condensation nuclei and ice phase nucleation. A Lagrangian dynamical framework was utilized in the model. The model was used to compare orographic precipitation values under natural and seeded conditions and to calculate precipitation efficiency for each case. Other models have been presented by various researchers (Fukuta et al., 1973; Plooster and

Fukuta,1975; Plooster and Vardiman,1976; Derickson,1974; Brown and Rottner,1976).

Preliminary studies of cold orographic cloud systems using a three dimensional, primitive equation, mesoscale dynamic model developed by Nickerson and Magaziner (1976) and a microphysical model developed by Chappell and Smith (1976) have been reported by Nickerson et al. (1976). This model was used to simulate cloud seeding over the San Juan Mountains (Chappell et al.,1979).

Microphysical Growth and Fall Velocity Equations

Growth equations developed for ice crystals have been based on the laws of Fickian diffusion and the assumption of equilibrium between the rate of molecular diffusion of heat away from a crystal and the production of latent heat at the crystal surface due to vapor deposition. Byers (1965) presents a complete development for the case of growth due to vapor deposition alone. This equation is used in most of the models described in the previous section. Cotton (1970,1972) developed this equation further by including the effects of riming.

The effects of ventilation on the growth equation for the ice crystals with various shapes has not been satisfactorily investigated. The work of Frossling (1938) and Zikmundova (1968) indicates that the ventilation factor for spheres can be expressed as

$$F = 1 + b(RE)^{0.5} \quad (1)$$

where b is a constant ≈ 0.2 and RE is the Reynolds number for the crystal. The equation is valid only for Reynolds numbers between 10 and 100. Models utilizing a ventilation factor in the growth equations (Middleton,1971; Cotton,1972) have adopted this formulation. Because of the restrictive assumptions in determining this empirical relationship

(e.g. sphericity, limited Reynolds number) it is unlikely that the ventilation factor is applicable over a wide range of crystal shapes and terminal velocities (Cornford,1965; Brownscombe and Hallet,1967). For this reason, other modelers (e.g. Hobbs et al.,1973) ignore the ventilation factor. In this work, the ventilation factor is assumed to be unity.

The earliest studies of ice crystal terminal velocities include those of Nakaya and Terada (1935), Nakaya (1954), Magono (1951,1954, 1957), Langleben (1954), and Litvinov (1956). Nakaya and Terada as well as Litvinov measured terminal velocities by visually observing crystals fall a known distance while timing the fall with a stopwatch. Magono (1951) also measured fall velocities of crystals and aggregates visually, photographing them while falling and estimating the crystal diameters from the photographs. In 1954, Magono presented a theoretical development relating fall velocity of snowflakes to snowflake radius and density, using an assumed drag coefficient of 0.5. Later, Magono expanded his work by developing equations for various crystal types (Magono, 1957). In each case, his terminal velocity equations were formulated by equating the gravitational and drag forces acting on the falling crystal.

Investigations of crystal terminal velocities were continued in the 1960's and 1970's by many researchers: Baskirova and Pershina (1964), Podzimek (1965,1968,1969), Jayaweera and Cottis (1969), Jayaweera and Ryan (1972), Brown (1970), Kajikawa (1971,1972,1973,1975a,b), Zikmunda and Vali (1972), Davis and Auer (1974), Davis (1974), Locatelli and Hobbs (1974).

Theoretical work concerned with fall velocity determinations has been directed toward development of relations between drag coefficients, the Best number and the Reynolds number. Cornford (1965) developed some generalized relationships from data on free falling crystals. Measurements of the fall velocities of model plastic crystals settling in various fluids were made by Jayaweera et al. (1964), Jayaweera and Mason (1965,1966), Podzimek (1965,1968,1969), Willmarth et al. (1964), Stringham (1965) and List and Schemenauer (1971). In studies such as these, vertical velocities are calculated from relationships between Best and Reynolds numbers and then applied to real ice crystals falling through the atmosphere by invoking dynamic similarity arguments. Jayaweera and Ryan (1972) compared measured terminal velocities of small columns and plates with that predicted by the earlier theoretical work of Jayaweera and Cottis (1969). They found good agreement between calculated and measured terminal velocities, although their study was restricted to small size ranges and terminal velocities less than 6 cm/s.

Extensive work on the measurement of fall velocities of ice crystal models under conditions of small Reynolds numbers was reported by Kajikawa (1971). In later work, Kajikawa (1972,1973,1975a,1975b), using stroboscopic methods, measured the fall speeds of a large number of crystals, particularly dendritic and platelike crystals, and compared these with the results of his earlier investigation. In 1975, Kajikawa presented a large number of empirical equations relating fall velocities of dendritic crystals and plates to their diameters (1975a) as well as equations relating the velocities and diameters of falling graupel particles (1975b).

Brown (1970), using a stroboscopic technique, measured the terminal velocities of a number of crystal types and developed empirical equations for the cases in which sufficient data were collected. Davis (1974) and Davis and Auer (1974) have fitted the terminal velocities observed by Bashkirova and Pershina (1964), Fukuta (1969), Brown (1970), Jayaweera and Ryan (1972) and Locatelli and Hobbs (1974) to empirical equations of the form $V_T = AD^B$ where D is the maximum dimension of the crystal and A and B are constants.

Fall velocities of rimed particles and graupel particles were measured by Zikmunda and Vali (1972) and Locatelli and Hobbs (1974). The former group fitted their data to empirical equations of the form $V=A+B(\log D)$ while the latter used the same form as that of Davis (1974).

For the purposes of this study, the empirical equations given by Davis (1974), Brown (1970) and Locatelli and Hobbs (1974) are used to calculate the terminal velocities of crystals of different habits and degrees of rime.

1.3 Data Sources

Data used to develop the two case studies presented in this thesis were collected during the second Colorado State University Orographic Seeding Experiment (COSE II) conducted by CSU during November and December of 1979 in the Park Range area of Northwest Colorado (see Figures 1 and 2). The specific objectives of the CSU experiments were:

i) to describe the microphysical processes governing the growth and development of precipitation in Northern Colorado orographic systems.

ii) to quantitatively define the dispersion and transport of seeding materials in complex terrain.

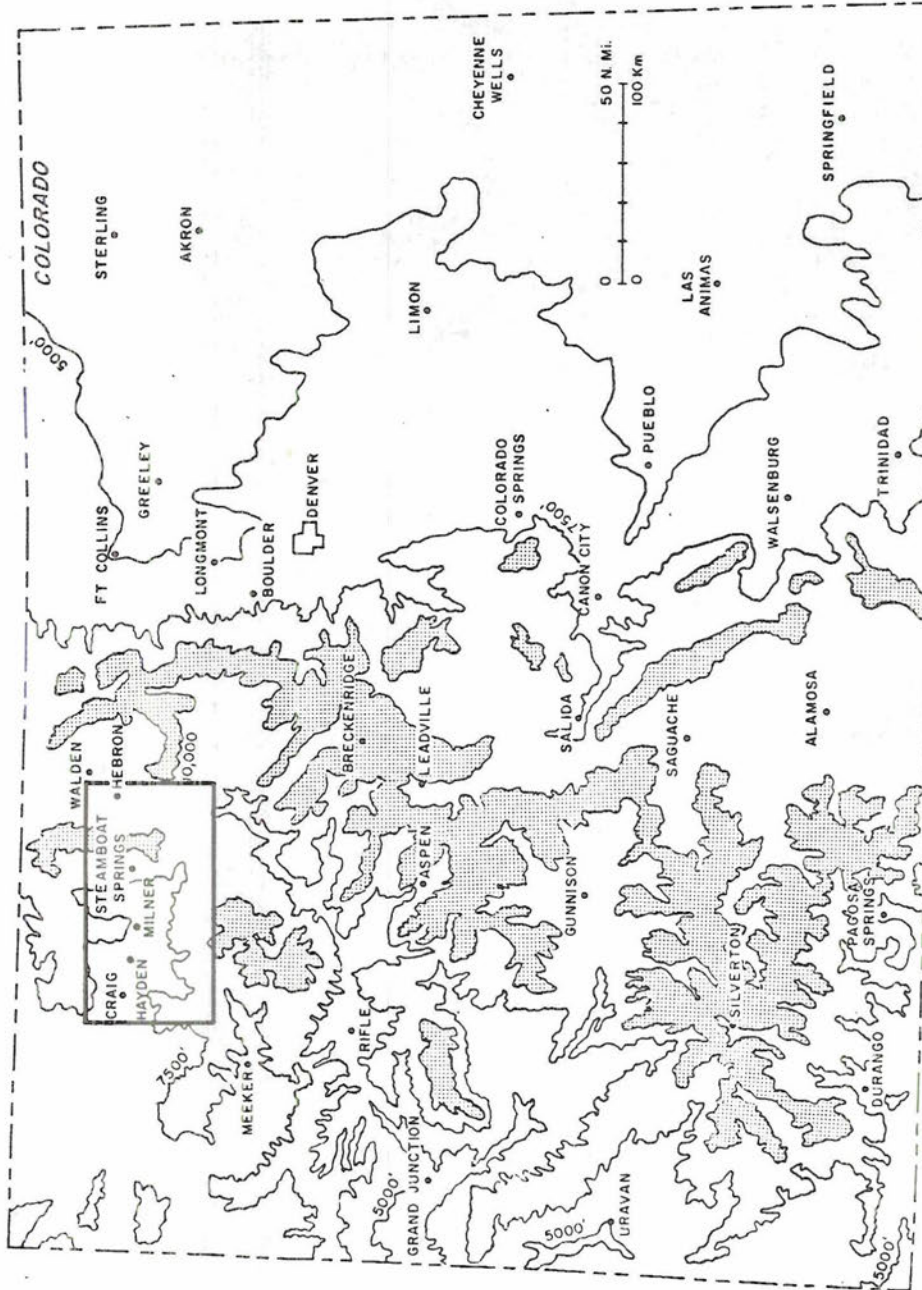


Figure 1. The state of Colorado and the COSE study area.



Figure 2. The COSE study area. Letters indicate positions of ground instrumentation described in the text.

iii) to identify atmospheric covariates (predictors) needed for analyses of weather modification programs.

COSE II project data sources included: observations with two cloud physics aircraft (NCAR Queen Air N306D and CIC Learjet N88TC), vertically pointing ku, k, and x band (Dopplerized) radars, rawinsonde observations upwind and downwind of the Park Range, ice crystal replicators at various mountain sites, surface meteorological observations of wind, temperature, humidity and precipitation, and observations of atmospheric aerosols and nuclei with both ice nucleus counters and high volume samplers, observations of boundary layer turbulent structure with an acoustic sounder. Specific data used in this analysis is discussed in the following chapter.

CHAPTER II INSTRUMENTATION

This section contains a detailed discussion of the cloud microphysics instrumentation used during the COSE II Project and a review of other instrumentation used to collect the data presented in this thesis. Two aircraft were used to provide in-cloud microphysical data and aerosol tracer information during the program. Cloud physics instrumentation on the NCAR Queen Air included a Particle Measuring Systems' forward scattering spectrometer probe (FSSP) and a two dimensional optical array spectrometer (2-D probe), (Knollenberg, 1976), as well as a Johnson-Williams hot wire liquid water content meter (JW). The Queen Air contained an inertial navigation system so that continuous observations of horizontal windspeed and direction were available. Data were logged through two independent on-board computer systems. State parameters, winds, aircraft position, pitch, roll and yaw angles were recorded by the Queen Air Airborne Research Instrumentation System (ARIS IV) described by Brown and Post (1978). Microphysical data were logged through an independent data acquisition system (DAS) provided by CSU. A complete list of the instrumentation aboard the NCAR Queen Air including range, accuracy and resolution of each instrument is provided in Table 1. The CIC Learjet was utilized in the project because of its high speed and consequent capability to cover a large area of cloud in a short time. The Learjet instrument package included a 2-D probe and a JW liquid water content meter. Aircraft position was determined by a VOR/DME, multiple DME tracking system. Data were recorded through a data acquisition system provided by CIC. A complete listing of Learjet instrumentation is provided in Table 2.

INSTRUMENTATION LIST
 COLORADO OROGRAPHIC SEEDING EXPERIMENT
 QUEEN AIR N306D

Instrument	Range	Accuracy	Resolution
Rosemount Temp	-40 C to +40 C	0.5 C	0.02 C
Reverse Flow Temp	-40 C to +40 C	0.5 C	0.02C
E G G Dewpoint	-50 C to +30 C	0.5 C > 0 C 1.0 C < 0 C	0.02 C
Static Pressure	30 to 103.5 Kpa	0.1 KPa	0.01 Kpa
Dynamic Pressure	0 to 6.5 KPa	0.05 KPa	0.002 KPa ₃
J-W liquid water	0 to 2 g/m ³	---	0.005 g/m ³
Wind Speed (WSPD)	---	1+0.5t m/sec t=hours in flight	0.01 m/sec
Wind Direction	0-360 deg	Cot ⁻¹ (WSPD)	
Aircraft Position		1.2 nm/hour	0.1 nm
Pitch, Roll	45 deg	0.05 deg	0.005 deg
Heading	0-360 deg	0.05 deg	0.005 deg
Attack angle	20 deg	0.2 deg	0.01 deg
Sideslip angle	20 deg	0.2 deg	0.01 deg
PMS FSSP	3-45 microns	---	15 channels
Radio altitude	0-2500 ft	5%	10 ft

Photography—One forward looking 16mm color film

time and date encoded, 1 frame per 5 sec.

Colorado State University supplied instrumentation:

PMS 2-D probe with Data Acquisition System

Langer ice nuclei counter

Table 1. Queen Air Instrumentation

INSTRUMENTATION LIST
 COLORADO OROGRAPHIC SEEDING EXPERIMENT
 LEARJET N88TC

Instrument	Range	Accuracy	Resolution
Rosemount temp	-50 C to +50 C	0.5 C	0.1 C
Reverse flow temp	-50 C to +50 C	0.5 C	0.1 C
Cambridge dewpt	-50 C to +50 C	1.0 C	0.3 C
JW liquid water	0-3 g/m ³	0.3 g/m ³	0.1g/m ³
Altitude	0-15 psia	0.015 psia	0.007 psia
Ind. air speed	-2.5 to +2.5 psid	0.0025 psid	0.0025 psid
Heading	0-360 deg	1 deg	.1 deg
Pitch	-85 to +85 deg	2 deg	0.1 deg
Roll	-180 to +180 deg	2 deg	0.1 deg
Azimuth position	0-360 deg	1 deg	0.1 deg
Distance position	0-400 km	0.07 km	0.01 km
Angle of attack	-20 to +20 deg	0.25 deg	0.1 deg

Colorado State University supplied instrumentation:
 MEE industries ice nuclei counter

Table 2. Lear Instrumentation

2.1 The Two Dimensional Optical Array Spectrometers

The two dimensional optical array spectrometer was developed by Particle Measuring Systems as a particle imaging system capable of recording and displaying two dimensional images of atmospheric particles with sizes greater than 25 microns (37.5 microns for the Lear) passing through an object plane at typical aircraft speeds. Analytical techniques for transforming raw 2-D data to effective crystal concentration have been primarily developed by Cooper (1977).

Crystal concentrations are calculated from 2-D probe data according to various criteria which are related to buffer storage capacity and characteristic shadow pattern. Under conditions when ambient crystal concentrations are 10/liter and crystal sizes in the 0.5-1.0 mm range, the storage buffer loads to capacity in about 0.35 seconds. Under normal experimental conditions, transfer of data to tape storage at this rate would consume several tapes and leave large data gaps during tape rewind and installation. To eliminate this problem, data are normally transferred once every second to tape, unless a high data rate is required. This means that only 35% of the data passing through the storage buffer is retained for later use.

Two parameters are calculated from the full body of data as it passes through the storage register. These are the number of distinct shadows and the total sample volume, a function of crystal size. If all of the distinct shadows are assumed to be individual crystals, the average crystal concentration over the one second leg can be calculated by dividing the number of distinct shadows by the sample volume. This number is referred to as the 'shadow-or' concentration.

Unfortunately, the shadow-or determination of crystal concentration can be inaccurate due to artifacts produced by liquid water droplets, crystals smaller than the resolution of the instrument, and the occasional inadvertant triggering of a photodiode by the probe electronics. Liquid water droplets often produce artifacts which appear as long narrow streaks. These occur when the droplets collide with the probe arm and then streak across the optical path. This problem is not major in stable orographic systems. Counts also occur when single diodes fire due to shadowing by sub-25 micron particles. However, the probe will occasionally fire a single photodiode when no particle can be identified. To obtain a reliable count, only particles which shadow at least two adjacent photodiodes are counted. Figure 3, taken from Queen Air data collected during the CSU experiment in 1979, shows examples of the single trigger artifact and streaker artifacts.

Representative values of true crystal concentration can be obtained by considering the image data retained in the buffer at the time of tape transfer. Crystal concentration is determined by first removing the artifacts from the data by applying rejection criteria. The criteria used for CSU data, first outlined by Cooper (1977), is as follows:

- 1) Streakers are rejected if they are six times as long (longitudinal dimension) as they are wide (lateral dimension). If the image is less than 150 microns wide, the criteria is lowered to three times as long as it is wide.
- 2) To eliminate images due to splashes from the edge of the aperture, when the time interval between images corresponds to a spatial distance of 2.5 cm or less, the second image is rejected.

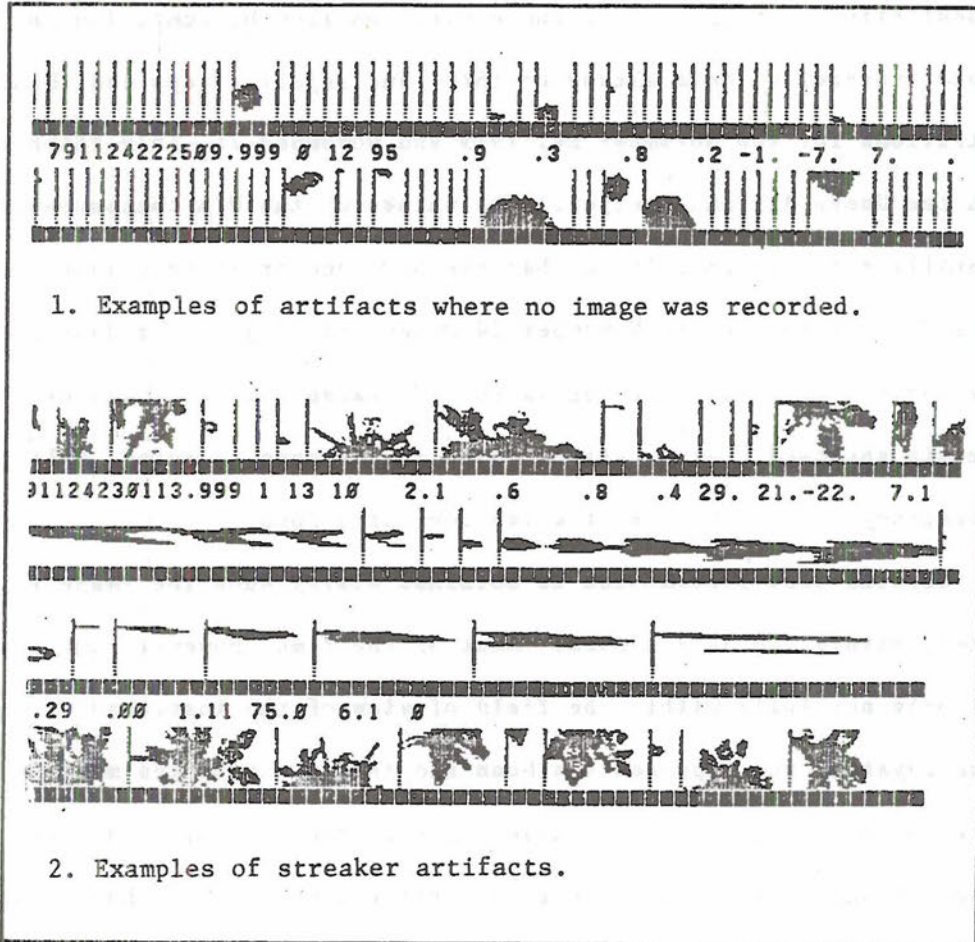


Figure 3. Artifacts of the 2-D probe.

- 3) Cases in which the probe recording circuitry is triggered but no elements are recorded as shadowed are rejected.

With these criteria applied to the images in the buffer, a new concentration is calculated which is more representative of actual crystal concentrations. Figures 4, 5 and 6 were compiled by computing one minute averages of both shadow-or (S/O) and rejection applied (R/A) concentrations for the November 24, 1979 and November 26, 1979 flights of both the Queen Air and Learjet. The values of the R/A concentration are generally a few percent lower than the S/O concentration except during the early portion of the November 24 Queen Air flight. The data during this portion of the flight consisted of a large number of images with no elements shadowed. Since all of these images were rejected, a larger discrepancy existed between the two concentrations.

Crystal size information is obtained easily when the image is completely within the data record. Most of the time, however, the crystals fall only partially within the field of view of the instrument. For these crystals the approach has been adopted to define the maximum dimension of the image as the major axis of the crystal. This has the effect of undersizing many crystals. Alternative methods have been developed by Heymsfield and Parrish (1979) who try to fit images to a circle but these methods are not valid for many habits and have not been included in CSU's software.

At present, no good analysis techniques exist for categorizing ice crystal habit from 2-D data. Current research by the electrical engineering department at the University of Wyoming is concerned with pattern recognition from 2-D images but this work has yet to be published. Using information relating areal coverage of the crystals to

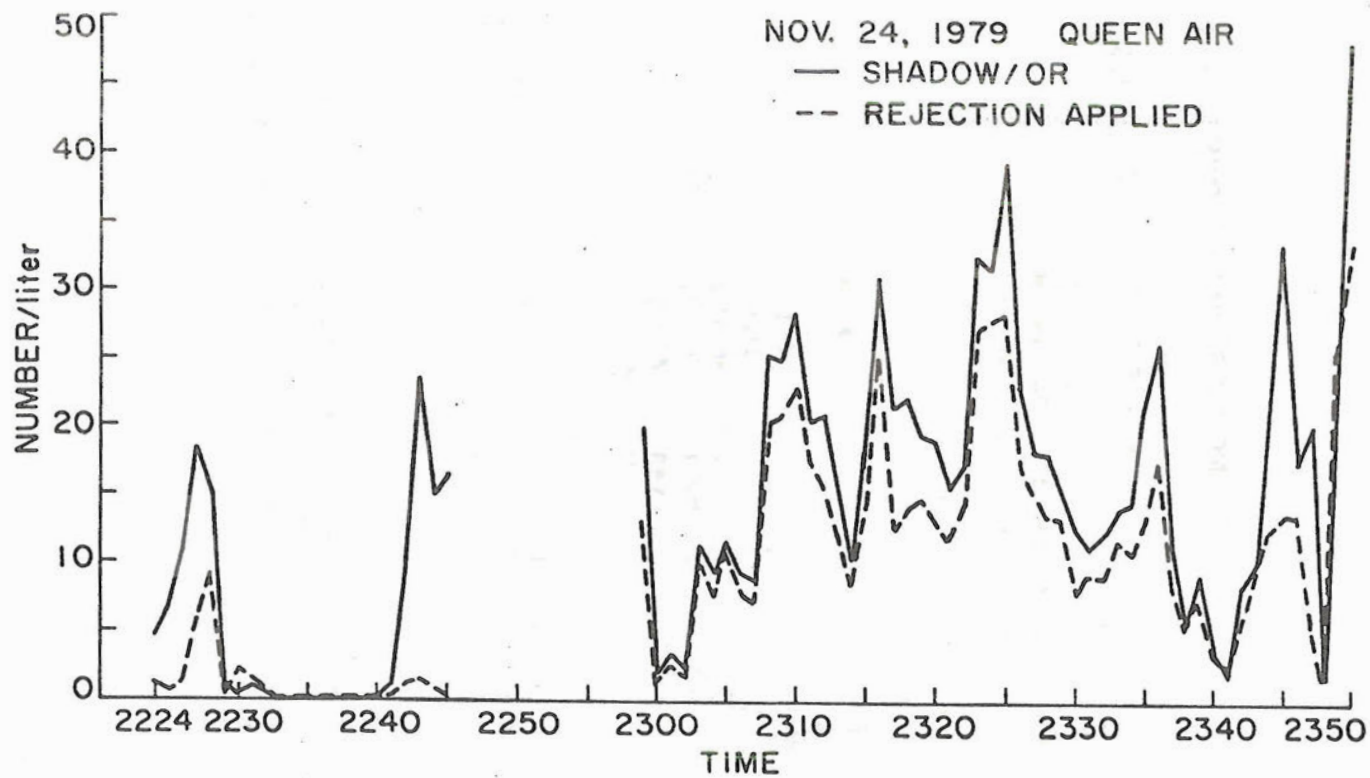


Figure 4. Shadow-or crystal concentrations vs. concentrations with rejection criteria applied for the November 24, 1979 Queen Air flight. Concentrations were averaged over one minute intervals.

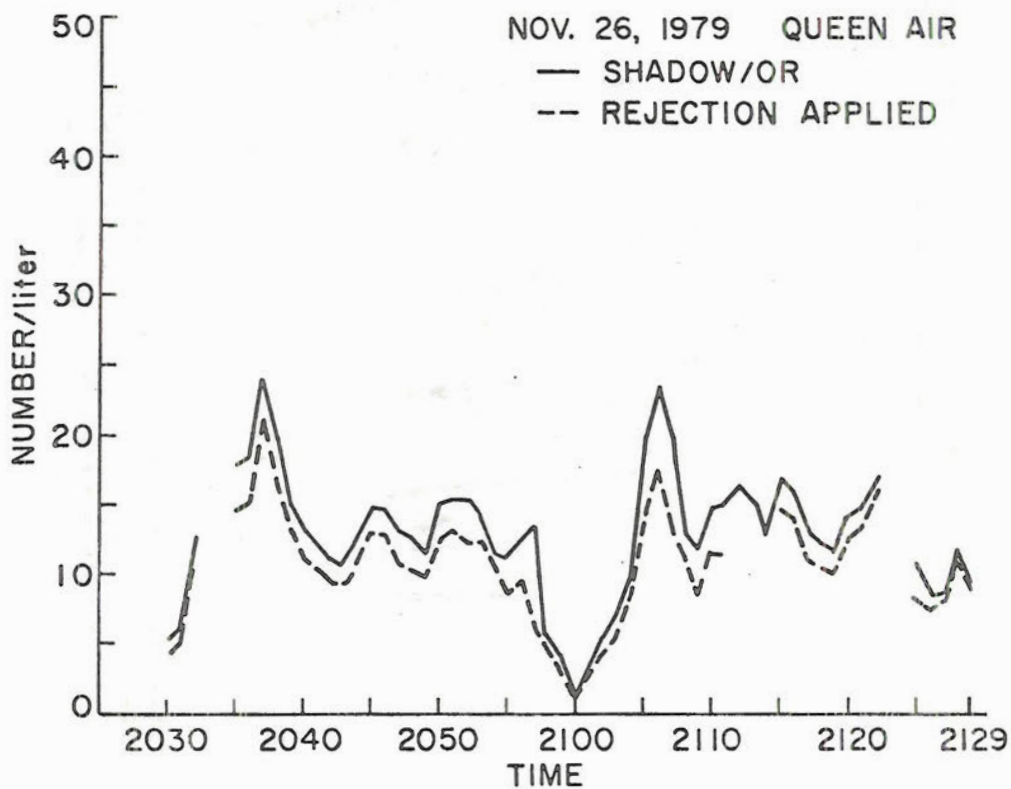


Figure 5. Shadow-or crystal concentrations vs. concentrations with rejection criteria applied for the November 26, 1979 Queen Air flight. Concentrations were averaged over one minute intervals.

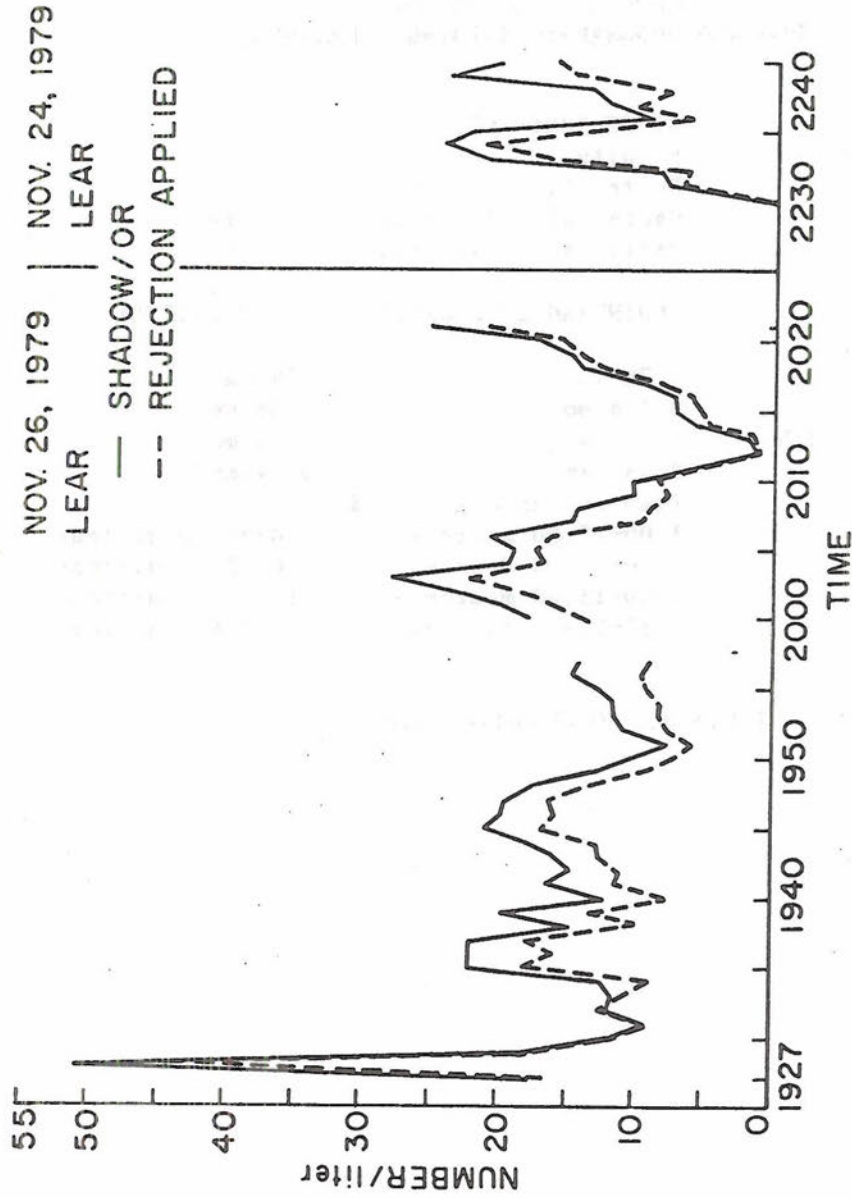


Figure 6. Shadow-or crystal concentrations vs. concentrations with rejection criteria applied for the November 24 and November 26, 1979 Lear flights. Concentrations were averaged over one minute intervals.

FSSP CALIBRATION DATA
COLORADO OROGRAPHIC SEEDING EXPERIMENT

Laser Serial No.	80-5T 7806-4066	
Reference Voltage	8 volts	
De-icing power	Heater #1	35 watts 28 volts
	Heater #2	250 watts 28 volts
	Heater #3	35 watts 28 volts
PARAMETER	BEGINNING OF PROJECT	END OF PROJECT
Depth-of-field	2.76 mm	1.58 mm
Beam width	0.186 mm	0.186 mm
Effective beam width	0.093 mm ²	0.093 mm ²
Sampling area	0.257 mm ²	0.147mm ²
Sample Volume	Sampling area X velocity	
Size Ranges #1	3.00-45.00 microns	3.54-53.10 microns
#2	2.00-30.00 microns	2.36-35.40 microns
#3	1.00-15.00 microns	1.18-17.70 microns
#4	0.50-7.50 microns	0.59-8.85 microns

Table 3. FSSP calibration data

area of encompassing circles and areal coverage of crystals to mass of crystals (Knollenberg,1976), Heymsfield and Parrish (1979) developed crude routines to identify crystal habit, but these routines have yet to be implemented in any actual operations. By far, the best technique available is visual inspection of the data, although it is the most time consuming.

2.2 Liquid Water Content Measurements

2.21 The forward scattering spectrometer probe

The forward scattering spectrometer probe (FSSP) is designed to measure the amount of light scattered into collecting optics during particle transit through a focused laser beam (Knollenberg,1976). The FSSP sizes droplets passing through the sample volume into 15 size ranges. The instrument has a primary size range of 2-30 microns in diameter. Auxiliary size range selections allows determination of cloud liquid water content.

The FSSP was calibrated before and after the field program by Particle Measuring Systems. Calibration on arrival at PMS after the end of the CSU field season indicated that the probe was low by a factor of 1.18, that is, range 1 was 3.54-53.1 microns, etc. Table 3 shows pertinent data for the NCAR FSSP probe from calibrations made before and after the field program.

2.22 The Johnson-Williams Liquid Water Detector

The JW liquid water content detector contains two heated wires, a sensing wire normal to the airflow and a compensative wire parallel to the airflow. The sensing wire encounters droplets which subsequently evaporate, lower the wire's temperature and change its resistance. The second wire, which remains dry, is used to compensate for changes in

heat transfer due to variations in airspeed, ambient air temperatures or altitude. The current through the detector varies proportionally to the decrease in resistance of the sensing wire as it is cooled by impinging droplets, and is therefore a measure of liquid water content. The JW probe is operated with a positive zero offset to compensate for negative drift. Values of data from the JW presented herein include this offset and should be adjusted downward by simultaneous comparison of FSSP liquid water contents using the information stated in the following section.

2.23 Comparison of the JW and FSSP

The most comprehensive work available on comparison of instruments designed to measure liquid water content has been completed recently by Baumgardner (1980). His work did not include the FSSP, but did include the Axially Scattering Spectrometer Probe (ASSP), also designed by PMS. No comprehensive comparison between the FSSP and other liquid water content instruments has been found in the literature. Many of the errors inherent in the FSSP are also common to the ASSP instrument designed by PMS. Baumgardner (1980) determined that ASSP errors arise primarily from the large uncertainty in the sample volume of the instrument. Droplets are mis-sized due to background scattering outside the depth of field, uneven intensity of laser illumination, multiple scattering in the depth of field at higher concentrations and inaccurate sizing calibrations. Inaccurate sizing of droplets leads to significant errors because the liquid water content is dependent on the cube of the diameter of the particles.

The JW probes' measurement errors are caused primarily by faulty design (Baumgardner, 1980). The hot wire's temperature is non-uniform

due to heat conduction to the shield. The zero LWC baseline drifts excessively due to poor grounding, lack of voltage regulation and lack of temperature compensation in the bridge circuitry. The baseline drift is not a serious problem in cumulus cloud research but can cause more significant errors in horizontally stratified clouds where the aircraft may in cloud for long time periods. Baumgardner (1980) sites other reasons for the JW errors.

A comparison of the JW and the FSSP instruments for low liquid water contents observed in orographic systems was made for the November 24, 1979 Queen Air flight during the CSU experiment. The results are shown in Figure 7. The JW offset appears as the intercept of the best fit (dashed) line on the figure. The intercept is 0.085 g/m^3 , the slope of the line 1.64 and the correlation coefficient 0.80.

No comparison was made for the November 26 flight because of the scarcity of liquid water in the system. By using the FSSP zero values as an indicator, the JW bias for the November 26, 1979 flight was determined to be 0.18 g/m^3 .

Baumgardner (1980) discusses comparisons between liquid water contents measured by the JW, ASSP, a cloud gun and a CSIRO hot wire probe. No comparisons are available for the FSSP. In general, the ASSP liquid water contents exceed the cloud gun and CSIRO probe by a factor of 2-3. The JW demonstrates anomalously high values when other instruments indicate smaller liquid water levels. In general, the value of the FSSP as an indicator of liquid water content has never been properly researched.

2.3 Ground Based Instrumentation

Rawinsonde data were collected during the project with RD-65 rawinsonde units at two sites, the first upwind of the Park Range at Craig,

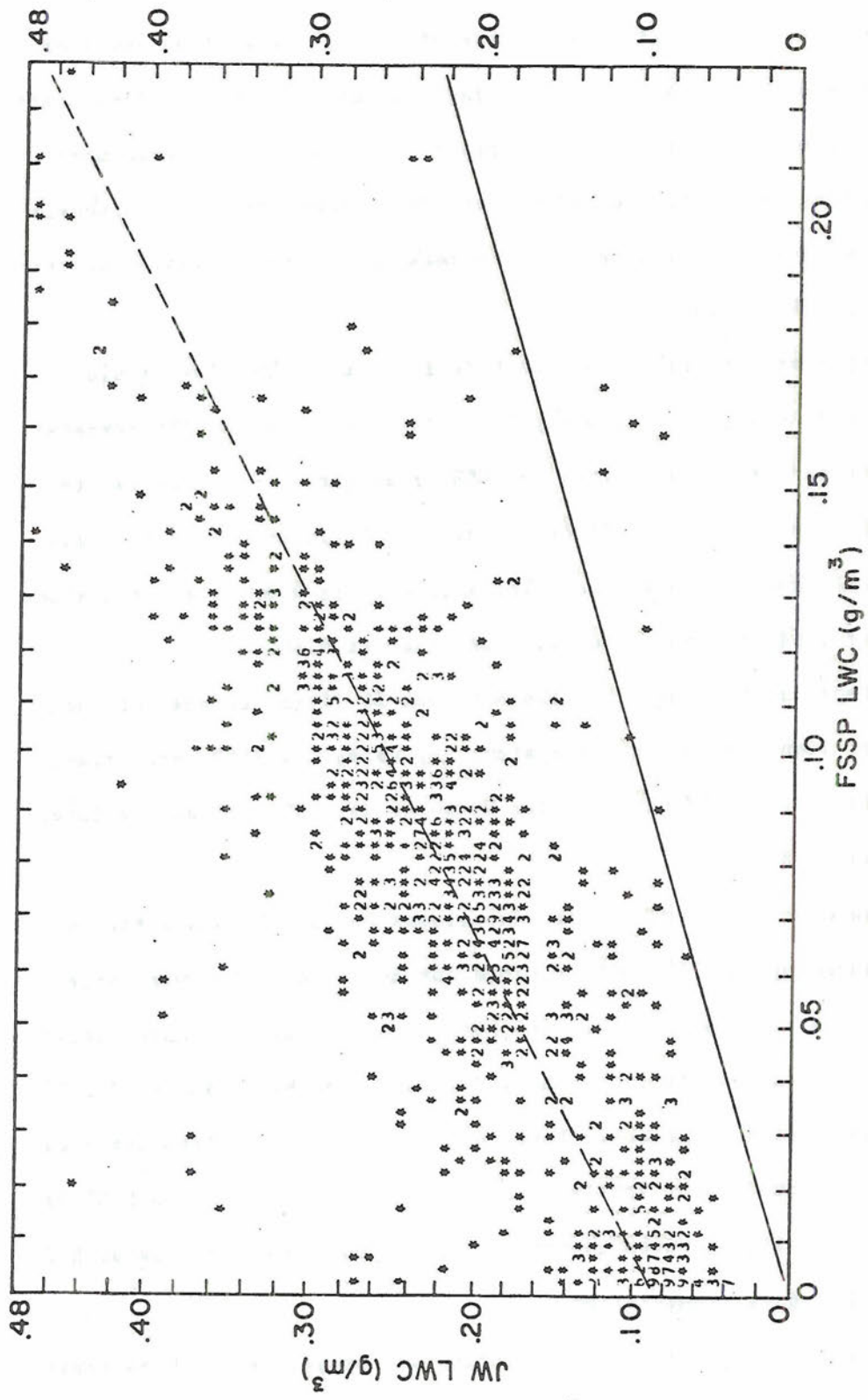


Figure 7. FSSP vs. JW determined liquid water contents. For the November 24, 1979 data set, the intercept was 0.085 g/m³, the slope of the line was 1.64 and the correlation coefficient 0.80.

Colorado and the second downwind at Hebron, Colorado (see Figure 2). Generally, balloons were launched as often as every three hours during storm periods and less often between storm events, unless a transport and dispersion experiment was declared. All raw rawinsonde data were carefully checked and then reduced by the Environmental Data Network System operated by the Bureau of Reclamation.

Three radars were used during the entire COSE II experiment but only one was placed on fully operational status on the dates when these case studies occurred early in the experimental period. Radar data presented in this study were taken by NOAA's vertically pointing x-band (M-33, $\lambda=3.2$ cm, frequency =9.4 GHz, optional Doppler) operating in the Doppler mode.

Surface observations of precipitation, winds and temperature with hourly resolution were taken at a number of stations in the Yampa Valley and on the Park Range. Table 4 summarizes the locations and types of observations taken by the surface network. The letters to the left of each location refer to Figure 2, a map of the COSE area. In addition to these observations, Formvar crystal replicas were made at two locations, the Timbers Lodge (R) and Thunderhead Lodge (O).

**GROUND INSTRUMENTATION
COLORADO OROGRAPHIC SEEDING EXPERIMENT**

Location Identifier (Figure 2)	Location Name	Reduced Data
Precipitation network		
A	Columbine Lodge	Hourly Precipitation
B	Rabbit Ears Highway	Hourly Precipitation
C	False Top	Hourly Precipitation
D	Picnic Area	Hourly Precipitation
E	Priest Creek (ski area)	Hourly Precipitation
Wind Instrumentation		
G	Storm Peak	Hourly wind speed
H	Gondola Tower 3	Hourly wind direction
I	Milner	Wind run and wind direction
J	Mt Harris	Wind run and wind direction
K	Yampa Valley	Wind run and wind direction
L	Emerald Mountain	Wind speed and direction
M	Hayden Power Plant	Wind speed and direction
N	Craig Power Plant	Wind speed and direction at three levels on stack
Temperature Sensors		
G	Storm Peak	Hourly Temperature
O	Thunderhead Lodge	Hourly Temperature
P	Cristie Base	Hourly Temperature
L	Emerald Mountain	Hourly Temperature
J	Mt Harris	Hourly Temperature
K	Yampa	Hourly Temperature
M	Hayden Power Plant	Hourly Temperature
N	Craig Power Plant	Hourly Temperature

Table 4. Ground instrumentation network. Location identifiers refer to figure 2.

CHAPTER III THEORETICAL CONSIDERATIONS

As part of the research effort to describe physical processes which generate stable orographic cloud systems, two models of cloud physical and microphysical processes were developed. The first model is designed to calculate streamlines, potential condensate production, and condensate production rates under steady-state conditions as air passes over a mountain barrier. The second model was developed to estimate crystal trajectories within the cloud system. The physical basis for these models will be discussed in this chapter. In section one, the vertical velocity equation used in both models will be derived. The method of calculating streamlines and potential condensate will be discussed in the next section. The last section will describe the microphysical growth and fall velocity equations used to calculate crystal trajectories.

3.1 Vertical Velocity

The following derivation results largely from the work of Scorer (1949) in his treatment of mountain lee waves. A complete discussion of the derivation is given in Smith (1979). Willis (1970) adapted the work of Scorer into a parameterized model of precipitation on the Park Range (Rhea et al., 1969). The vertical velocity equation presented by Willis is used in the present model to calculate air parcel trajectories.

Assuming adiabatic steady-state frictionless motion over a small enough scale that the coriolis terms may be neglected, the linearized governing equations in two dimensions can be expressed as:

$$\text{Horizontal Momentum Eqn.} \quad \rho_0 \left(U \frac{\partial u}{\partial x} + w \frac{\partial U}{\partial z} \right) = - \frac{\partial p}{\partial x} \quad (1)$$

Vertical Momentum Eqn. $\rho_0 U \frac{\partial w}{\partial x} = - \frac{\partial p}{\partial z} - \rho g$ (2)

Continuity Eqn. $\frac{\partial u}{\partial x} + (\frac{\partial}{\partial z} + S)w = 0$ (3)

Thermodynamic Eqn. $\frac{wN^2}{g} = \frac{U}{\rho_0} \frac{\partial}{\partial x} (\rho - \frac{p}{c_s^2})$ (4)

where U is the undisturbed flow (a function only of z), u and w are the perturbations on the flow, ρ_0 is the base state density and ρ and p are the perturbation density and pressure respectively. The quantities S , N and c_s in these equations are defined as follows:

$$S = \frac{1}{\rho_0} \frac{\partial \rho_0}{\partial z} \quad (5)$$

$$N^2 = \frac{g}{\Theta} \frac{\partial \Theta}{\partial z} \quad (6)$$

$$c_s^2 = \gamma R T_0 \quad (7)$$

where T_0 is the base state temperature, a function only of z .

By assuming $\rho \gg \frac{p}{c_s^2}$ in (4) (Smith, 1979), eliminating u between (1)

and (3), p between (2) and (4) and p from the resulting two equations,

the following equation in w is obtained:

$$\frac{\partial^2 w}{\partial x^2} + \frac{\partial^2 w}{\partial z^2} + S \frac{\partial w}{\partial z} + \left(\frac{N^2}{U^2} + \frac{S}{U} \frac{\partial u}{\partial z} + \frac{\partial S}{\partial z} - \frac{1}{U} \frac{\partial^2 u}{\partial z^2} \right) w = 0 \quad (8)$$

By applying the Boussinesq approximation, terms in S vanish and the equation reduces to

$$\frac{\partial^2 w}{\partial x^2} + \frac{\partial^2 w}{\partial z^2} + \left(\frac{N^2}{U^2} - \frac{1}{U} \frac{\partial^2 u}{\partial z^2} \right) w = 0 \quad (9)$$

By assuming that the vertical wind profile over the model domain is approximately linear such that $U(z) = U(0) + \beta z$, and that a wave solution of the form $w = w^* e^{ikx}$ exists, equation (9) becomes

$$\frac{\partial^2 w^*}{\partial z^2} + l^2 w^* = 0 \quad (10)$$

where $l^2 = \frac{N^2}{U^2} - k^2$.

The lower boundary condition is given by $w(0) = U(0) \frac{\partial h}{\partial x}$ where h is the height of the topography. This can be expressed as $w^*(k, 0) = U(0) ik h^*(k)$ where $h^*(k)$ is the Fourier transform of the mountain shape. The vertical velocity w^* may be written as the Fourier integral

$$w^*(x, z) = \text{RE} \int_0^{\infty} w^*(k, z) e^{ikx} dk \quad (11)$$

For the case of $l^2 = \text{constant}$, the solution for $w^*(k, z)$ is

$$w^*(k, z) = w^*(k, 0) \exp(-(k^2 - l^2)^{0.5} z) \quad k^2 > l^2 \quad (12)$$

$$w^*(k, z) = w^*(k, 0) \exp(i(l^2 - k^2)^{0.5} z) \quad l^2 > k^2 \quad (13)$$

Solving for the vertical displacement of the streamline η where

$$w = U \frac{\partial \eta}{\partial x};$$

$$\begin{aligned} \eta(z) = \text{RE} & \int_0^l h(k) \exp(i(l^2 - k^2)^{0.5} z) \exp ikx dk \\ & + \int_l^{\infty} h(k) \exp((-k^2 - l^2)^{0.5} z) \exp ikx dk \end{aligned} \quad (14)$$

A bell shaped mountain of the form

$$h(x) = \frac{h_m a^2}{x^2 + a^2} \quad (15)$$

where h_m is the maximum height of the mountain and a is its half width has the Fourier transform

$$h(k) = h_m a e^{-ka} \quad (16)$$

For the broad mountain solution with strong stability, the first integral in (14) vanishes and integration of the second using (16) produces

$$\eta(x, z) = h_m a \left(\frac{a \cos(lz) - x \sin(lz)}{a^2 + x^2} \right) \quad (17)$$

Solving for the vertical velocity:

$$w(x, z) = \frac{-2axhu (a \cos(lz) - x \sin(lz))}{a^2 + x^2} - \frac{ahu}{a^2 + x^2} \sin(lz) \quad (18)$$

Smith (1979) discusses the validity and limitations of this simplified theory of mountain airflow.

In his total model development Willis (1970) determines values of a and h for the Park Range by comparing his model of orographic precipitation with data taken during the Park Range Atmospheric Water Resources Program (Rhea et al., 1969). Willis found values of a and h which best represent the Park Range as $h = 1400\text{m}$ and $a = 8000\text{m}$. Figure 8 shows the ideal profile and an actual profile along $40^{\circ}30'$ N latitude.

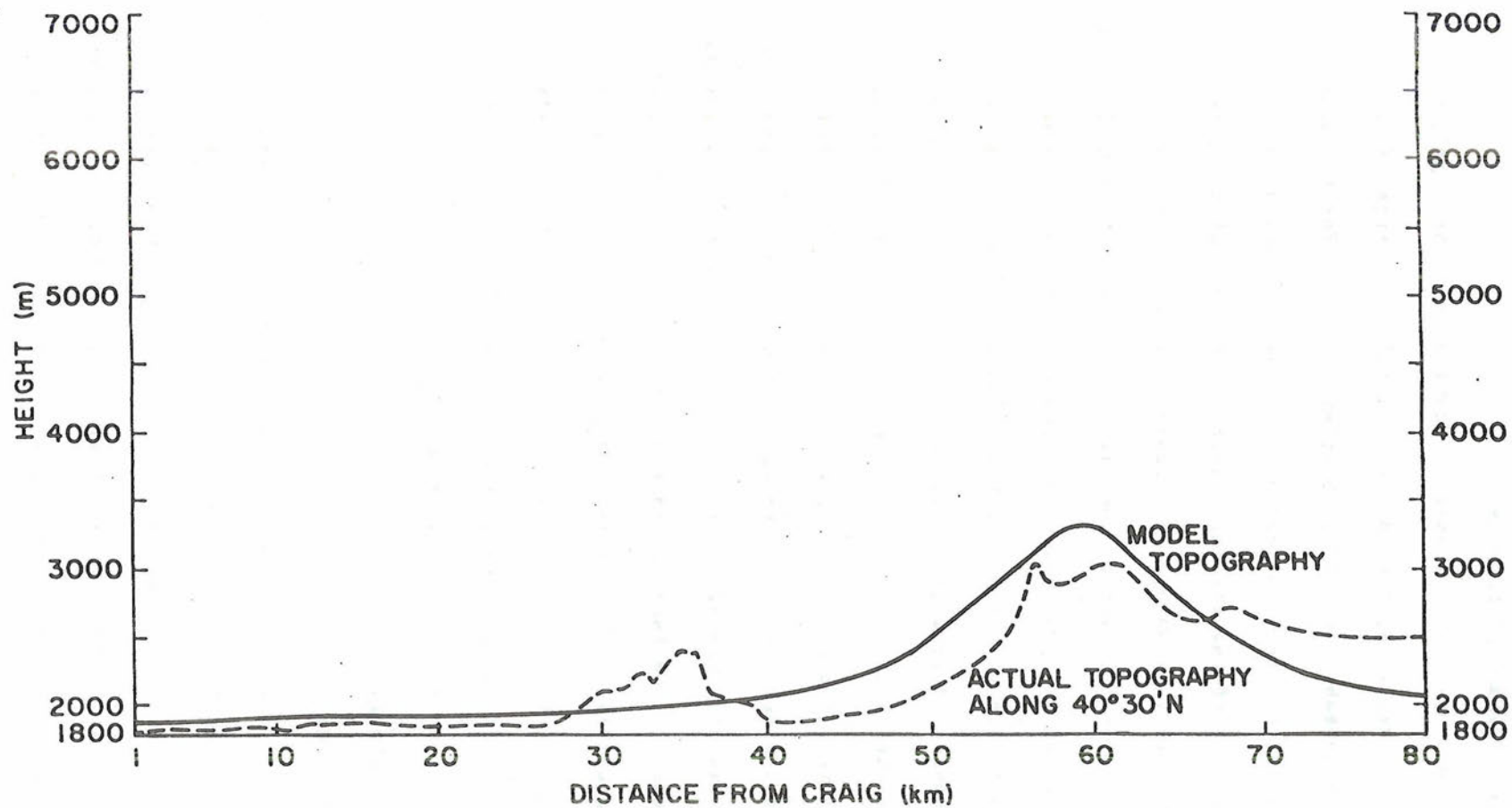


Figure 8. Actual and simulated mountain profiles used in the airflow model. Topography was taken along the 40°30' North parallel.

3.2 Airflow and Condensate Production

Values of vertical velocity were calculated on a 25x80 grid (200m x 1000m resolution) using input data from aircraft soundings taken on November 24 and November 26, 1979. Supplemental data for the uppermost and lowest gridpoints were provided by the Craig, Colorado sounding taken near the time of the aircraft flights. Air parcel trajectories over the barrier were calculated by considering the measured horizontal and predicted vertical motion of the air as it passed through the grid. To calculate condensate production and production rates, the equivalent potential temperature of the parcel was calculated from the upwind sounding and conserved from the origin point throughout the parcels transit across the barrier. When a parcel is lifted beyond its lifting condensation level, condensation begins to occur. Since droplet growth is slow, droplet sizes are small during the time period of transit and fallout is negligible, the droplets are assumed to remain with the parcel during transit. The temperature and saturation mixing ratio of the parcel are calculated as the parcel undergoes moist adiabatic ascent and descent. The total condensate in the parcel is then calculated by considering the difference in saturation mixing ratios at its current location and at its lifting condensation level.

3.3 Crystal Trajectories

3.31 Growth Equations

In this model, crystal trajectories are determined by growing single crystals by the vapor diffusion process and advecting them with the horizontal wind while falling against a predicted updraft. Crystals can be grown or evaporated by running trajectories forwards or backwards. The effects of crystal competition for vapor are controlled by varying

the supersaturation from water to ice saturation. Crystals growing under water saturated conditions will have the lowest trajectory (fastest fall) while those growing at conditions just above ice saturation will have the highest trajectory (slowest fall). These trajectories represent the limits of actual trajectories in a cloud with spatially varying supersaturations.

The growth equations used are derived in Byers (1965) and Cotton (1970) by considering an equilibrium condition between the latent heat production due to mass growth of an ice crystal and the rate of molecular diffusion of heat away from the crystal.

The rate of latent heat release due to mass deposition on the surface of an ice crystal is given by

$$L_s \frac{dx_i}{dt} = 4\pi CD_v (\rho_w - \rho_w(r)) L_s \quad (19)$$

where

x_i = mass of the crystal

L_s = latent heat of sublimation

C = capacitance (using electrostatic analogy)

D_v = diffusivity of water vapor in air

ρ_w = vapor density at a distance crystal

$\rho_w(r)$ = vapor density at the crystal surface

The rate of molecular diffusion of heat away from the crystal is given by:

$$\frac{dQ}{dt} = 4\pi CK_i (T_r - T) \quad (20)$$

where

K_i = thermal conductivity

T_r = temperature at crystal surface

T = temperature at a distance the crystal

At equilibrium, the terms on the right sides of (19) and (20) are equal. Thus:

$$\frac{\rho_w - \rho_w(r)}{(T_r - T)} = \frac{K_i}{D_v L_s} \quad (21)$$

Substituting the approximate relationship:

$$\rho_w - \rho_w(r) = \frac{m_w (e - e_r)}{RT} \quad (22)$$

where

m_w = molecular weight of water

R = universal gas constant

e = vapor pressure

e_r = vapor pressure near crystal surface

into (21) and the result into (19) gives:

$$T_r - T = \frac{L_s}{4\pi C K_i} \frac{dx_i}{dt} \quad (23)$$

The integrated form of the Clausius-Clapeyron equation is

$$\frac{e_s(T_r)}{e_s(T)} = \exp\left(\frac{m_w L_s}{RT^2}(T_r - T)\right) \quad (24)$$

Substituting (23) into (24)

$$\frac{e_s(T_r)}{e_s(T)} = \exp\left(\frac{m_w L_s^2}{4RT^2 \pi C K_i} \frac{dx_i}{dt}\right) \quad (25)$$

Substituting (22) into (19) and rearranging

$$\frac{e}{e_s(T)} = \frac{e_s(T_r)}{e_s(T)} + \frac{RT}{4\pi C D_v m_w e_s(T)} \frac{dx_i}{dt} \quad (26)$$

After substituting (25) into (26), expanding the exponent and dropping higher order terms

$$\frac{e}{e_s(T)} = 1 + \frac{m L_s^2}{4\pi C K_i R T^2} \frac{dx_i}{dt} + \frac{RT}{4\pi C D \frac{m}{v} e_s(T)} \frac{dx_i}{dt} \quad (27)$$

Letting $\frac{e}{e_s(T)} = S$ and rearranging

$$\frac{dx_i}{dt} = 4\pi C(S-1)G(T,p) \quad (28)$$

where

$$G(T,P) = \frac{1}{\frac{m L_s^2}{K_i R T^2} + \frac{RT}{m \frac{D}{v} e_s(T)}} \quad (29)$$

In this work, the range of temperatures involved in the calculation of crystal trajectories are all within the boundaries of plate and dendritic crystals ($-8^\circ\text{C} \geq T \geq -25^\circ\text{C}$). Dendrites are assumed to grow between -12°C and -16°C . Cotton (1970) gives a detailed description of the growth criteria, capacitance, density and resulting growth equations for individual habits. His results are summarized in Table 5 and are the equations used in this model.

3.32 Terminal Velocity Equations

The terminal velocity equations used in this model are from Brown (1970), Locatelli and Hobbs (1974) and Davis (1974). A simple parameterization to estimate crystal trajectories under conditions of medium riming was used to calculate some trajectories. Basically a weighted transition from the equation for unrimed to rimed crystals was carried out over a specified period under which riming was assumed to occur. The crystal continues to grow two-dimensionally but its fall velocity increases as a function of time due to riming. This parameterization is

Parameter	Small Plates (c axis < 30 μ m)	Large Plates (c axis > 30 μ m)	Dendrites
Capacitance	$C = \frac{ae}{2 \sin^{-1} e}$ $e = \left(1 - \frac{c^2}{a^2}\right)^{0.5}$	$C = \frac{a}{\pi}$	$C = \frac{a}{\pi}$
Relationship Between Axes	$\frac{dc}{dt} = K_{HP} \frac{da}{dt}$ $K_{HP} = 0.12$	$c=30\mu\text{m}$	$c=30\mu\text{m}$
Density	$\delta_s = 0.9\text{g/cm}^3$	$\delta_s = 0.9\text{g/cm}^3$	$\delta_s = 0.162\text{g/cm}^3$
Growth Equations	$\frac{da}{dt} = \frac{4.0 \frac{dx_i}{dt}}{\pi \delta_s (a^2 K_{HP} + 2ac)}$	$\frac{da}{dt} = \frac{2.0 \frac{dx_i}{dt}}{\pi ac \delta_s}$	$\frac{da}{dt} = \frac{dx_i}{2ka}$

$$k=38.0 \times 10^{-5} \text{g/cm}^2$$

Table 5. Growth equations used in trajectory model

not unrealistic since growth by riming occurs along the prism axis for flat platelike crystals. The fall velocity equations are then:

$V_T = 61.97a^{0.217}$	dendrites	Brown(1970)
$V_T = 132.55a^{0.250}$	rimed dendrites	Locatelli and Hobbs(1974)
$V_T = 296.0a^{0.284}$	plates	Davis(1974)
$V_T = 152.9a^{0.250}$	rimed plates	Locatelli and Hobbs(1974).br

CHAPTER IV NOVEMBER 24, 1979 CASE STUDY

Two case studies of stable orographic cloud systems over Colorado's Park Range are presented in Chapter 4 and 5. Data presented from aircraft observations during each case are compared with airflow model results. A crystal trajectory analysis is completed for the more complex case of November 24, 1979. By considering the information obtained through observations and theoretical considerations, a hypothesis concerning the dominant microphysical mechanisms by which crystals grow and precipitate during these type of storm events is developed.

November 24, 1979 Case Study

4.1 Major Synoptic Features

Conditions Prior to the Mesoanalysis

At 12Z on November 24, 1979, a low pressure system located just south of Salem, Oregon produced a wide area of precipitation extending eastward to Montana and southward into northern Utah, Nevada and California. Associated with this system, a cold front extended west-southwest into the Pacific. Directly south of the low, a warm front produced clouds and light rain into California. Figure 9 indicates the most important surface and upper level features at 12Z.

Between 85 and 70 KPa, westerly flow through the east side of a strong thermal ridge centered on the Oregon coast produced a region of warm air advection which extended as far as Montana, Utah, and Nevada. Precipitation reports were widespread throughout this area. Aloft at 50 KPa, the thermal ridge was displaced eastward so that weak cold air advection occurred over the northwest. East of the warm advection zone, a thermal trough extended southward from Montana to New Mexico. This

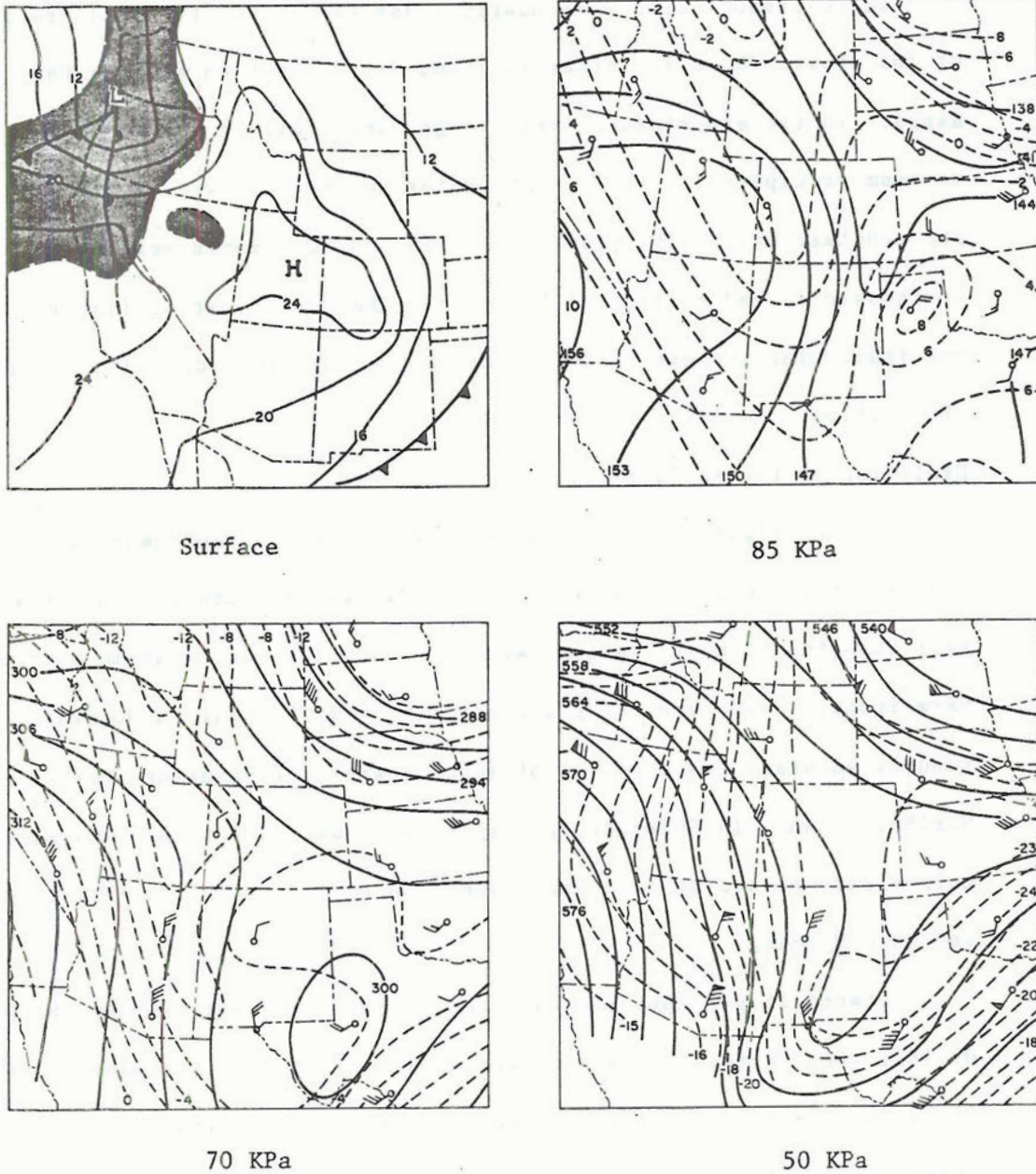


Figure 9. Major synoptic features at 12Z on November 24, 1979. Heights are in decameters, temperatures in $^{\circ}\text{C}$, pressures on the surface map are in (hectopascals - 1000).

mass of cold air moved into the central mountains behind a cold front which was already crossing the Great Plains.

In Colorado, skies were mostly clear except for two small regions of the state. These two areas included Grand Junction and the Park Range. In the experimental area, light snow fell in the mountains with maximum precipitation (0.15 cm/hr water equivalent (w.e.)) occurring at the mountain base. The flow between 50 and 70 KPa was west-northwesterly and moist at low levels. The precipitation zone was narrow indicating the precipitation originated due to orographic forcing of the airflow.

Evolution of the surface low

By 15Z (Figure 10), the low center had shifted northward into the coastal areas south of Seattle, Wa. Post frontal rain and rainshowers were reported at most stations west of the cold front. Ahead of the warm front, a wide area of precipitation, mostly light to moderate continuous snowfall, covered all of Idaho, Eastern Washington, Oregon and Northern Utah. In Colorado, precipitation continued to be limited to a narrow band extending from Grand Junction northeast to the Park Range and into Wyoming.

Between 15 and 18Z, the surface low began to move rapidly eastward. By 18Z, the low was positioned over Lewiston, Idaho. A tongue of warmer air wedged between the surface frontal positions continued to supply moisture into the clouds over the warm front as snow and snowshowers continued to be reported throughout Utah, Idaho, and western Wyoming. Post frontal showers continued to be reported in a widespread area west of the cold front.

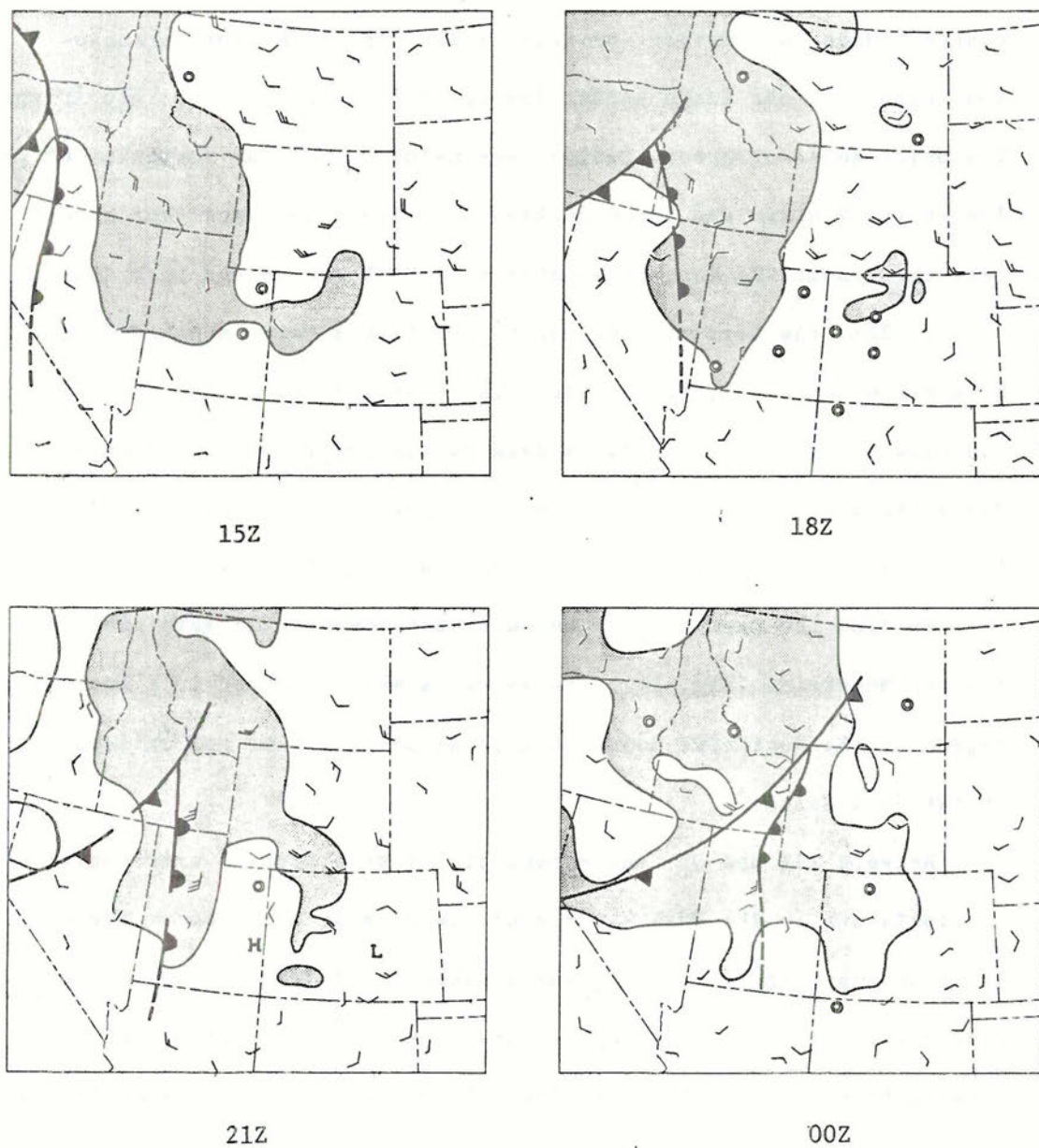


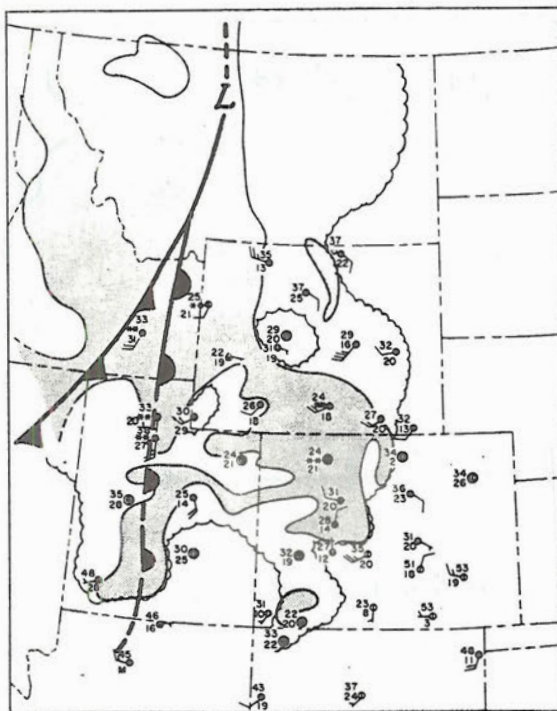
Figure 10. Evolution of the surface features during the analysis period of November 24, 1979.

At 21Z, the low pressure center was located over Helena, Montana. The cold front associated with the low now extended southwest across central Idaho into Nevada and California. The warm front branched southward from the Idaho border through Salt Lake City and into Arizona. The major zones of precipitation were mainly north and northwest of the low in the Montana and Idaho Rockies. In addition, snow continued to fall throughout the Wasatch Mountains of Utah and in the Park Range.

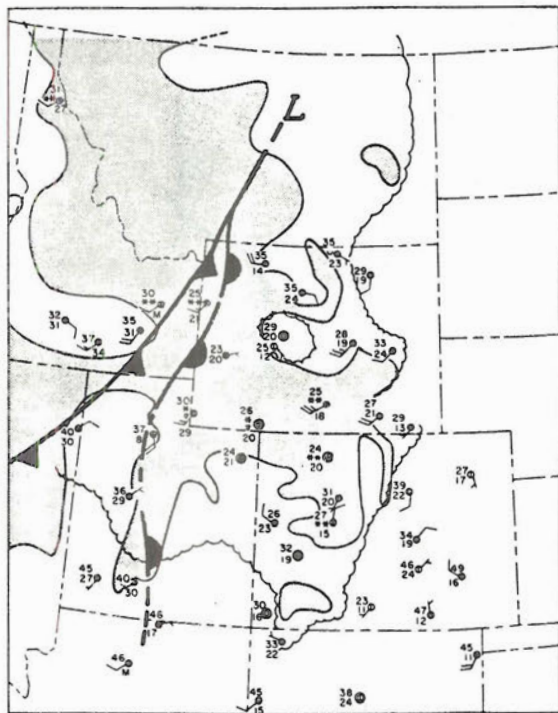
By 22Z, the Learjet and Queen Air flights were launched from their base airports east of the divide. The Lear arrived in the area at 2224Z and remained until 2241Z when a data system power failure occurred. The Queen Air also arrived in the area at 2224Z and remained until 2356Z. The mesoanalysis is from data collected during this period.

At 22Z, the warm frontal boundary had reached the west side of Wasatch Mountains (Fig. 11). Snowshowers were reported in a much larger region of the Northwest Colorado mountains, including the valleys west of the Park Range.

Between 22Z and 0Z, the effect of the warm frontal overrunning on precipitation in the Park Range could be clearly observed on the Queen Air sounding (Fig. 12). From the surface to 68 KPa, the air was somewhat moist, with dewpoint depressions around 3°C throughout the layer. Between 68 and 63 KPa the warm frontal inversion occurred and the air became completely saturated. The effect of this inversion on the production of cloud water and precipitating crystals will be discussed in a later section. Above the inversion to 50 KPa, the air remained completely saturated. Winds below the inversion veered from southwest to northwest with height through inversion level. Above the inversion the winds were northwesterly.

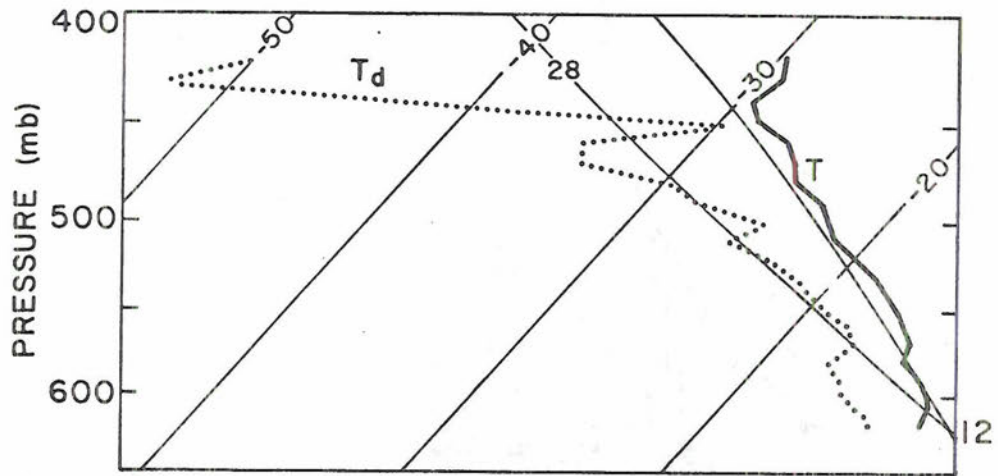


22Z

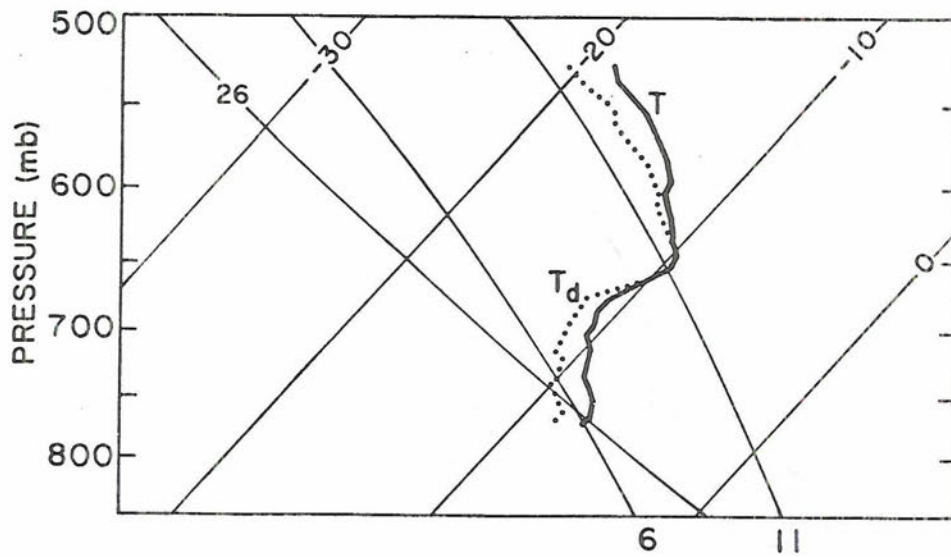


23Z

Figure 11. Detailed surface analyses at times coinciding with the aircraft microphysical analyses on November 24, 1979 over Hayden, Colorado.



Lear Sounding (2230-2238 Z)



Queen Air Sounding (2330-2353 Z)

Figure 12. Aircraft soundings taken during the November 24, 1979 storm.

By 23Z (Fig. 11) the warm front had stalled in the south at the Wasatch Barrier but continued eastward in northern Utah and Wyoming, so that the surface position of the front curved slightly conforming more to the topography. Snow continued to intensify in the Park Range and the Hayden Valley area during the period. At 2330Z, a landing approach to the Hayden airport by the NCAR Queen Air had to be aborted because of heavy snowfall and poor visability. Snow was reported at the airport during the entire period of the mesoanalysis. Evidence from aircraft sounding data indicated that the existence of the warm frontal surface over the Park Range region accounted not only for the presence of precipitation but strongly affected the microphysical processes associated with the production of cloud water and the growth and development of precipitation particles.

Post Analysis Conditions

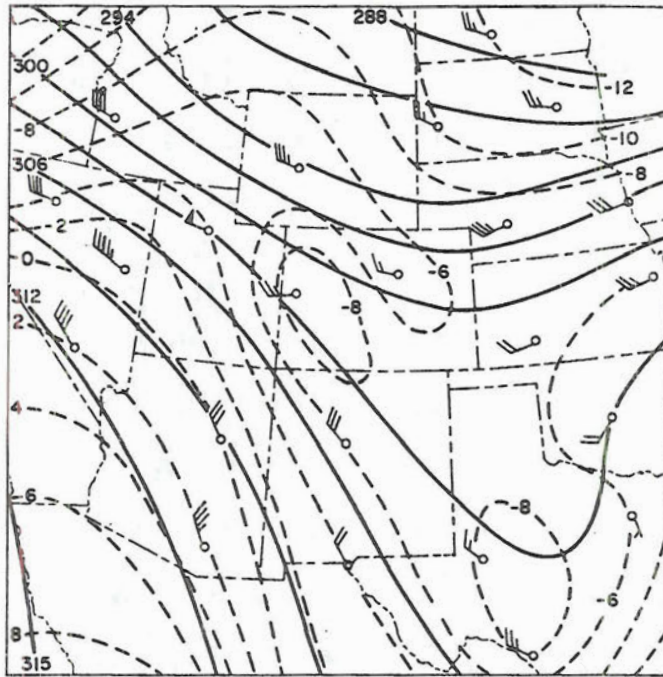
By 00Z on November 25 both aircraft had left the Park Range area. At 00Z, the surface analysis indicated that the low center was located in eastern Montana with the warm front extending south into Wyoming through the eastern tip of Idaho and into Utah (Fig. 10). The cold front trailed the warm front, passing through central Idaho southward into Nevada. Post-frontal precipitation occurred throughout Idaho and western Montana. Ahead of the warm front in Colorado and Wyoming, precipitation reports were numerous, extending from the Wyoming Mountains south into the Park and Front Ranges, the central Colorado Mountains and the west slopes of the San Juans. During the next four hours, precipitation in the experimental area continued to intensify, reaching a maximum around 04Z.

Aloft at 00Z, the strong thermal ridge at 70 KPa (Fig. 13) had moved westward so that its axis now extended from central Montana into northern Utah. Between the ridge and continental divide, warm air advection continued to enhance precipitation and produce widespread cloudiness. The ridge was also evident at 50 KPa in the northern states, but was displaced eastward in the Colorado/Wyoming region so that slight cold air advection occurred in western Colorado (Fig. 13). This, combined with the warm air advection at 70 KPa probably enhanced precipitation later in the storm by producing some destabilization of the atmosphere. During the flights, no convection or strong turbulence was observed by either aircraft and the presence of convection during that period of the storm was unlikely. A vertical cross-section of the θ_E and θ surfaces from Medford, Oregon to Denver, Colorado indicates the frontal positions at the end of the mesoanalysis period (Fig. 14).

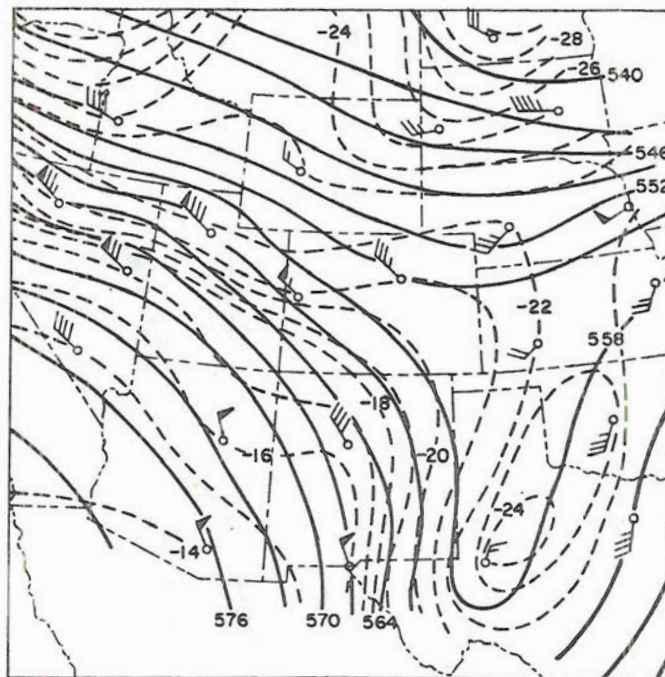
4.2 Flight Track Descriptions

The Queen Air and Lear flights both arrived in the experimental area at 2224Z (Figure 15). The Lear entered the area at an altitude of 6822 meters msl just north of $40^{\circ}30'N$ latitude and proceeded westward to the Hayden vortac (Fig. 15). After reaching the vortac, the Lear descended in a double loop pattern to an elevation of 3931 meters and proceeded east-southeast 28 kilometers, maintaining a constant altitude. At this point, a power failure occurred in the data acquisition system and the flight had to be terminated.

The Queen Air entered the area from the southeast at an altitude of 4878 meters and proceeded northward along the immediate lee side of the Park Range to $40^{\circ}53'N$ latitude in the Mt. Zirkel wilderness area (Figure 15). The aircraft then descended to 4270 meters and turned 180° ,



70 KPa



50 KPa

Figure 13. Upper air analyses for November 25, 1979 at 00Z. Heights are in decameters, temperatures in °C.

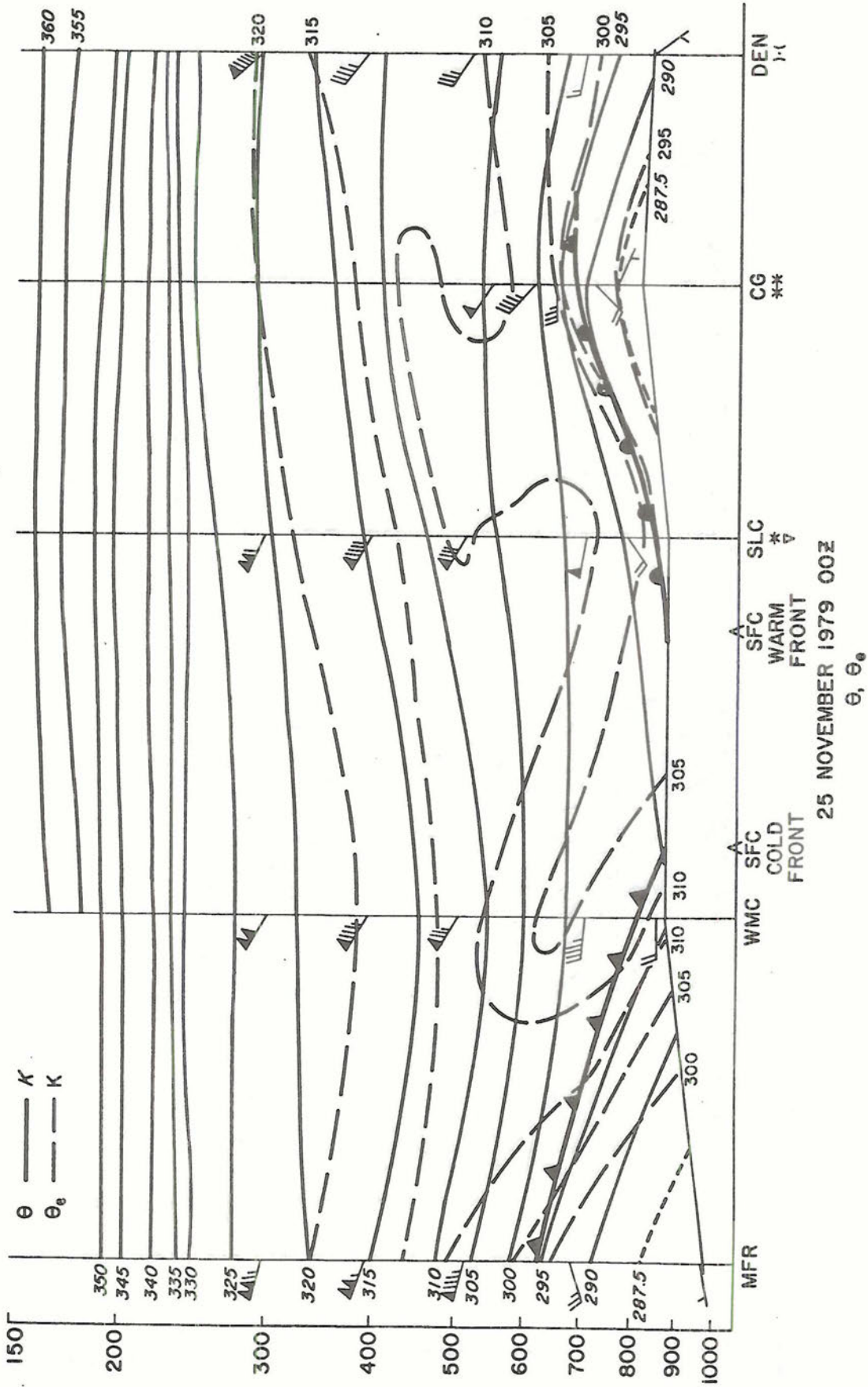


Figure 14. Vertical cross-section of potential and equivalent potential temperature from Medford, Oregon to Denver, Colorado showing frontal positions.

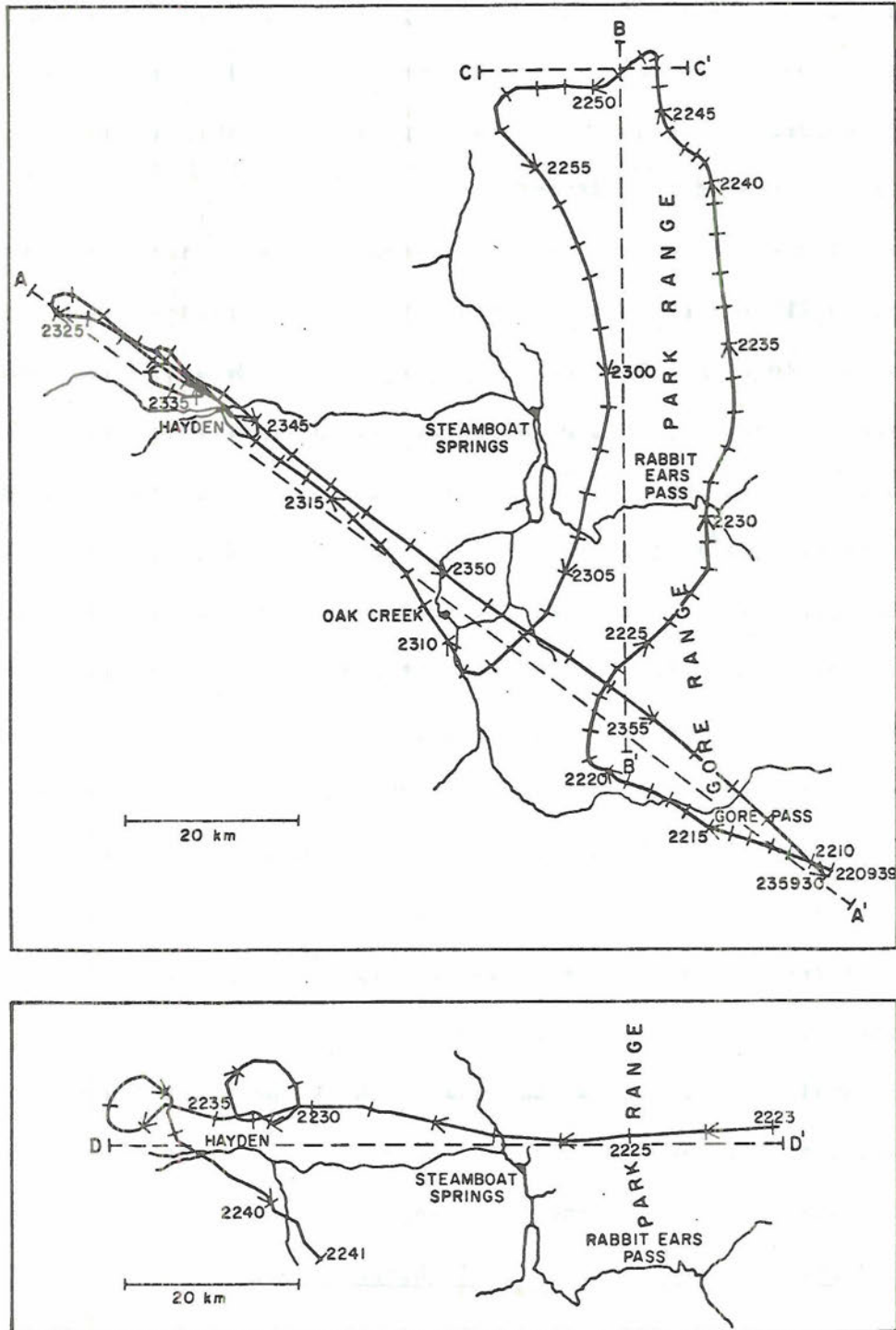


Figure 15. Queen Air and Lear flight tracks for November 24, 1979. The Queen Air flight track is the top figure.

proceeding southward along the windward side of the range to $40^{\circ}22'N$ latitude. The aircraft turned northwest, descended to 3950 meters and proceeded to the Hayden vortac. After performing a descent and ascent sounding between 3950 meters and 2236 meters over the vortac, the aircraft proceeded southeast out of the experimental area, climbing to 4100 meters as it crossed the barrier.

Data for the Queen Air flight are represented on six cross-sections (Figures 16-21). The topography indicated on the cross-sections is taken along lines AA', BB' and CC' on Figure 15. Data on each Queen Air cross-section consists of 2-D shadow-or crystal concentration (#/liter), JW liquid water content (g/m^3) (positive bias included), FSSP liquid water content (g/m^3), temperature ($^{\circ}C$), dewpoint ($^{\circ}C$), wind direction and wind speed (kt). Data were averaged over 10 second periods before they were plotted. Wind barbs are plotted in the usual manner such that a vertical barb indicates a north wind.

Lear flight data are presented on two cross-sections (Figures 22-23). Topography for the cross-sections is taken along line DD' on Figure 15. Lear cross-sections include 2-D shadow-or crystal concentration (#/liter), JW liquid water content (g/m^3) temperature ($^{\circ}C$) and dewpoint ($^{\circ}C$), all 10 second averages.

The small letters below the base of the temperature scale on all cross-sections are used to indicate the precise location of the microphysical data presented in the following sections.

4.3 Cloud physical and microphysical characteristics

In this section, references will be made continuously to figures 16- 23, the cross-sections of the flights. In the text that follows, exact locations of the measurements under discussion will be indicated by a small letter beneath the temperature scale on these eight figures.

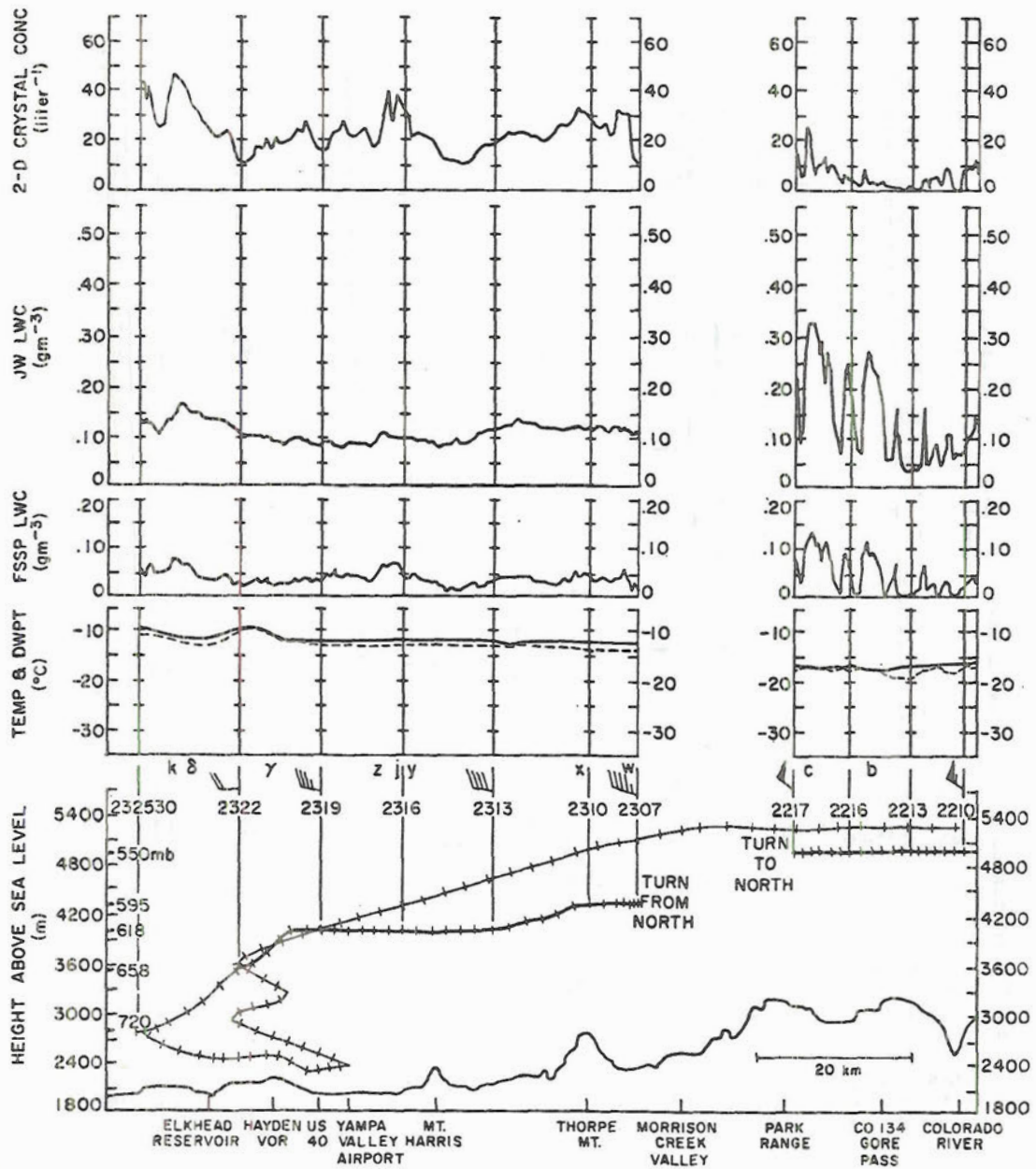


Figure 16. Vertical cross-section along line AA' on Figure 15 showing state, wind and microphysical data collected by the Queen Air on November 24, 1979. Data were averaged over ten second periods.

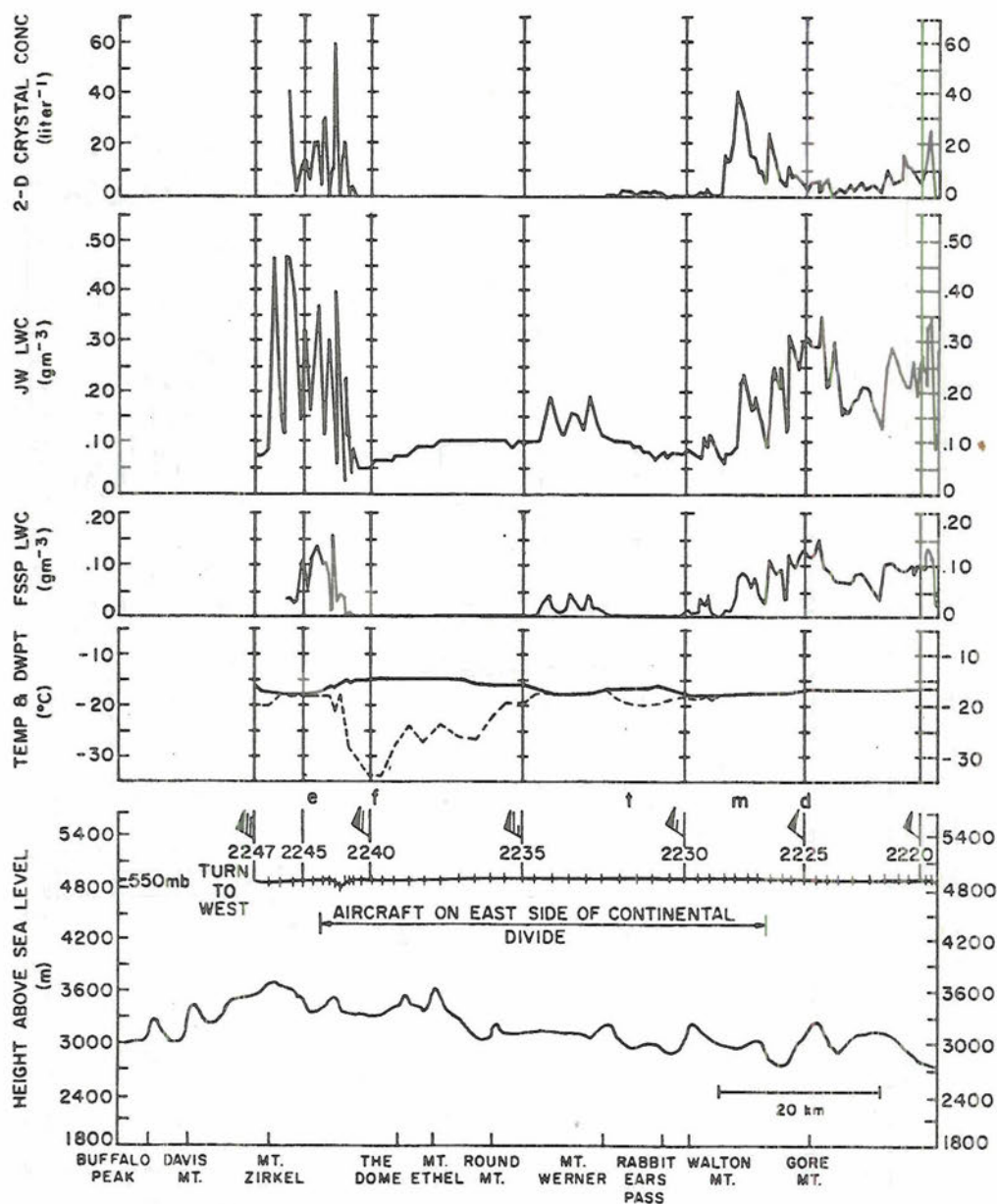


Figure 17. Vertical cross-section along line BB' on Figure 15 showing state, wind and microphysical data collected by the Queen Air on November 24, 1979. Data were averaged over ten second periods.

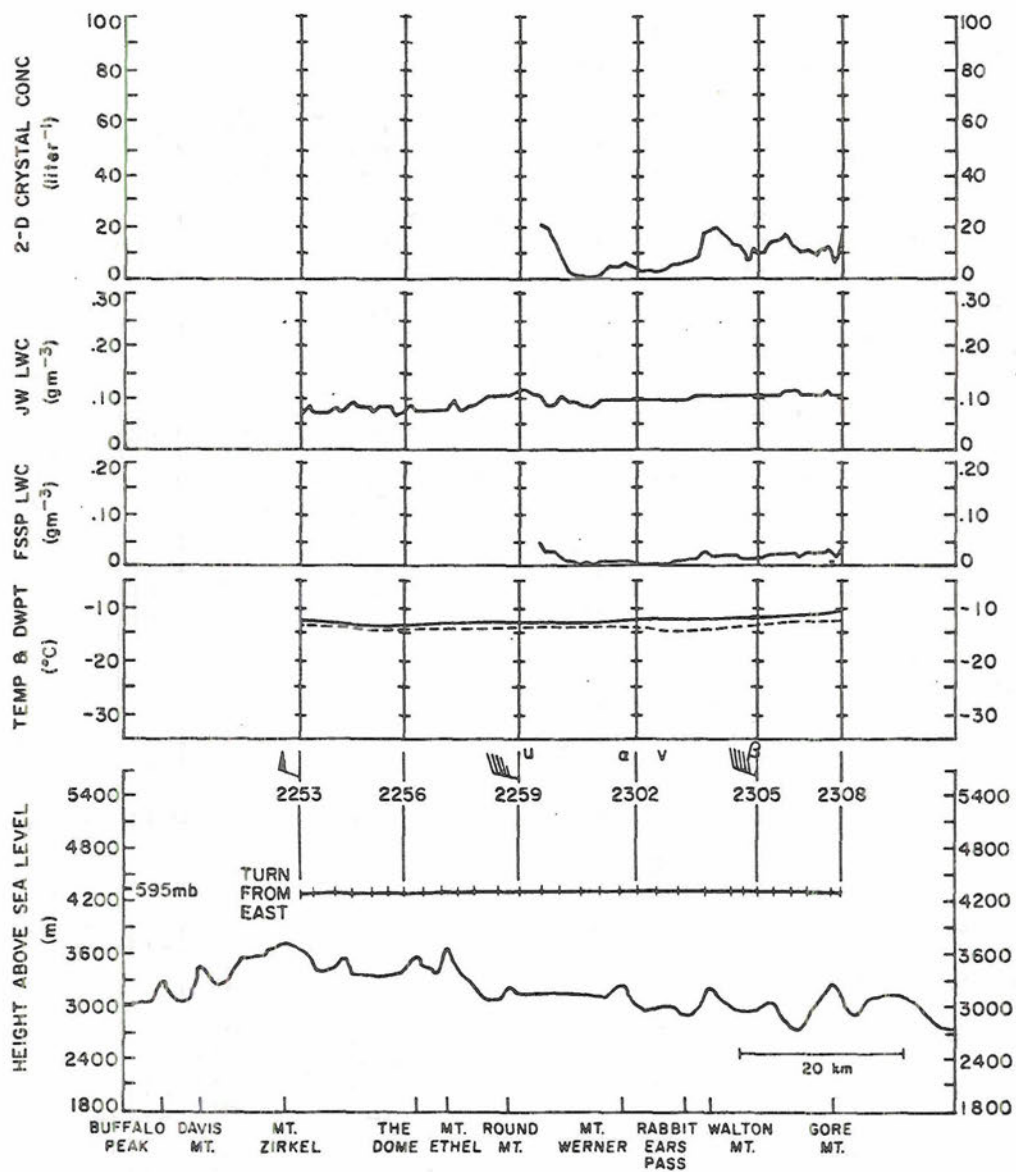


Figure 18. Vertical cross-section along line BB' on Figure 15 showing state, wind and microphysical data collected by the Queen Air on November 24, 1979. Data were averaged over ten second periods.

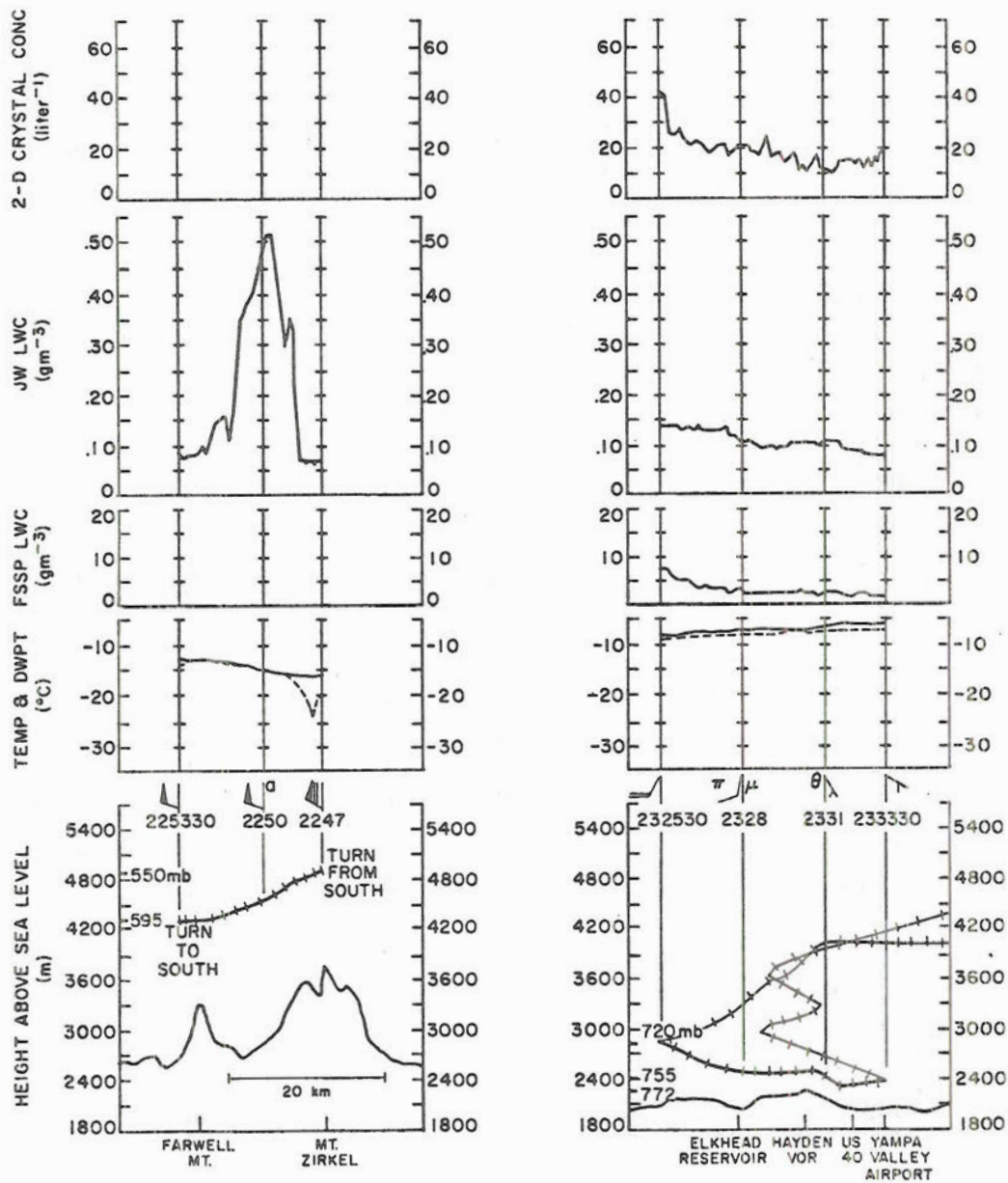


Figure 19. Vertical cross-sections along line CC' (left) and AA' (right) on Figure 15 showing state, wind and microphysical data collected by the Queen Air on November 24, 1979. Data were averaged over ten second periods.

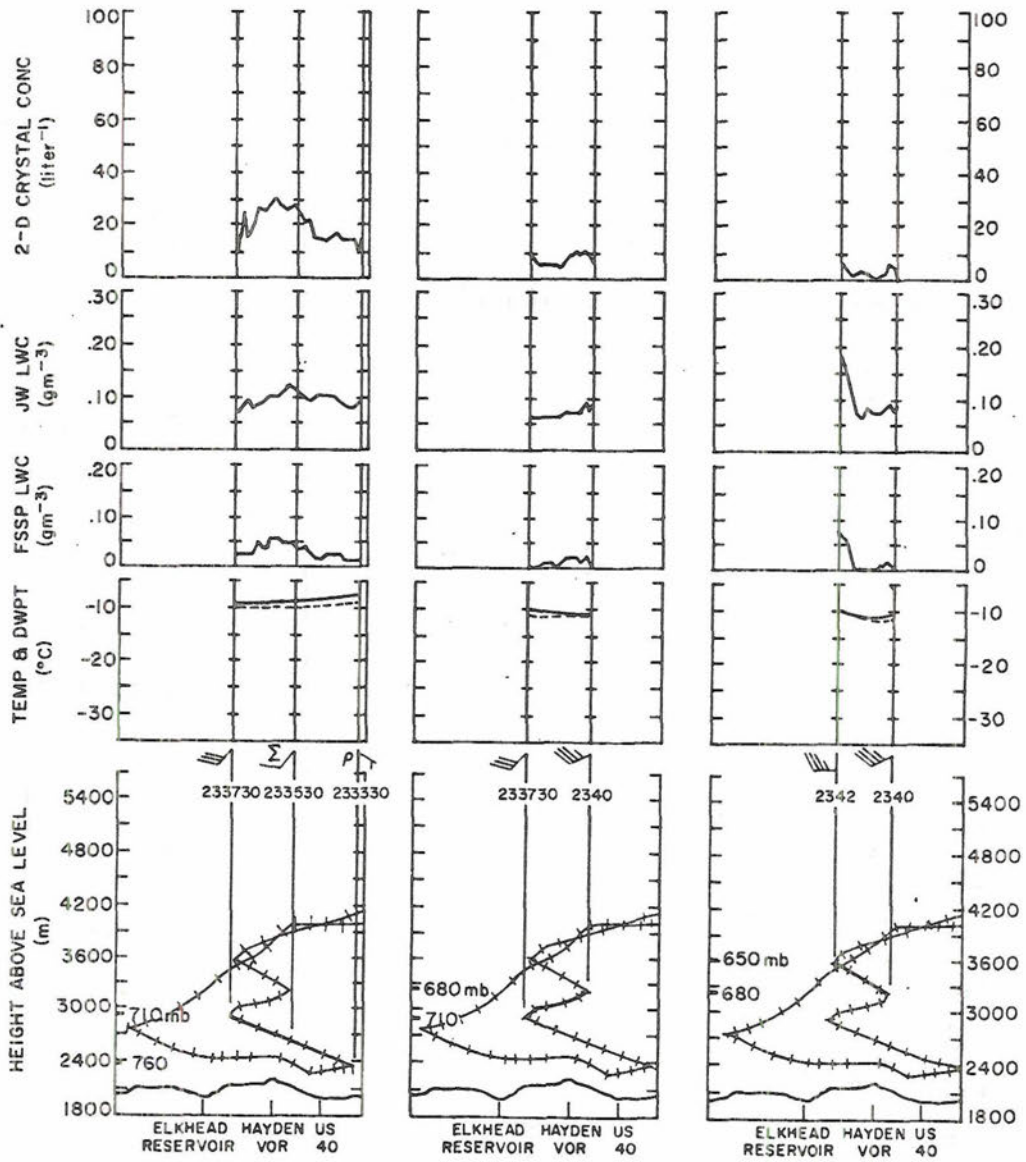


Figure 20. Vertical cross-sections along line AA' on Figure 15 showing state, wind and microphysical data collected by the Queen Air on November 24, 1979. Data were averaged over ten second periods.

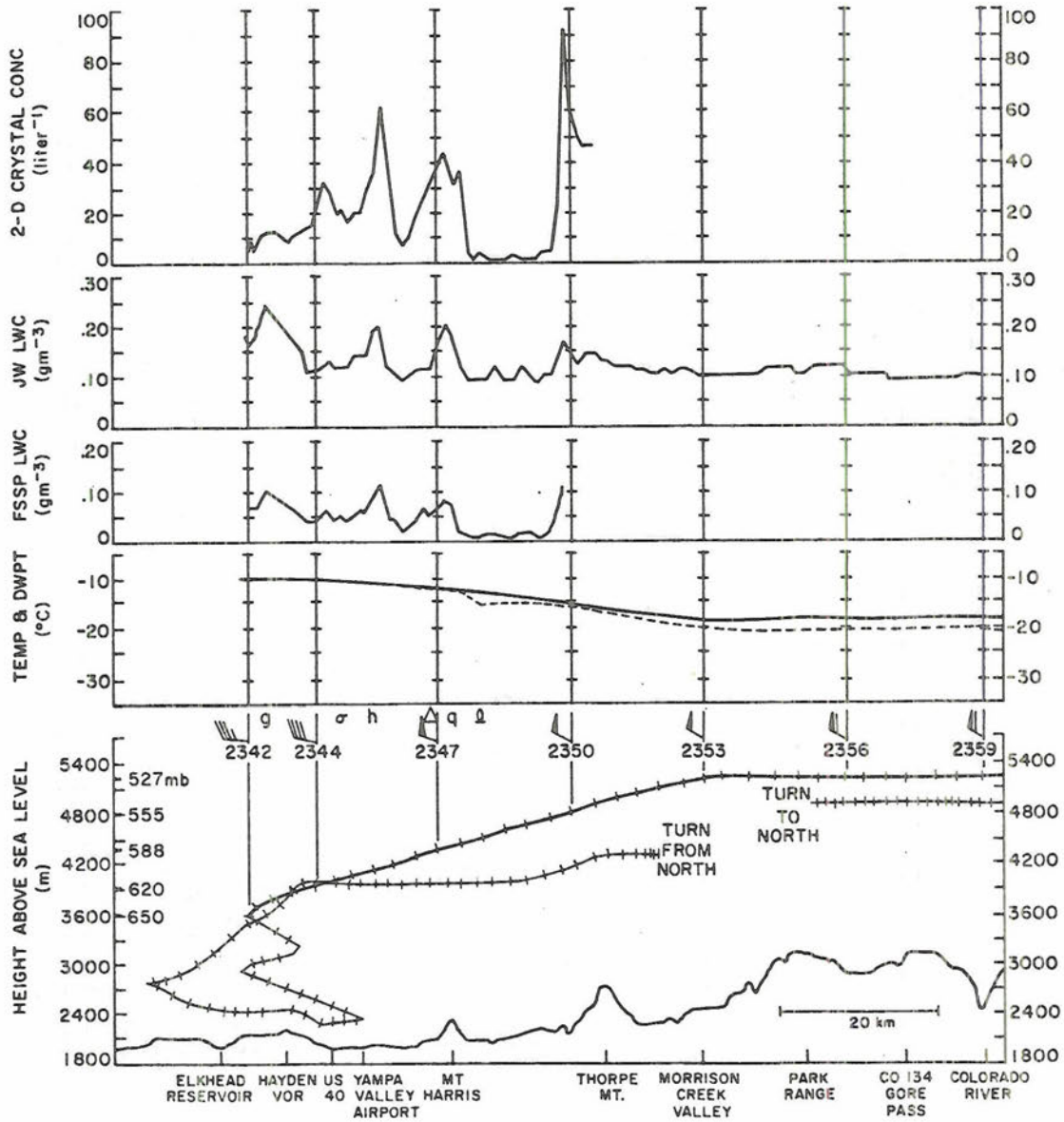


Figure 21. Vertical cross-section along line AA' on Figure 15 showing state, wind and microphysical data collected by the Queen Air on November 24, 1979. Data were averaged over ten second periods.

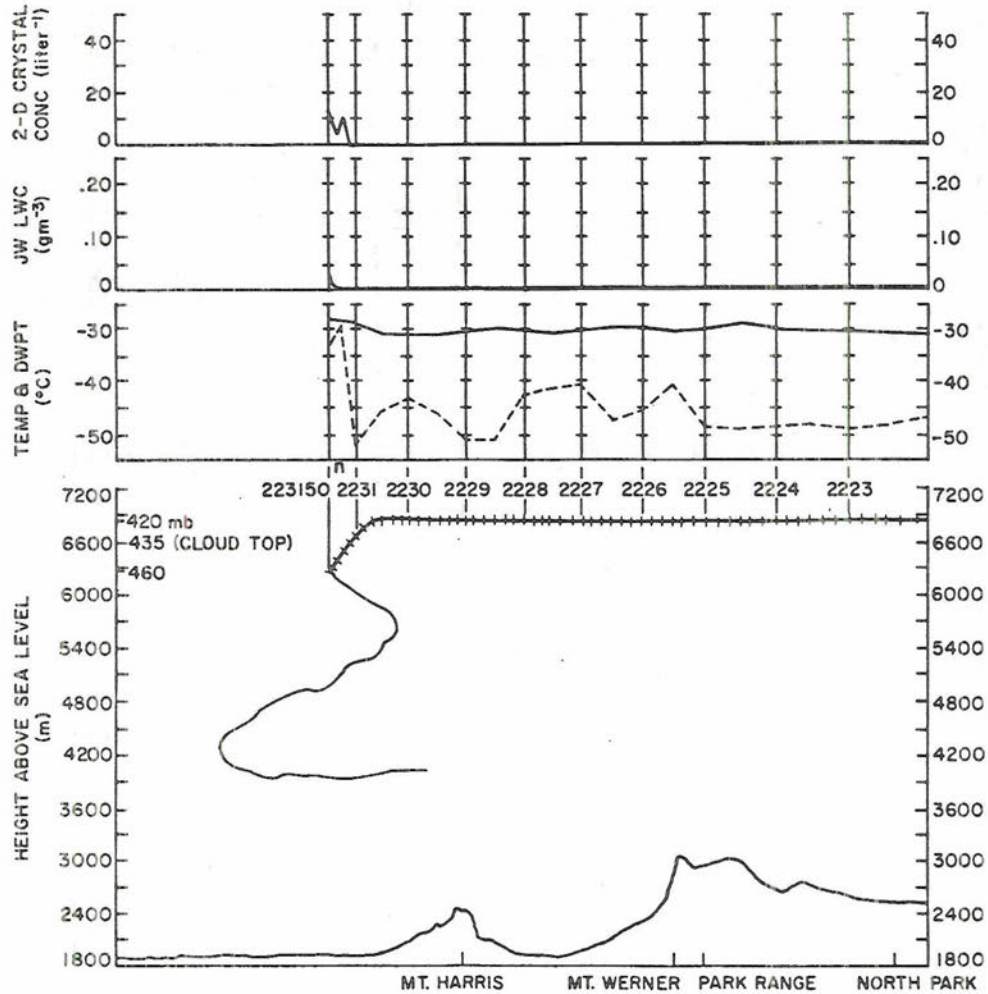


Figure 22. Vertical cross-section along line DD' on Figure 15 showing state and microphysical data collected by the Learjet on November 24, 1979. Data were averaged over ten second periods.

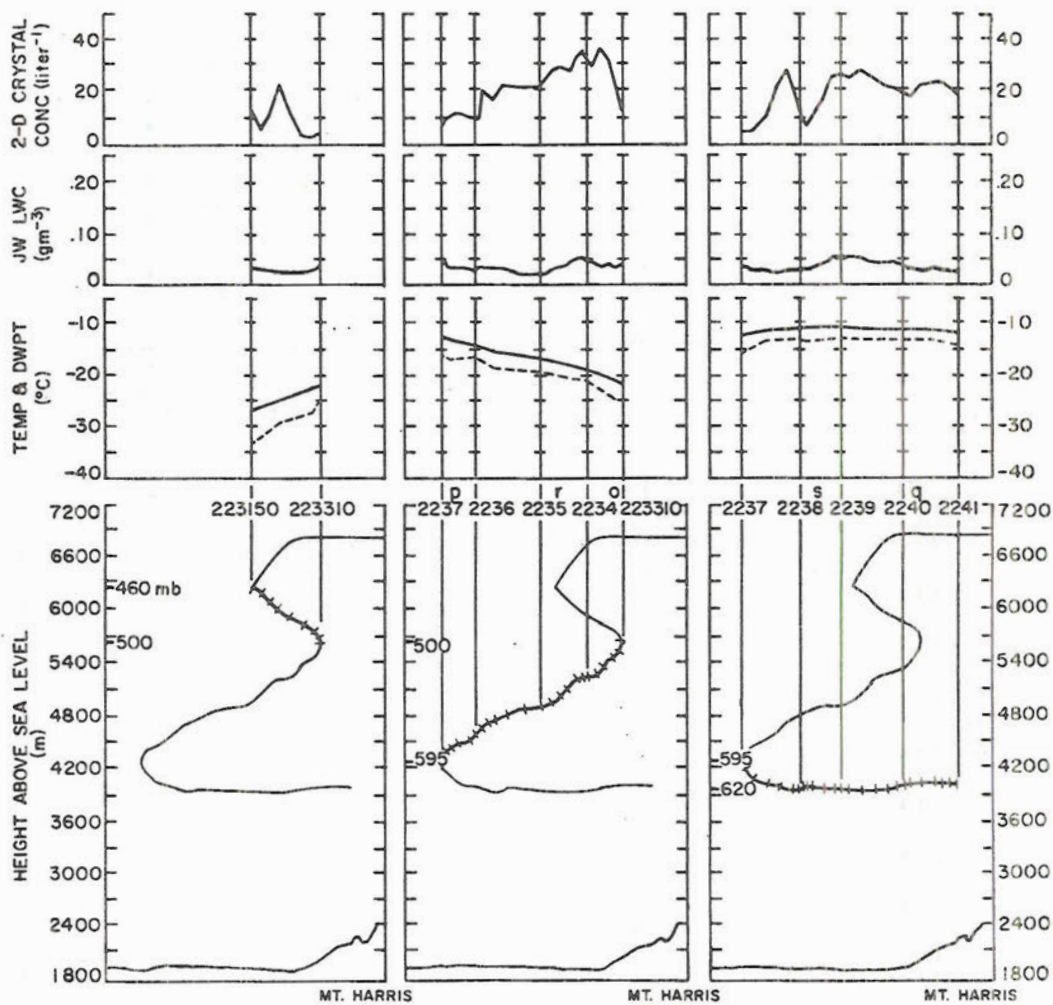


Figure 23. Vertical cross-sections along line DD' on Figure 15 showing state and microphysical data collected by the Learjet on November 24, 1979. Data were averaged over ten second periods.

The JW bias of 0.09 g/m^3 is included on the November 24, 1979 flight track cross-sections. In the text, JW values quoted will have the bias subtracted out. 2-D crystal concentrations labeled on Figures 16-23 are determined by the shadow-or method. Crystal size spectra are based on concentrations with rejection criteria applied. The data are presented in this manner because of the structure of the data as it is stored. Concentrations determined by the shadow-or method are recorded each second and can be averaged simply, while reject concentrations are based on the contents of a storage buffer which fills at irregular times, depending on the ambient crystal concentrations.

On November 24, 1979 at the time of the aircraft cloud penetrations, warm moist air overrunning of Pacific air was occurring over a shallow cold air mass that had settled into the region during a previous cold air intrusion (Figure 24). The frontal inversion was located at 65 KPa. To the west of the Park Range, a large cloud, primarily orographically induced, extended from the 43.5 KPa level (-29°C) to approximately 200 meters above the Yampa Valley (-8°C). To the lee of the Range, rapid evaporation of the cloud occurred due to strong downslope motion. The Queen Air pilot at one point was unable to maintain altitude due to strong downslope forcing. Lear and Queen Air observers were able to see the ground through broken clouds much of the time on the leeward side. Winds veered with height throughout the atmosphere, exceeding 20 m/s above 62 KPa.

Snow fell over much of the valley where reports were available. Aggregates of plates were observed at the replicator station at Thunderhead Lodge. Precipitation gauges on the barrier recorded snowfall at the rate of 0.05-0.13 cm per hour during the flight period.

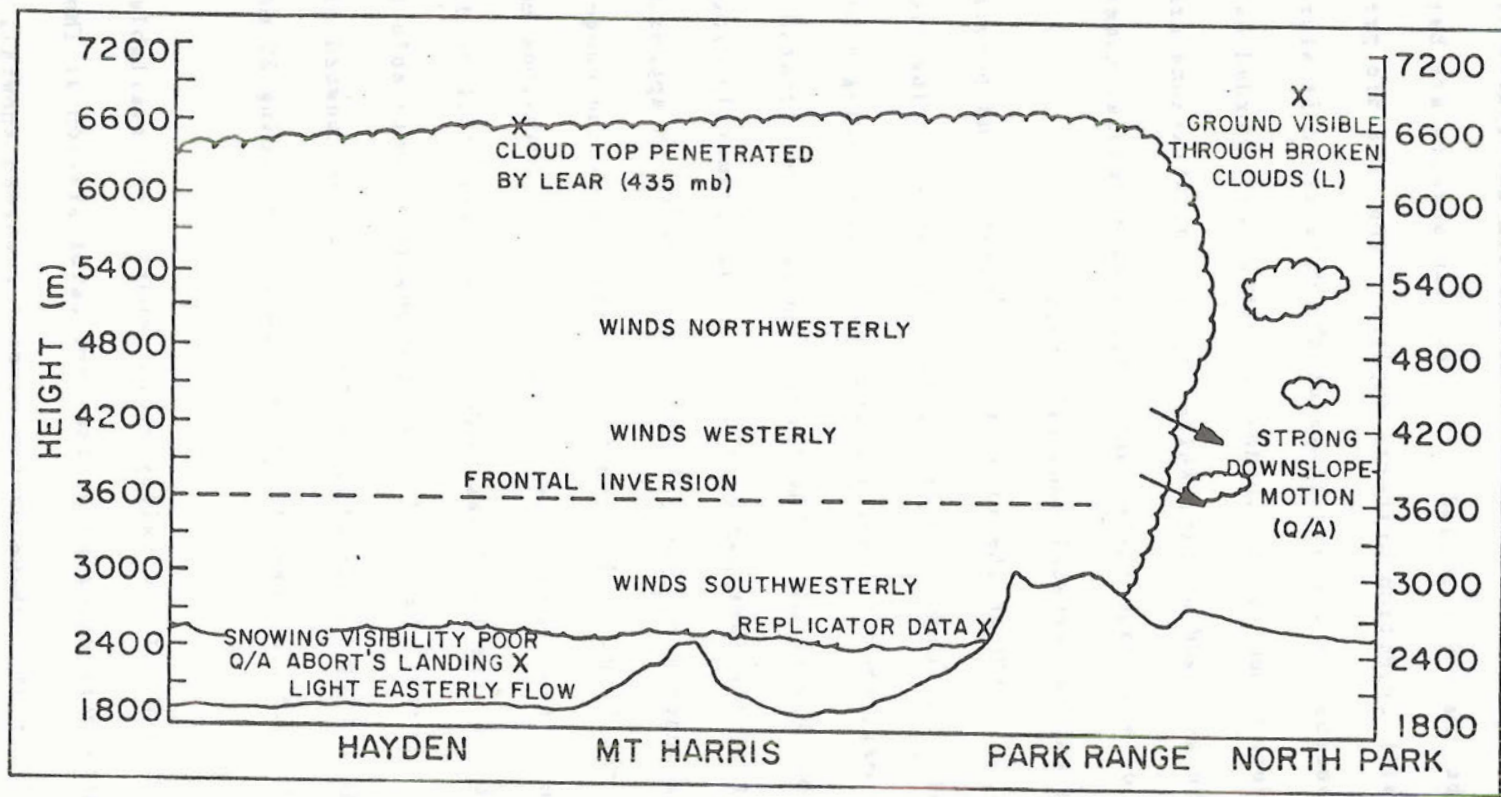


Figure 24. Schematic cross-section of the November 24, 1979 cloud system.

Snow continued to intensify during and after the flights as the major synoptic disturbance approached the COSE experimental area.

4.31 Cloud Liquid Water and Droplet Spectra

The location and quantity of cloud liquid water present in the orographic system of November 24, 1979 was closely related to the underlying topography. The maximum liquid water content observed was 0.43 g/m^3 directly on the windward side of the Park Range (a, Figure 19). The cloud water was present at temperatures as cold as -15°C , and was confined to a narrow region directly over the slope and crest of the barrier. The presence of liquid water directly over the barrier crest was observed at several locations on the northbound leg of the flight. Liquid water contents varied from $0.10\text{--}0.25 \text{ g/m}^3$ directly over the barrier depending on location and aircraft position with respect to the immediate topographic structure below it (b,c, Figure 16; d,e, Figure 17). Immediate evaporation of this water was evident to the lee of the Range (f, Figure 17). The zone of liquid water in this system was confined to a narrow region over and along the immediate mountain slope. Virtually no liquid water was observed on the southbound leg of the flight (Figure 18) although the temperature was warmer (-12°C). Along this leg, the aircraft varied from 2-10 km west of the ridge base.

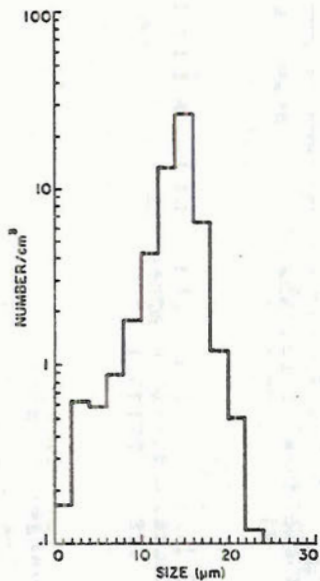
Approximately 40 km west of the Park Range, a small ridge crosses the Yampa Valley with a north-south orientation, varying in altitude from 2400-2700 meters (msl). To the northwest of this ridge, additional smaller hills are present. Cloud liquid water was observed at several locations directly upwind of these topographic features. Values seldom

exceeded 0.10 g/m^3 and were usually between $0.05\text{--}0.10 \text{ g/m}^3$ (g,h,i,Figure 21; j,k,Figure 16). The effect of the small ridge can be seen by noting the lee side evaporation zone it produces (l,Figure 21).

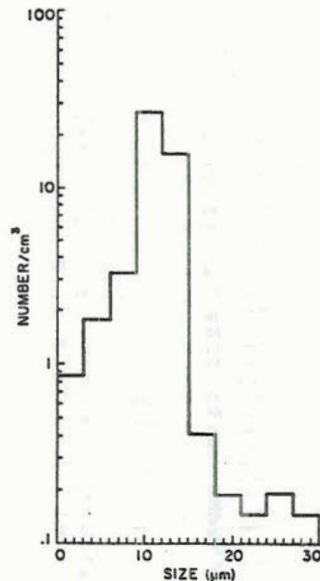
FSSP determined droplet spectra for 10 second samples in the cloud water zones are presented in Figure 25. Mean droplet diameters in zones near the ridge crest were near $15 \mu\text{m}$. The largest droplets observed by the FSSP were $28\text{--}30 \mu\text{m}$ but only in concentrations of $0.2/\text{cm}^3$. Measured droplet concentrations never exceeded $60/\text{cm}^3$ near the ridge crest. In the upwind zones, mean diameters were slightly smaller ($12 \mu\text{m}$). Concentrations varied substantially during this part of the flight with concentrations in the liquid water zones varying from $50/\text{cm}^3$ to $5/\text{cm}^3$ or less. These spectra were generally characteristic of an airmass with modified maritime characteristics. One possible reason for these characteristics was that the airmass was decoupled from the planetary boundary layer during its trajectory from central Utah over the underlying cold airmass. Parcel time within the precipitating system was sufficient to modify its aerosol characteristics by rainout, washout and nucleation processes.

4.32 Ice Crystal Structure and Crystal Size Spectra

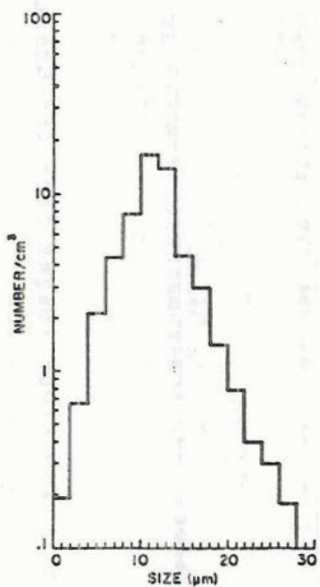
Selected 2-D images from the Queen Air and Lear flights are shown in Figures 26-28. Each row of images will be discussed in detail in the text. Accompanying crystal size spectra will be given in Figures 29-31. Because of the extensive referencing to these figures a shorthand notation will be used. For example, (Figure 26,Line 2; Figure 29,Spectra 3) will be abbreviated (F26,L2; F29,S3). All of the data in these figures can be cross referenced with Figures 16-23, the flight cross-sections



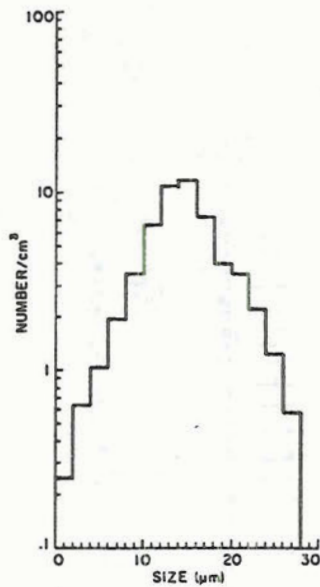
Time=222500 (figure 17,d)
 SV=163.7 cm³ ST=10 sec
 ND=9424 CD=57.6 cm⁻³



Time=234200 (figure 21,g)
 SV=168.2 cm³ ST=10 sec
 ND=8290 CD=49.3 cm⁻³



Time=222750 (figure 17,m)
 SV=153.6 cm³ ST=10 sec
 ND=8618 CD=56.1 cm⁻³



Time=224420 (figure 17,e)
 SV=171.5 cm³ ST=10 sec
 ND=9332 CD=54.4 cm⁻³

Figure 25. FSSP droplet spectra, November 24, 1979. The notation at the base of the diagrams include sample volume (SV), sample time (ST), number of droplets (ND), and concentration (CD).

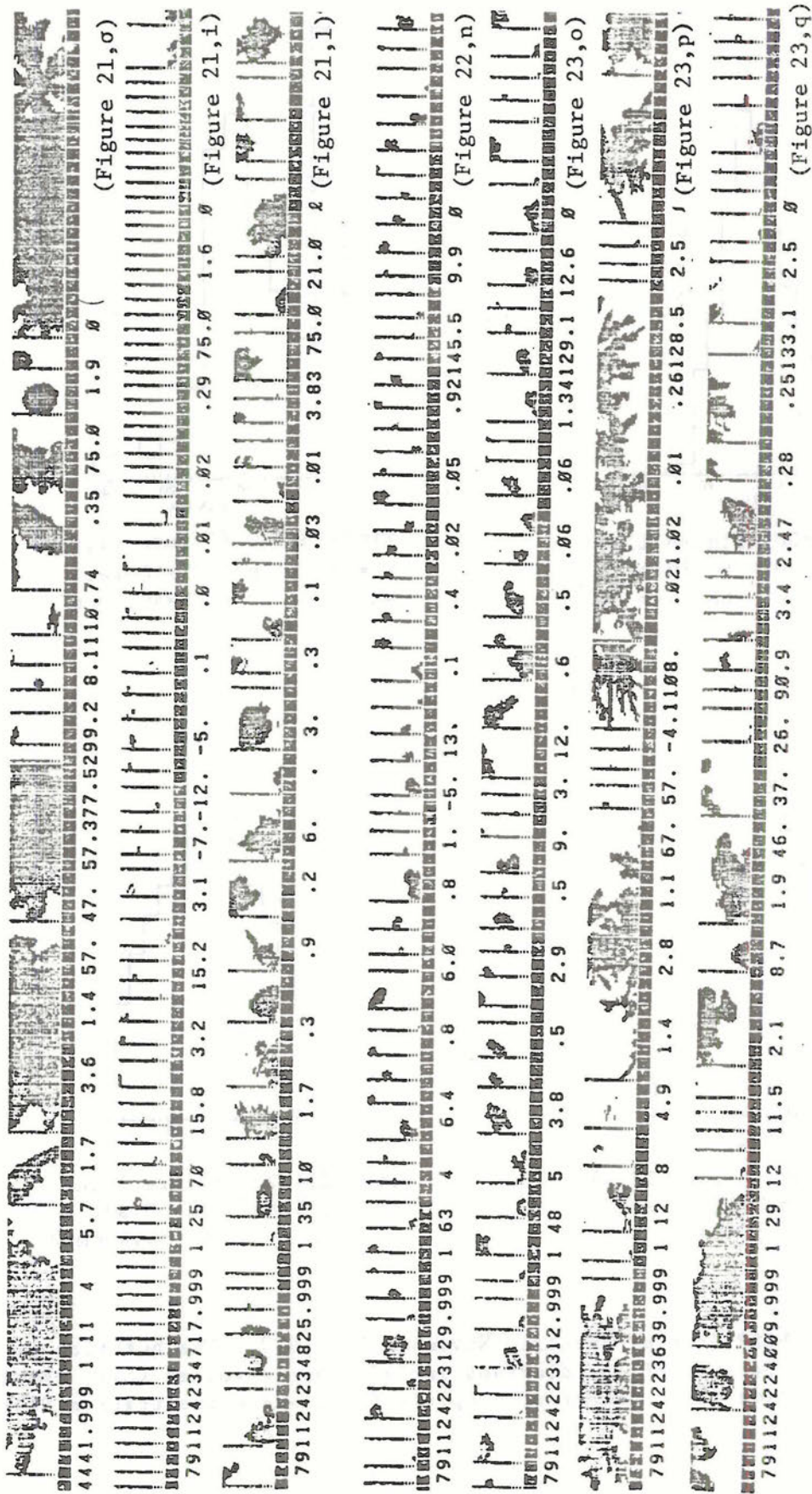


Figure 26.

2-D probe images from the Queen Air and Learjet flights. The reference at the bottom right of each image line refers to the precise location of the image on the flight cross-sections.

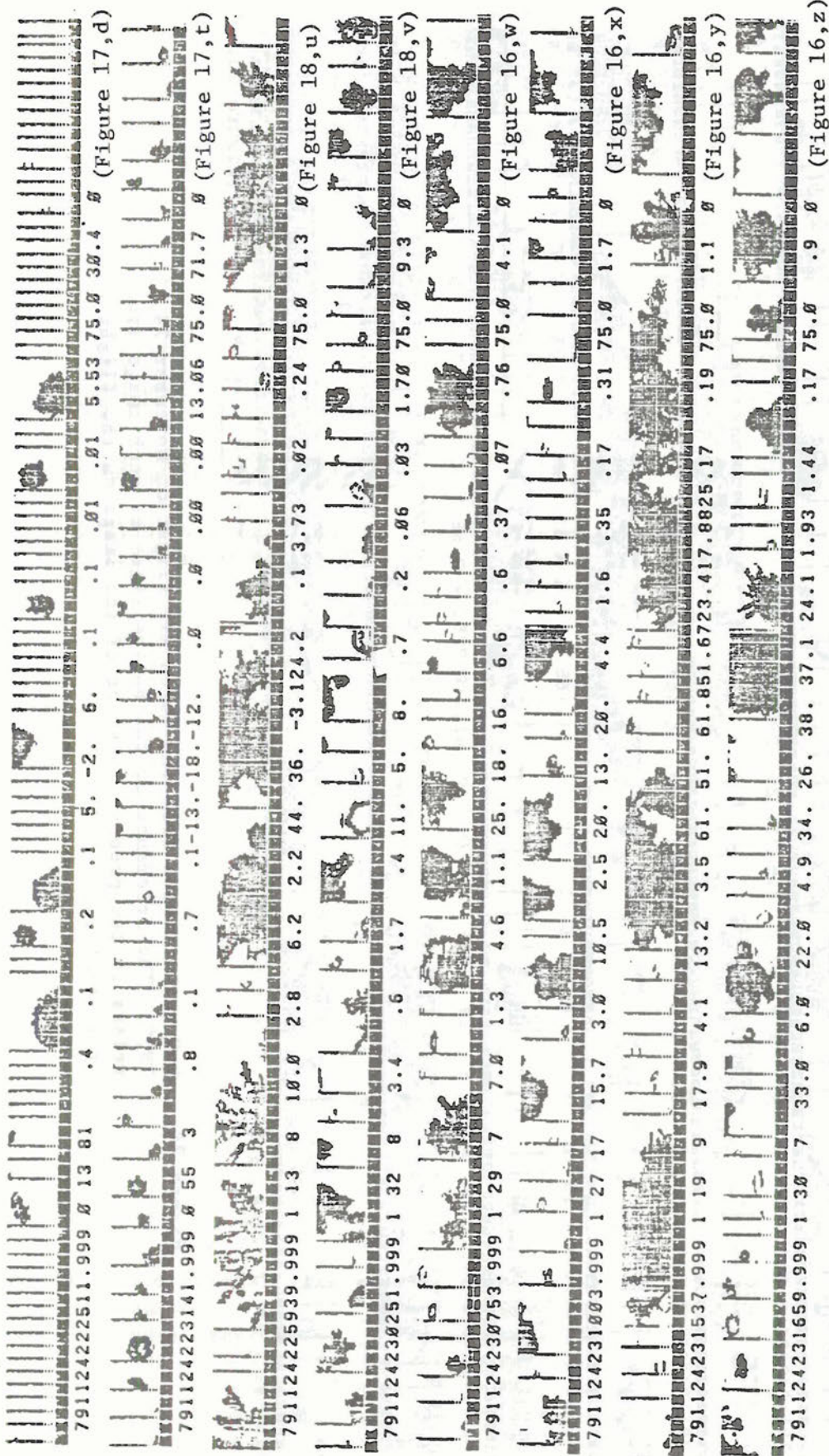


Figure 27. 2-D probe images from the Queen Air flight on November 24, 1979. The reference at the bottom right of each image line refers to the precise location of the image on the flight cross-sections.

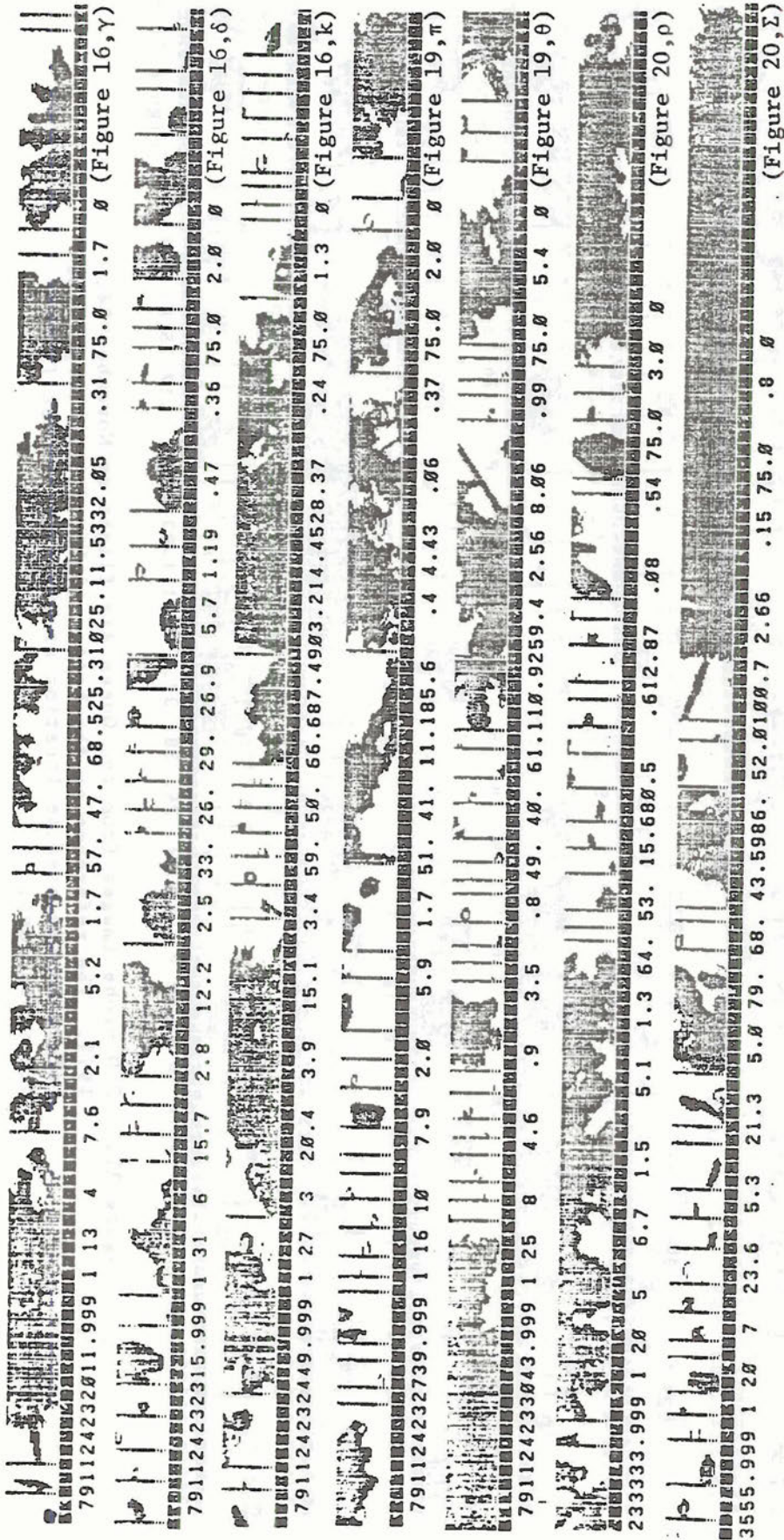
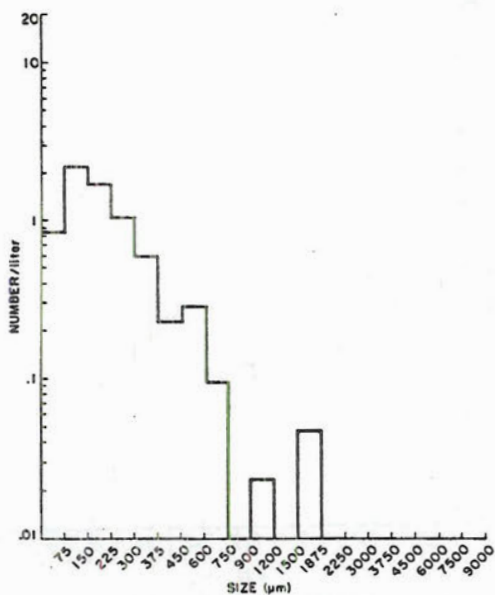
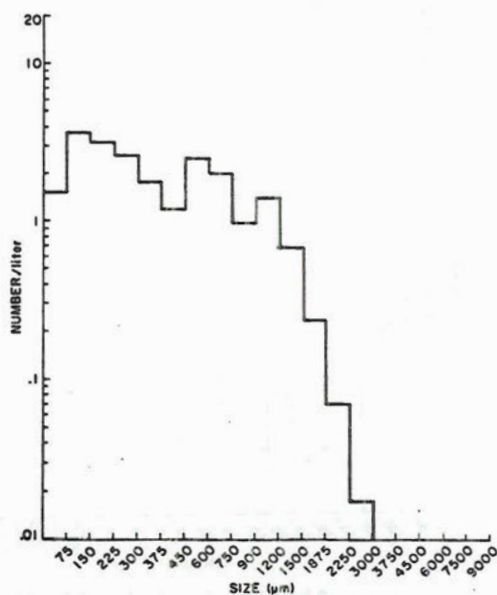


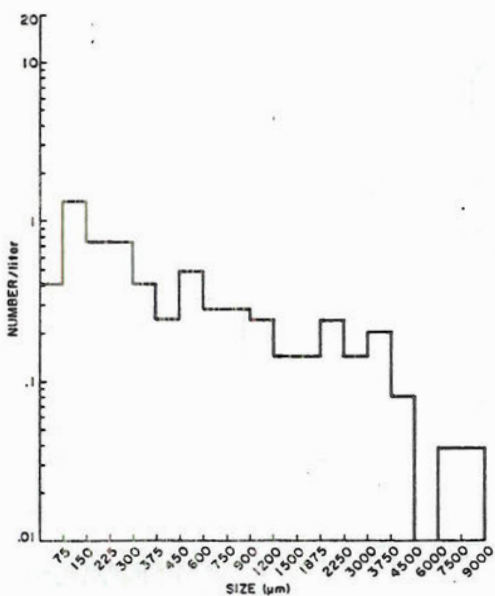
Figure 28. 2-D probe images from the Queen Air flight on November 24, 1979. The reference at the bottom right of each image line refers to the precise location of the image on the flight cross-sections.



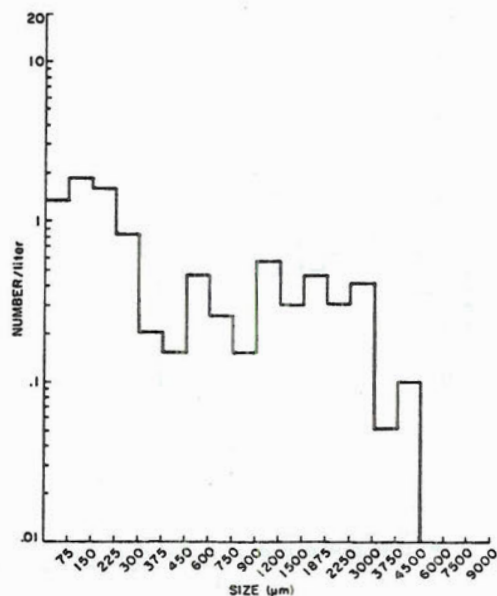
Time=223100-59 (Fig.23,n)
 SO=8.0 lit⁻¹ RA=7.0 lit⁻¹
 TS=294



Time=223400-59 (Fig.22,r)
 SO=29.7 lit⁻¹ RA=21.7 lit⁻¹
 TS=1215

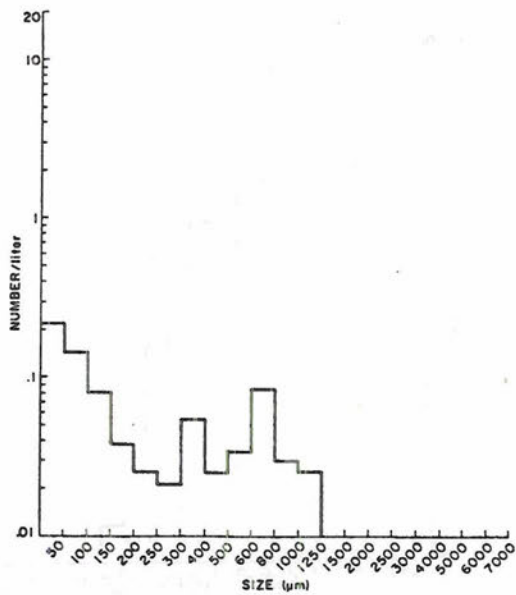


Time=223600-59 (Fig.22,p)
 SO=9.1 lit⁻¹ RA=6.2 lit⁻¹
 TS=150

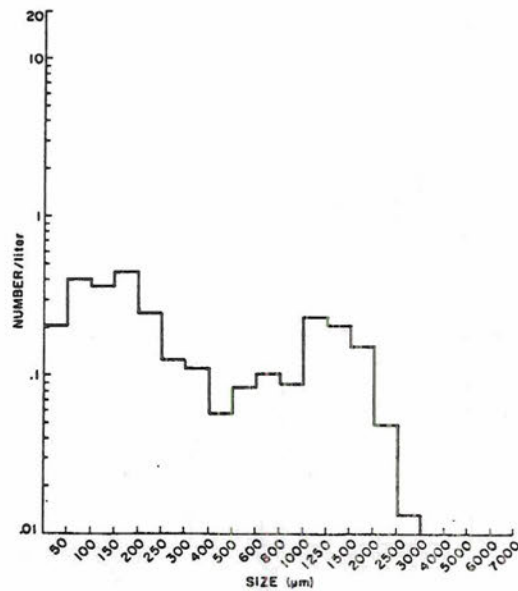


Time=223800-59 (Fig.22,s)
 SO=13.9 lit⁻¹ RA=8.1 lit⁻¹
 TS=157

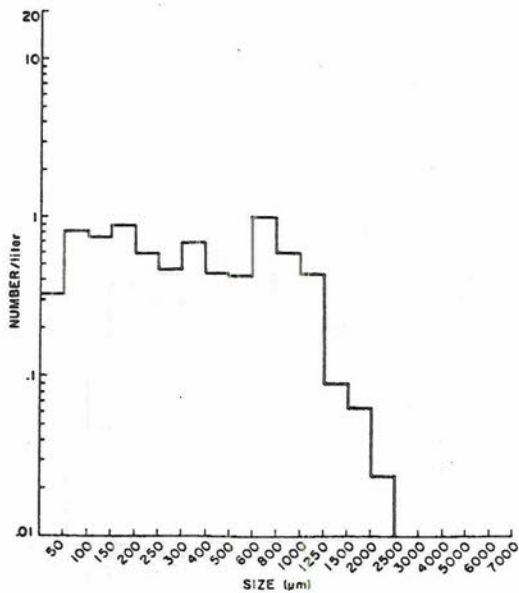
Figure 29. 2-D crystal size spectra taken during the November 24, 1979 Lear flight. Abbreviations refer to the concentrations determined by the shadow-or method (SO), the concentrations with the rejection criteria applied (RA), and the total number of crystals in the sample (TS). The figure reference under each spectra refers to the precise location of the image on the flight cross-sections.



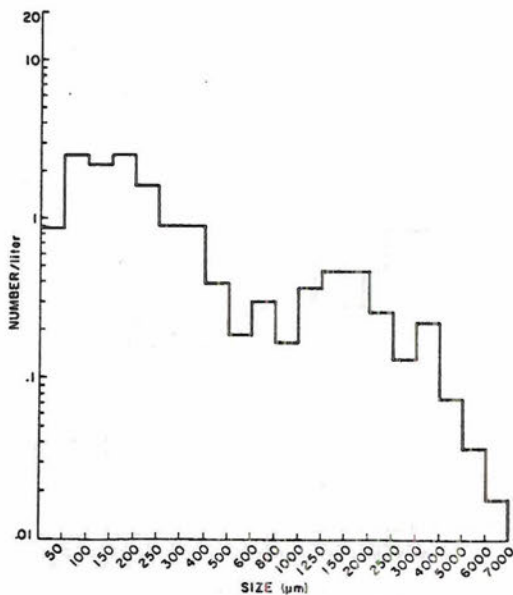
Time=222500-59 (Fig.17,d)
 SO=6.8 lit⁻¹ RA=0.8 lit⁻¹
 TS=186



Time=230100-59 (Fig.18,a)
 SO=3.7 lit⁻¹ RA=2.9 lit⁻¹
 TS=645

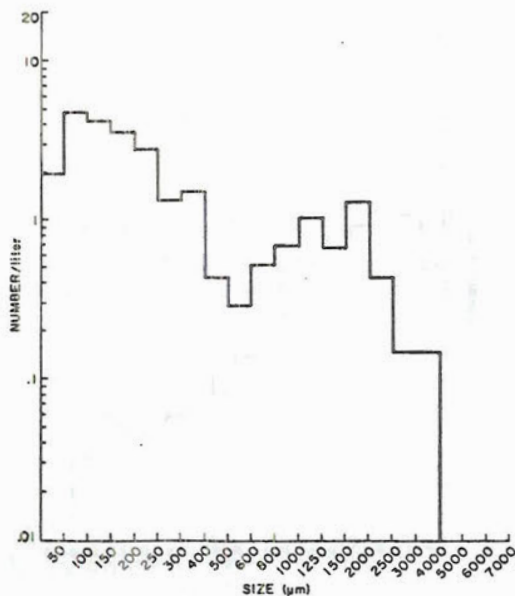


Time=230400-59 (Fig.18,β)
 SO=9.6 lit⁻¹ RA=7.5 lit⁻¹
 TS=917

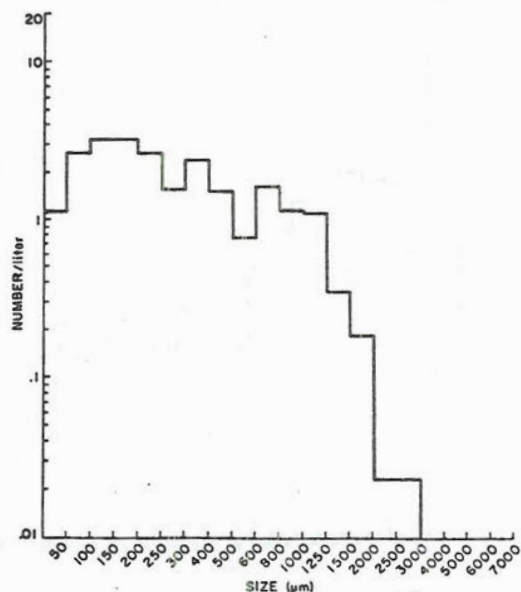


Time=231500-59 (Fig.16,y)
 SO=18.7 lit⁻¹ RA=14.6 lit⁻¹
 TS=773

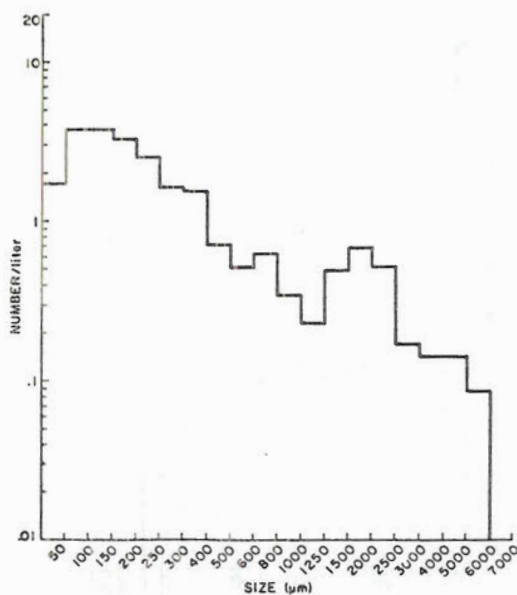
Figure 30. 2-D crystal size spectra taken during the November 24, 1979 Queen Air flight. Abbreviations refer to the concentrations determined by the shadow-or method (SO), the concentrations with the rejection criteria applied (RA), and the total number of crystals in the sample (TS). The figure reference under each spectra refers to the precise location of the image on the flight cross-sections.



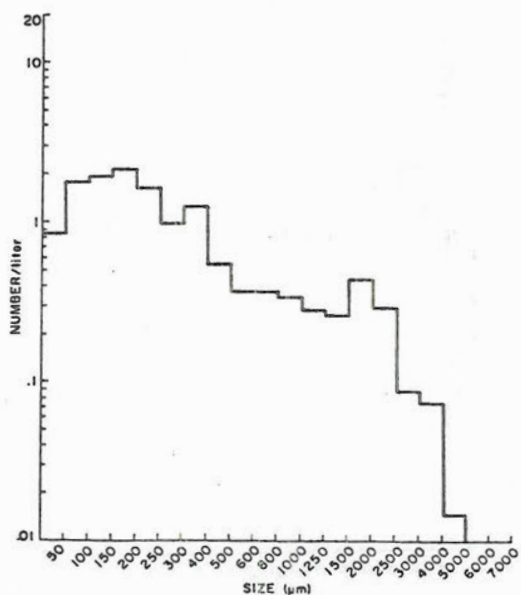
Time=231600-59 (Fig.16,j)
 SO=31.1 lit^{-1} RA=25.5 lit^{-1}
 TS=887



Time=231000-59 (Fig.16,x)
 SO=28.7 lit^{-1} RA=23.2 lit^{-1}
 TS=1010

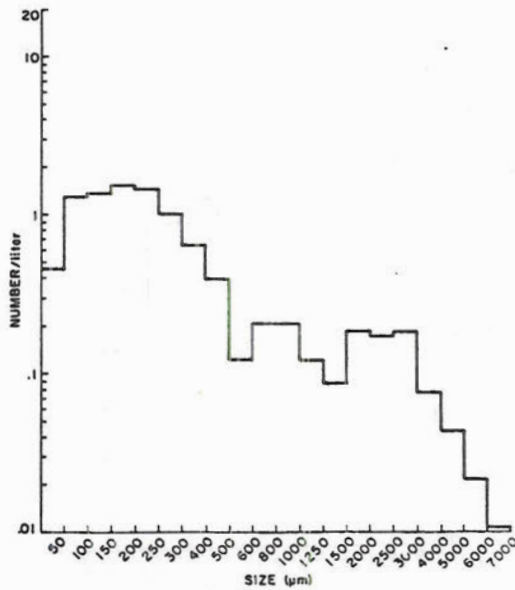


Time=232400-59 (Fig.16,k)
 SO=32.0 lit^{-1} RA=22.9 lit^{-1}
 TS=788

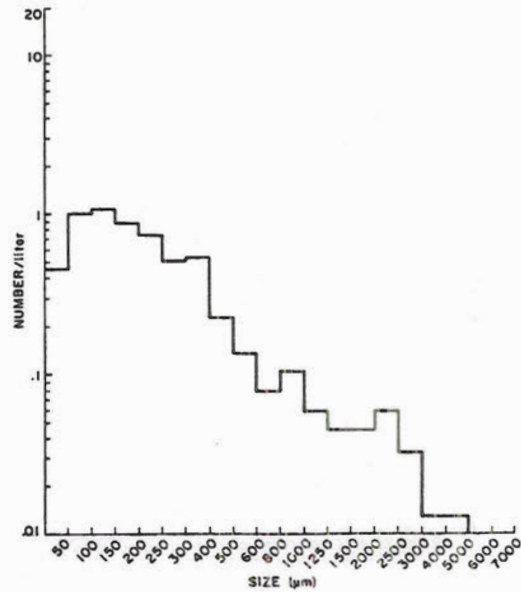


Time=232800-59 (Fig.19,μ)
 SO=18.2 lit^{-1} RA=13.7 lit^{-1}
 TS=920

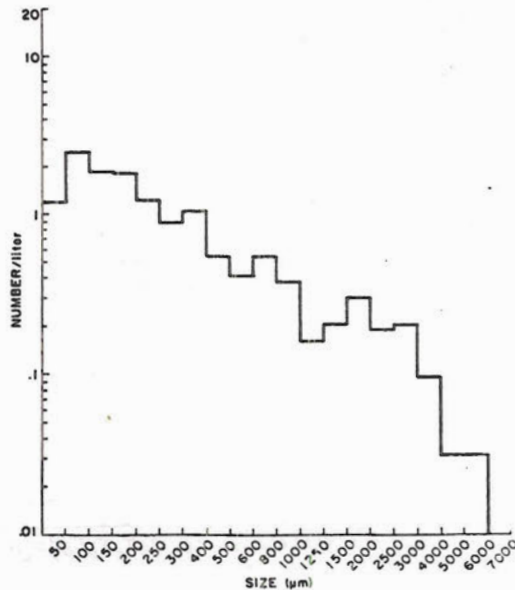
Figure 31. 2-D crystal size spectra taken during the November 24, 1979 Queen Air flight. Abbreviations refer to the concentrations determined by the shadow-or method (SO), the concentrations with the rejection criteria applied (RA), and the total number of crystals in the sample (TS). The figure reference under each spectra refers to the precise location of the image on the flight cross-sections.



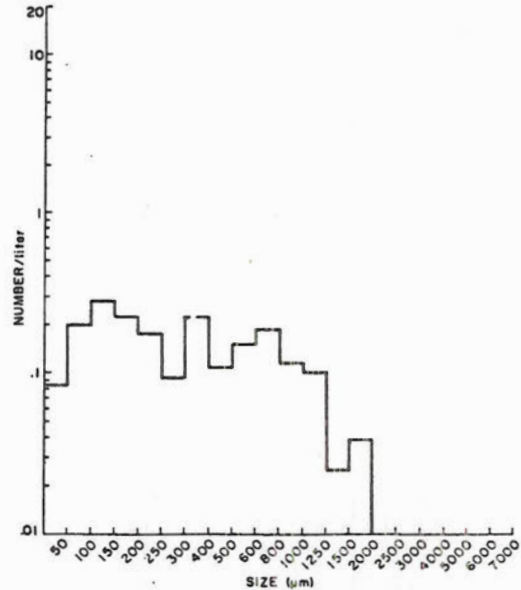
Time=233100-59 (Fig.19,θ)
 SO= 11.6 lit⁻¹ RA=9.5 lit⁻¹
 TS=860



Time=233800-59 (Fig.20,ω)
 SO=6.0 lit⁻¹ RA=6.0 lit⁻¹
 TS=916



Time=234600-59 (Fig.21,Δ)
 SO=17.7 lit⁻¹ RA=13.7 lit⁻¹
 TS=852



Time=234800-59 (Fig.21,1)
 SO=2.1 lit⁻¹ RA=2.0 lit⁻¹
 TS=474

Figure 32. 2-D crystal size spectra taken during the November 24, 1979 Queen Air flight. Abbreviations refer to the concentrations determined by the shadow-or method (SO), the concentrations with the rejection criteria applied (RA), and the total number of crystals in the sample (TS). The figure reference under each spectra refers to the precise location of the image on the flight cross-sections.

for exact location and comparison with other simultaneous state and microphysical data.

Lear Flight

Cloud top was penetrated by the Learjet at 43.5 KPa (-29°C). In this region of the cloud crystals were very small and in concentrations averaging 7.0/liter (F26,L4; F29,S1). By the time the aircraft had descended through the 50 KPa level, concentrations increased to approximately 20/liter. A few crystals had reached sizes greater than 2000 μm but most were small (F26,L5; F29,S2). At -15°C , a sharp transition in crystal habit and size occurred as the aircraft entered the dendritic growth zone. Images became larger and clear stellar structure was evident (F26,L6). Size spectra for this period indicate that some single crystals as large as 3000 μm existed (F29,S3). Images also indicate that some aggregation of dendrites occurred. A small number of particles at this level exceeded half millimeter size. Below the dendritic zone, images were smaller and habits harder to identify (F26,L7; F29,S4). Because dendrites do not appear in the data, the growth zone for larger dendritic crystals must not have extended far upwind or ambient vertical velocities were strong enough to suspend the crystals. If this were not true, dendritic crystals should have fallen into the path of the aircraft at lower altitudes and populated the lower zone.

Queen Air Flight

On the northbound leg of the Queen Air flight, the aircraft flew along the barrier crest and into the lee side evaporation zone. At the north end of the Range, it crossed the barrier crest again to the windward side of the ridge. Images during this period showed characteristically small crystals and a few large crystals with no edge

structure (F27,L1; F27,L2). The aircraft flew at 55 KPa (-17°C) during the leg and encountered areas of liquid water whenever it was windward of the crest. To the lee, both crystals and droplets were not observed indicating rapid evaporation in strong downslope motion. The trailing edge of the cloud (over the barrier crest) was characterized largely by few small crystals (F30,S1) and liquid water contents of the order $0.10\text{--}0.25\text{ g/m}^3$.

On the southbound leg, crystals during the early sampling were largely dendritic and showed little evidence of aggregation (F27,L3). No liquid water was observed during this period. The air temperature was -13°C during this time. The largest crystals observed were less than $4000\text{ }\mu\text{m}$ with concentrations between 3 and 10/liter (F30,S2). As the aircraft continued southbound, crystal habits changed to platelike structure (F27,L4) and temperature increased slightly (-12°C). Crystal concentrations increased slightly but the largest crystals observed were considerably smaller (F30,S3).

Very little change in crystal habit and size occurred over the westbound leg of the flight until the aircraft crossed the small upwind barrier. Many larger crystals appeared directly upwind of the ridge in a localized area which also was associated with higher liquid water contents (F27,L7; F30,S4). Apparently riming and/or enhanced aggregation of crystals was associated with this narrow zone of higher water contents. Crystals both upwind (F27,L6; F31,S1) and downwind (F27,L8; F31,S2) of the zone were consistently smaller.

The aircraft performed a descent and ascent sounding between 62 and 77 KPa over Hayden. Crystal images throughout the sounding exhibited the following characteristics. Two predominant crystal types

appeared: larger images which appear to be dendritic and numerous small images which appear to be hexagonal plates (F28). The larger images generally appear to be very small aggregates (F28,L1; F28,L2; F28,L4) except in regions where liquid water contents exceed 0.05 g/m^3 . In these regions of the cloud the aggregation process was significantly enhanced (F28,L7; F28,L3). Large aggregate images were observed occasionally outside of liquid water zones (F28,L6) but not in the significant numbers present in the zones. The image data indicates that the source region for the initiation of rapid aggregation of crystals is in regions of the cloud where some liquid water is present. These aggregated particles apparently attain fall velocities high enough to populate lower portions of the cloud, since they were observed occasionally throughout the lower segments of the sounding.

Crystal size spectra for the sounding (F31,S3; F31,S4; F32,S2), in addition to showing the smaller concentrations of large apparently aggregated crystals, also indicate the presence of a surprisingly large number of crystals with sizes smaller than $300 \mu\text{m}$. Many of these exhibit platelike structure. They consistently appear throughout the lower regions of the cloud at temperatures as warm as -8°C in concentrations exceeding 1/liter. Because of their small sizes, it is very unlikely that they have fallen a significant distance since formation. The concentrations of these crystals are orders of magnitude higher than that expected from theoretical ice nuclei concentrations, but generally agree with observations of ice crystal concentrations in natural clouds such as those by Cooper (1980) and others during previous studies of western orographic clouds.

There is no direct physical evidence for a known ice multiplication mechanism such as the Mossop-Hallet mechanism in this system. The large

number of crystals, particularly small crystals, at cloud temperatures between -8°C and -12°C indicates that either sufficiently large numbers of ice nuclei are present and active at warm cloud temperatures or multiplication mechanisms exist in the cloud which are not well understood. One possibility is that crystals are initiated by a contact nucleation process. If this were the case, collisions due to Brownian motion would require sufficient time that many nuclei would escape detection in current nuclei counters but would still be active in cloud systems.

The existence and possible mechanism for an ice multiplication process in these clouds is only speculative. Suggestions such as splintering of dendrites or seeding from higher cloud levels have been hypothesized for other cloud systems but are impossible to verify or deny from the available data. The question of the accuracy and limitations of current ice nuclei counters also confounds the problem of the large ice crystal concentrations observed in mountain cloud environments.

The last interesting evolution in the characteristics of the cloud crystal sizes and concentrations occurred as the aircraft crossed to the lee side of the small upwind ridge. In about a minute of flight crystal images changed from large aggregated crystals in concentrations between 10-15/liter (F26,L1; F32,S3) to very small images in concentrations of 2/liter (F26,L2; F32,S4). The transition occurred as the aircraft crossed the ridge crest. Downwind of the small ridge, larger single crystal images again appeared (F26, L3). Apparently even small topographic features can have substantial effects on cloud microphysical processes.

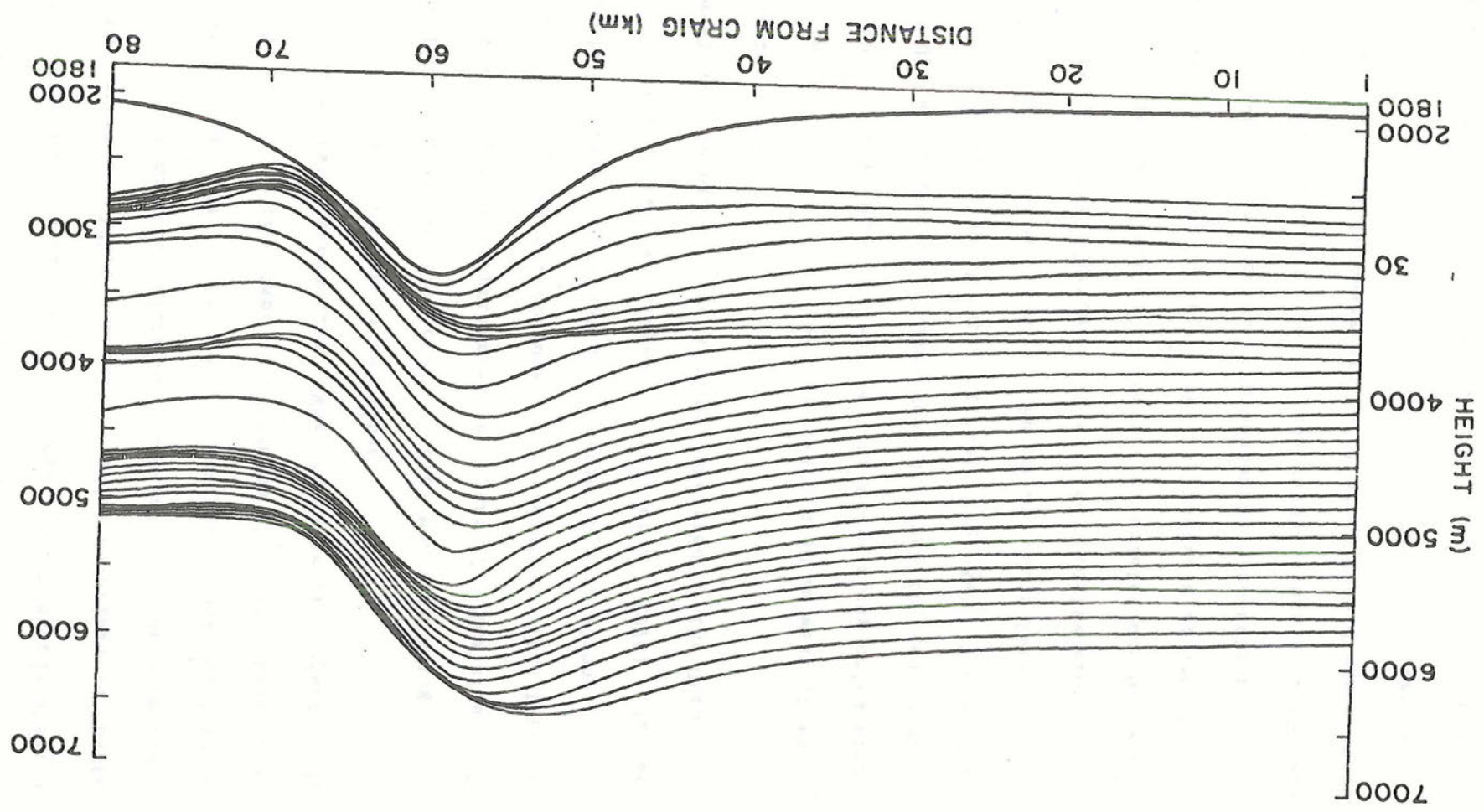
4.4 Condensate Production and Production Rates in the November 24 Cloud

Using input data based on aircraft soundings and rawinsonde observations taken on November 24, 1979, the airflow model described in Chapter 3 was used to determine maximum values of condensate available to precipitation processes and the location of the maximum production rates of condensate. The rates are important to determine the most likely location for cloud liquid water production. When the rate of production is maximized, cloud liquid water can be sustained.

A streamline analysis for flow over an ideal mountain using November 24, 1979 input data is presented in Figure 33. The effect of the inversion is to pack the streamlines above ridgetop. This type of inversion is often observed upstream of a barrier during strong downslope wind events on the lee slopes (Scheetz et al, 1976). In fact, a strong downslope component to the wind was observed by the Queen Air to the lee of the range.

The air parcels in the model were initialized 60 km west of the ridge with aircraft data and advected over the ridge along calculated streamlines. Maximum condensate values were observed to occur over ridgetop at the high point of the trajectories (Fig. 34). Two maxima occur on November 24 with a minimum just below inversion level. The minimum occurs because of a flattening of the trajectories along the inversion base. Maximum values of condensate calculated are 0.5 g/m^3 along the mountain crest and 0.7 g/m^3 over the mountain at 4800 meters (msl). Figure 35 shows the accompanying condensate production rates. A distinct vertical zone of maximum production rates occurs over the windward slope. When compared to observations of cloud liquid water by the Queen Air over the windward slopes, the observations agree very well with the predicted location and quantity of condensate based on rates

Figure 33. Model determined streamlines for the November 24, 1979 cloud system.



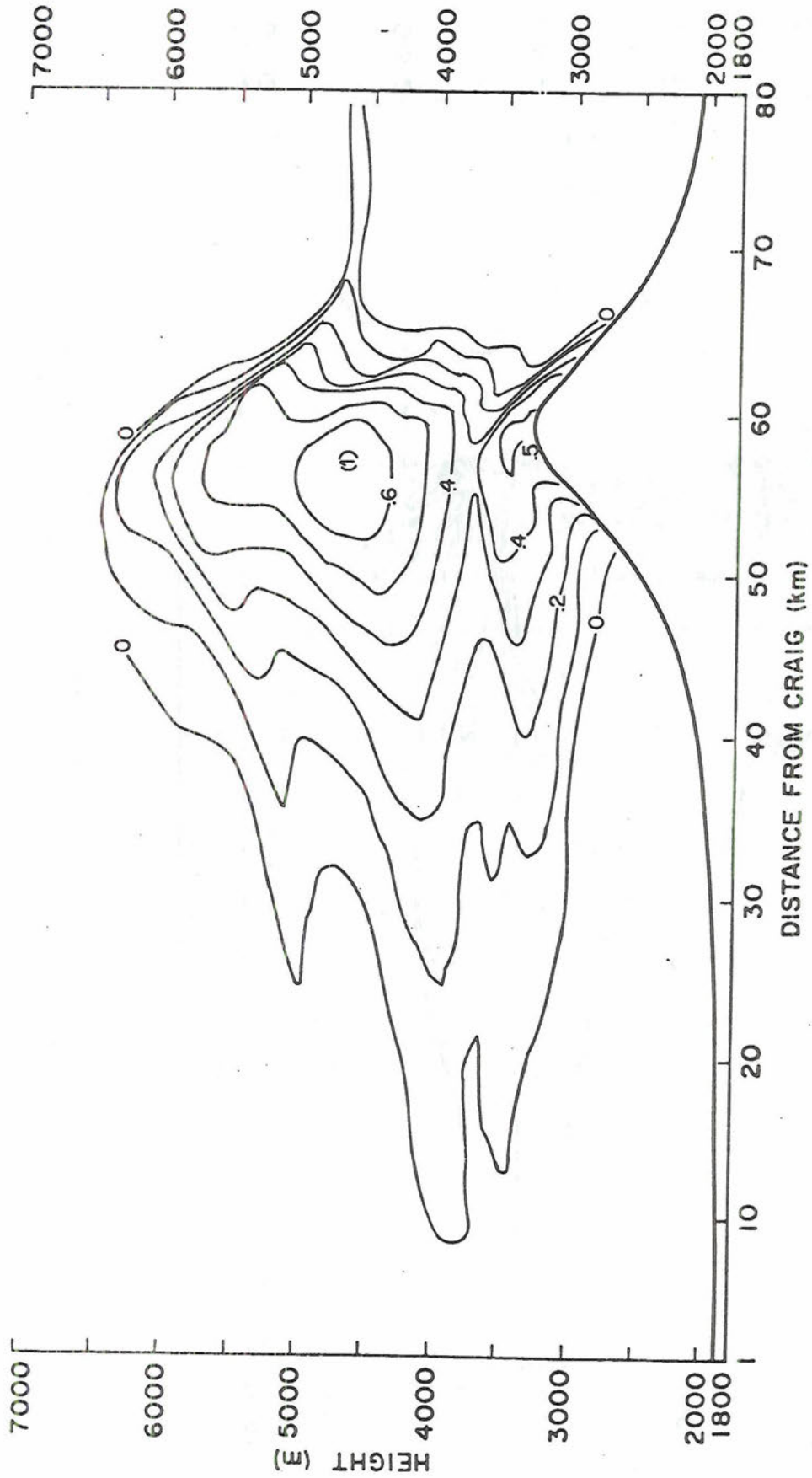


Figure 34. Steady-state potential condensate production in the -3 November 24, 1979 cloud system. Isopleths are in gm^{-3} .

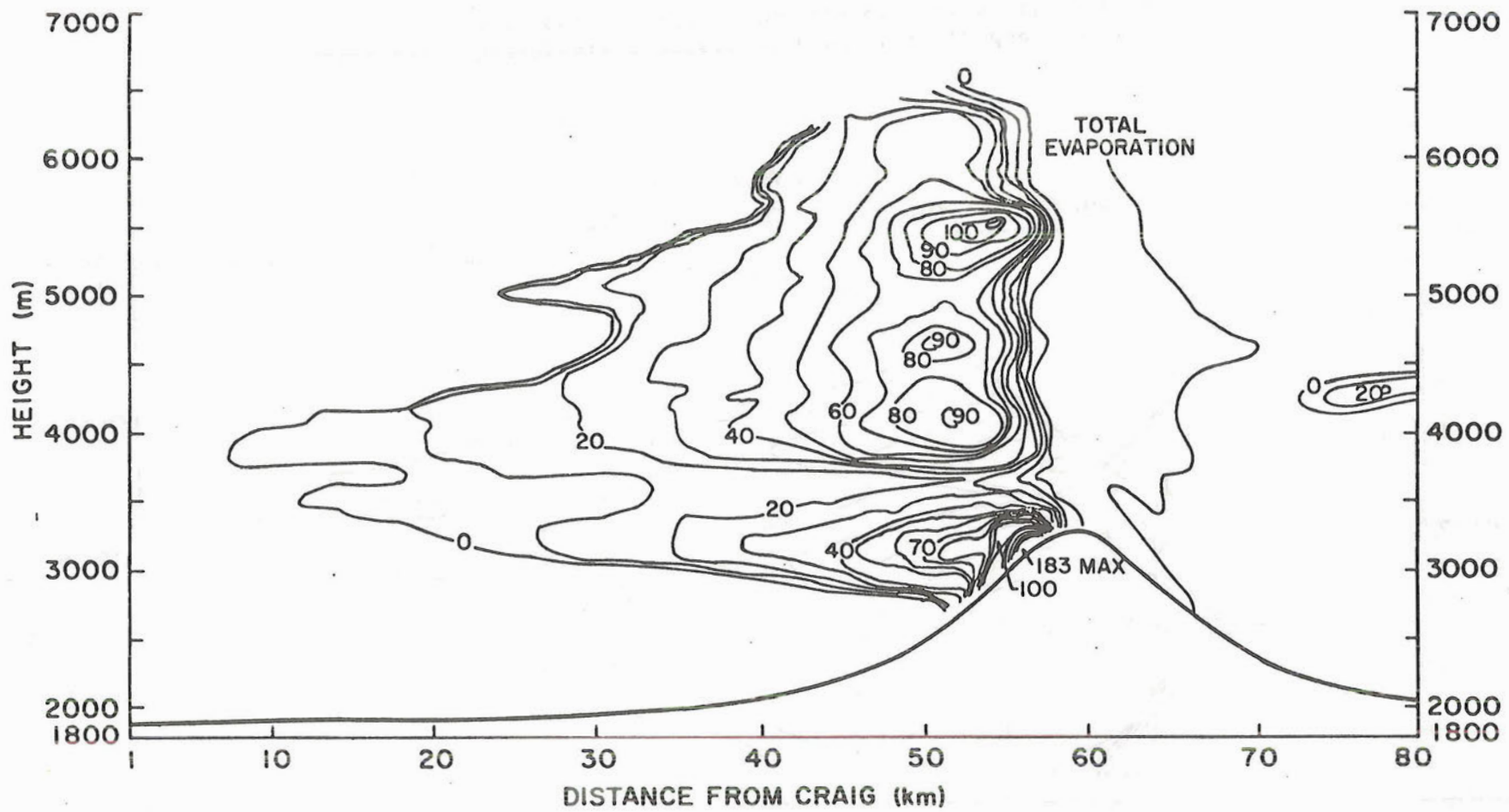


Figure 35. Potential condensate production rates in the November₃₋₂₄ 1979 cloud system. Isopleths are in units of 10^5 gm s^{-1} .

and total condensate available. The maximum liquid water content observed was 0.43 g/m^3 . Model predicted maximum potential condensate at approximately the same location on the grid was about 0.50 g/m^3 . Apparently in this narrow zone, most of the condensate produced was in the liquid state.

A second important point concerning model-derived production rates is the maximum occurring near the ridge. Observations at mountain locations have often recorded substantial amounts of surface rime associated with passage of liquid water over the barrier crest during storm periods (Hindman and Grant, 1981). Apparently the high liquid water contents associated with surface riming are due to the rapid condensation occurring in air moving directly up the surface slope. As indicated on the streamline analysis, the steepest slopes of the streamlines are very near the surface. For this reason, surface rime measurements can probably be used as a good indicator of the maximum liquid water contents which can be found in the cloud system under stable conditions.

4.5 Crystal Trajectories

Two approaches were taken to answer questions concerning the origin and path of crystals which fall to the barrier as precipitation. The first approach was to initialize crystals at a specific distance upwind and determine which crystals would have trajectories which intersect the barrier. The distance chosen was 45 km upwind of the main ridge crest. This distance corresponds to the location of cloud water zones associated with the smaller upwind ridge. It is a likely location for crystal nucleation due to high supersaturations with respect to ice. In addition, under artificial seeding conditions, this zone would likely be a source zone for additional crystals which may then interact with the

cloud water zone at the primary barrier. The second approach adopted was to assume that crystals of various sizes and habits were observed at the barrier crest, and to run the trajectory model in reverse to determine origin levels and upwind location of initial development.

Crystal trajectories were run under two supersaturation conditions, water saturation and slightly above ice saturation. These two limits represent physical limits in the cloud system and therefore represent the lowest and highest trajectories possible for the crystal. Actual crystal trajectories should be between these two limits, depending on the supply of moisture and the degree of competition for that moisture between crystals. Once crystals pass to the lee of the barrier, they enter the observed zone of rapid evaporation. In the model, the relative humidity is set at 50% and the crystal is allowed to evaporate.

Because a distinct zone of liquid water is evident in the data near the barrier crest, a simple riming parameterization was added to determine the effect of riming on crystal trajectories. The riming parameterization was accomplished using the following technique. When crystals reach the observed zone of liquid water, a smooth transfer from the fall velocity equations of unrimed to rimed crystals was effected over a specific time period. In one run, the time period was set at 30 seconds, corresponding to rapid riming. In the second case, the time period was extended to 300 seconds to simulate slow riming. Because riming of platelike and dendritic crystals is primarily along the c -axis, and the fall velocity equations are directly related to the a -axis, the effect of mass accumulation due to riming is still effectively accounted for in this simple parameterization.

Results:

Figure 36 shows several trajectories of crystals which remain in platelike temperature regimes throughout their path. Figure 37 shows trajectories of crystals which grow in dendritic regimes somewhere along their path. The most striking feature of these trajectories is that they are largely horizontal. The growth of the crystals and their accompanying increase in fall velocity in the model nearly counterbalances the increase in ambient air vertical velocity as the crystals approach the barrier. These results suggest that horizontal stratification of crystals according to habit and level of origin should have occurred in the November 24 cloud. For single crystals this appears to be the case. Dendritic crystals appeared in the 2-D data during the Lear sounding as the aircraft descended through -16 C, but seldom appeared below -13 C. The exception was aggregated dendrites. These attain higher fall velocities and can descend through the cloud. The same observations were generally true of Queen Air 2-D data.

Most crystals in plate regimes were able to impact on the barrier before complete evaporation even with near horizontal trajectories. The effect of riming was to lower trajectories about 150 meters by the time the crystals passed through the liquid water zone. Most single crystals originating within 45 km of the ridge crest and growing in the plate regime below -12 C reached the ground as precipitation. Because many of these crystals aggregate, with resultant increase in fall velocity, this region of the cloud is the most active in the formation of mountain precipitation. Crystal replicas taken on November 24 confirm that many of the precipitation particles were indeed aggregates of plates. In the case of crystals in the higher dendritic growth zone, the opposite is

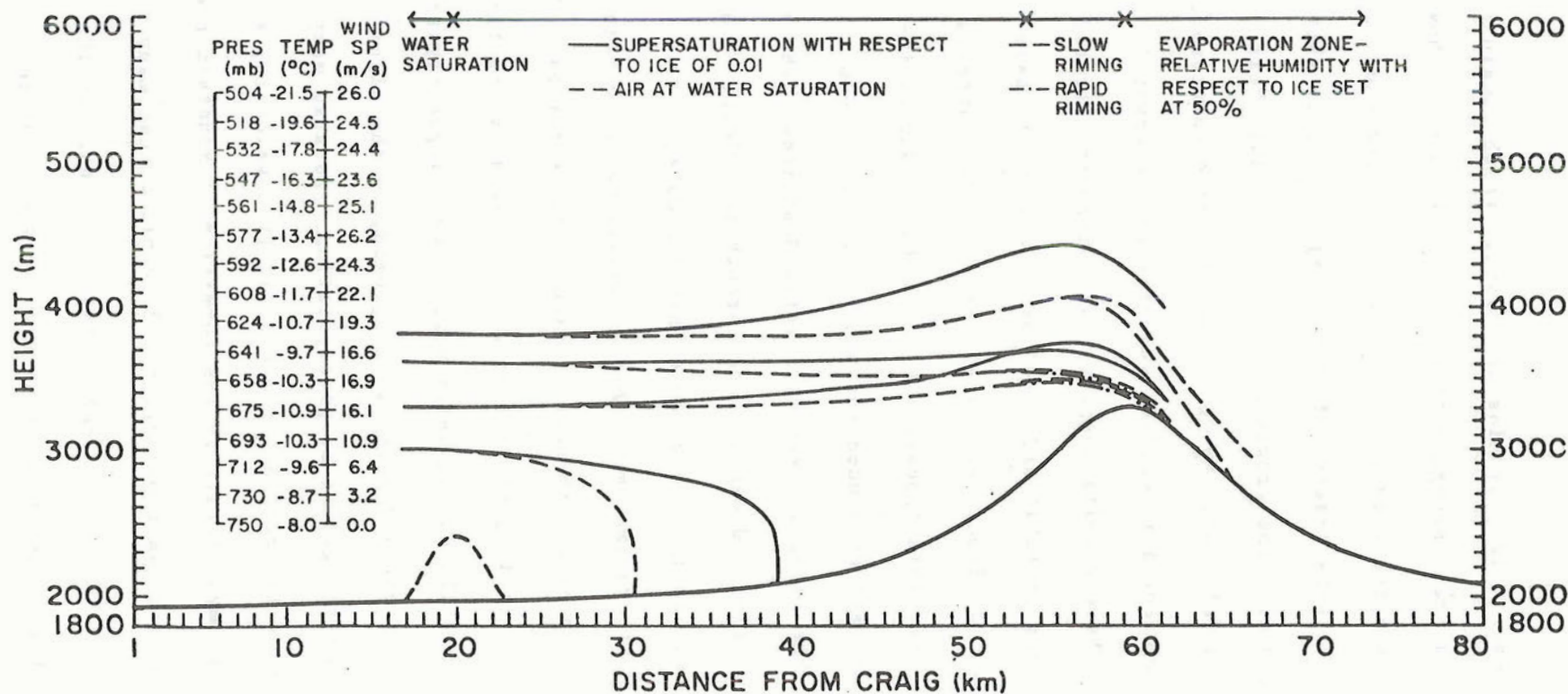


Figure 36. Trajectories of platelike crystals originating in the liquid water zone generated by the upwind ridgeline east of Hayden. The ridge is located 20 km east of Craig. Dashed lines indicate crystals growing at water saturation. Solid lines indicate crystals growing at conditions slightly above ice saturation. Heavy dashed lines indicate trajectories of crystals with the slow riming parameterization applied and dash-dot lines indicate trajectories with the parameterization applied rapidly.

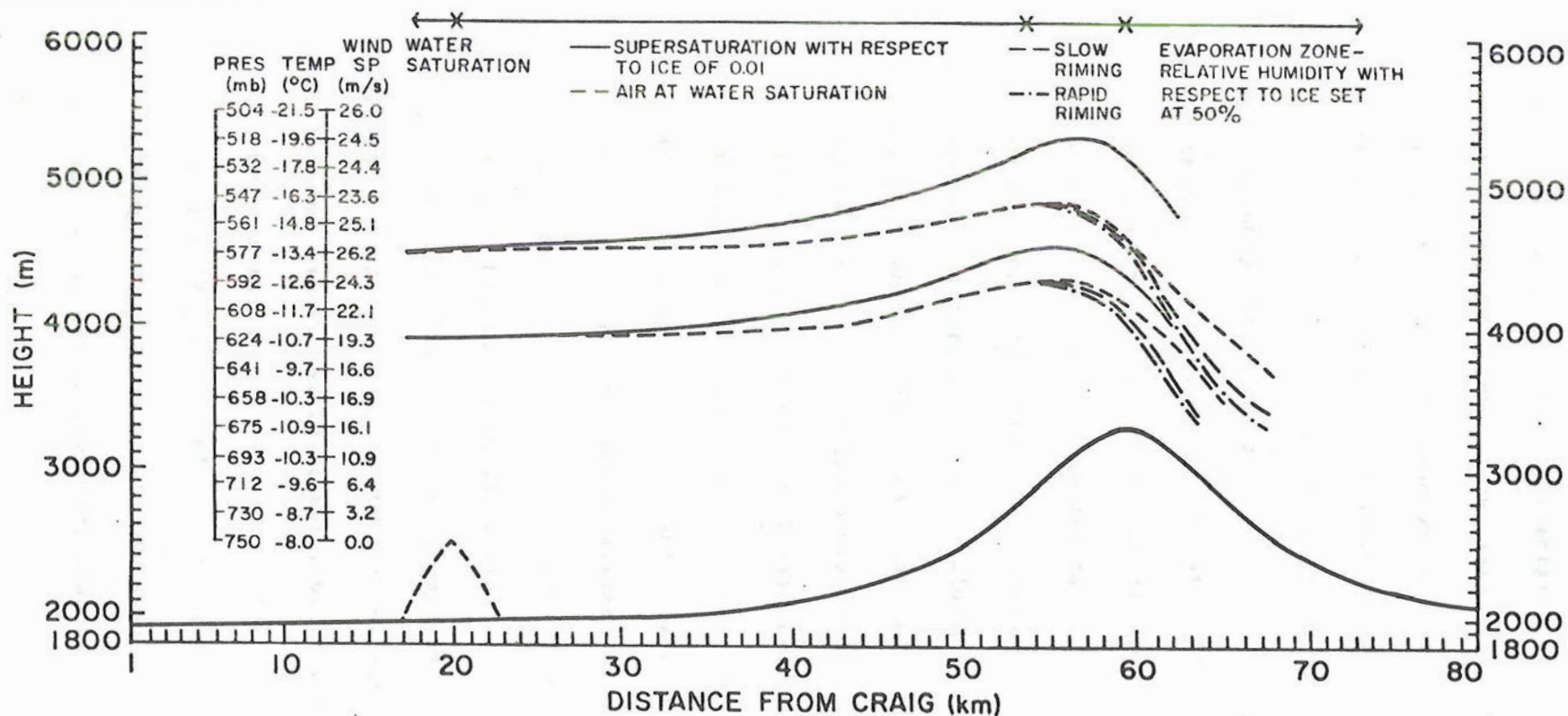


Figure 37. Trajectories of crystals which develop dendritic characteristics and originate in the liquid water zone generated by the upwind ridgeline east of Hayden. The ridge is located 20 km east of Craig. Dashed lines indicate crystals growing at water saturation. Solid lines indicate crystals growing at conditions slightly above ice saturation. Heavy dashed lines indicate trajectories of crystals with the slow riming parameterization applied and dash-dot lines indicate trajectories with the parameterization applied rapidly.

true. None of the dendrites originating within 45 km of the ridge should have impacted on the barrier, even under riming conditions. One major reason is that dendrite fall velocities are nearly independent of size. Although the crystals get quite large, they remain suspended unless they get involved in the aggregation process.

In figure 38, the assumption was made that small (2000 μm) and large (6000 μm) non-rimed dendrites are observed at the mountain crest. Crystal trajectories are then run backwards under four conditions, water saturation, slightly above ice saturation, and the same again but with the ambient air vertical velocity set at zero. The upper trajectories on the figure represent the absolute highest trajectories possible while the lower trajectories are more representative of actual trajectories. The results indicate that if the cloud exists in a water saturated state, dendritic crystals would not impact on the barrier in this type of flow regime unless their origin levels occurred far in excess of 60 km upstream. The same is true in ice saturation conditions. The most important implication of the results is that in this type of storm, there is little interaction between cloud upper levels and the precipitation process at the barrier, unless the clouds extend well over a hundred kilometers upwind of the range. Figure 39 shows the same type of analysis for a 3000 μm plate and a 1000 μm plate. These trajectories are steeper because the fall velocities of plates exceed those of dendrites. Even in this case, none of the crystals approach cloud upper levels within 60 km of the ridge crest. In fact the 3000 μm plate trajectories are contradictory since they begin in dendritic growth regions. These crystals would have shallower trajectories since they would grow as dendrites.

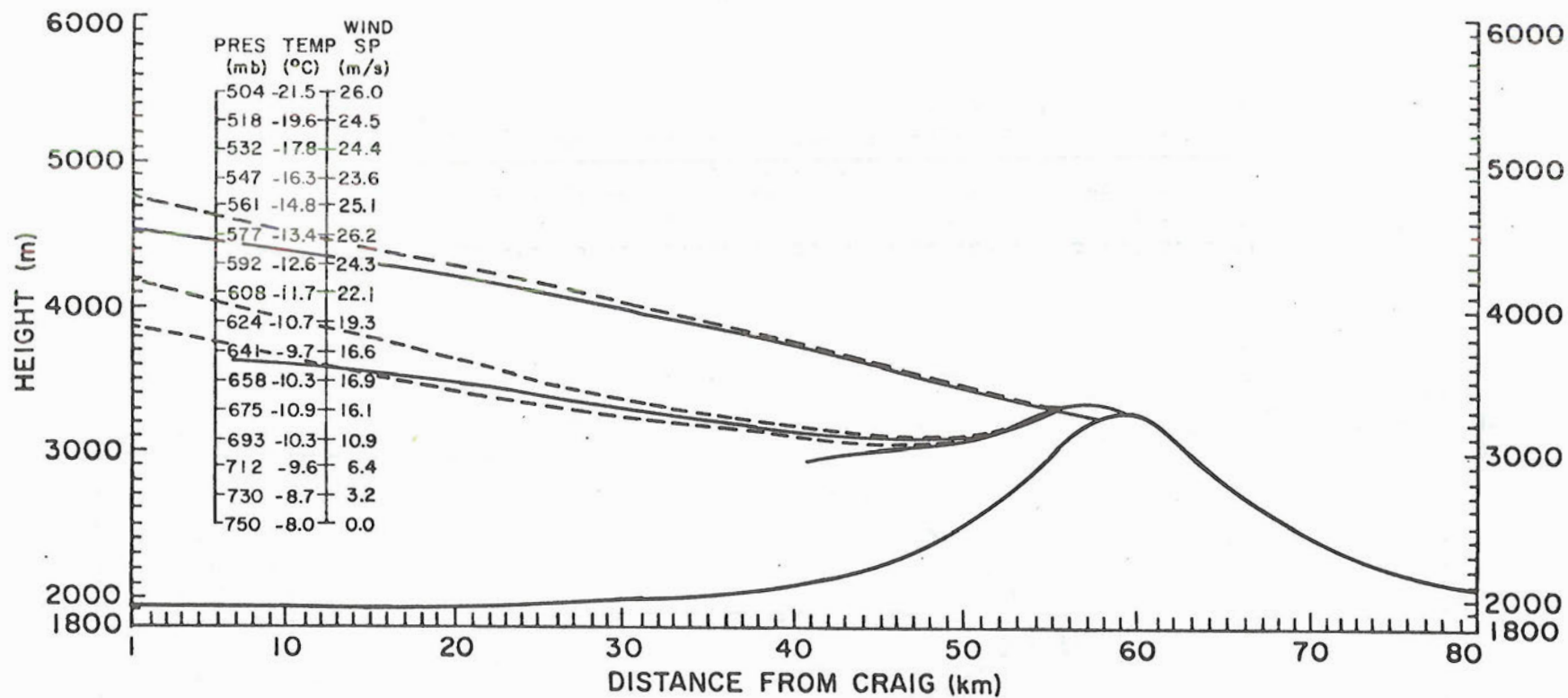


Figure 38. Trajectories of crystals which would impact on the barrier as small (2000 microns) and large (6000 microns) dendrites. The dashed lines indicate crystals growing under water saturation conditions, the solid lines indicate crystals growing under conditions slightly above ice saturation. The uppermost trajectories were calculated by assuming that the ambient air vertical velocity over the entire grid was zero.

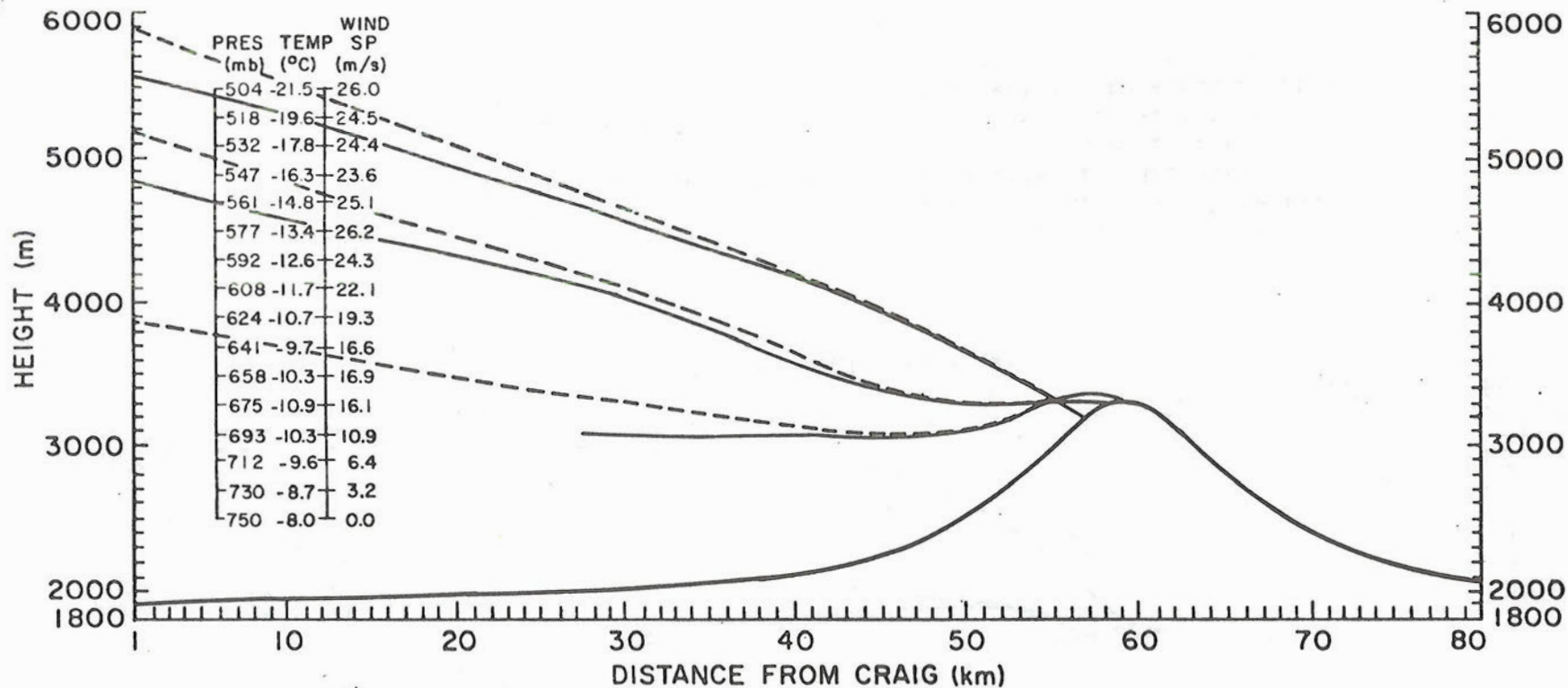


Figure 39. Trajectories of crystals which would impact on the barrier as small (1000 microns) and large (3000 microns) plates. The dashed lines indicate crystals growing under water saturation conditions, the solid lines indicate crystals growing under conditions slightly above ice saturation. The uppermost trajectories were calculated by assuming that the ambient air vertical velocity over the entire grid was zero.

4.6 Summary of November 24 Case Study

On November 24 1979, warm, moist stable overrunning of air was taking place over the top of a shallow cold air mass which had settled into the Northwest Colorado region during a previous cold air intrusion. The analysis indicates that the overrunning occurred for an extended period of time. The cloud physics aircraft observations show distinct and well-defined patterns of increased liquid water contents as well as significant crystal riming and aggregation associated with wave motion along the airmass boundary generated by the primary barrier (Park Range) and a smaller secondary barrier (Mt. Harris) located approximately 40 km upwind. Substantial liquid water contents of $0.3-0.4 \text{ g/m}^3$ were observed over the west slope of the Park Range barrier. Over one 75 km leg which paralleled the barrier crest, liquid water contents just windward of the crest ranged generally between 0.1 to 0.2 g/m^3 , while to the lee of the barrier strong downslope motion caused immediate evaporation of the cloud water and crystals.

Windward of the barrier over the valley, liquid water contents were consistently lower ($0.00-0.05 \text{ g/m}^3$), but did show increases ($0.05-0.10 \text{ g/m}^3$) in regions of upward motion in the overrunning warm air mass associated with wave motion generated by the smaller upwind topography. Although small, these increases clearly were associated with the development of large precipitation sized particles (3-10 mm) through the riming and aggregation processes and were very important in the total precipitation process in this cloud.

Theoretical calculations of condensate production rates indicate that almost all of the liquid water produced in the cloud will occur in a narrow zone corresponding in size to the half width of the mountain

over the western slope of the barrier. The maximum production is near the surface. This model predicted zone of liquid water corresponded very well in location and quantity with in-situ Queen Air observations. Comparison of predicted total condensate with observed liquid water contents indicates that the minimum efficiency with which potential condensate is converted to the ice phase was 14%. Outside of the narrow liquid water zone, the efficiency of conversion approached 100%.

Calculated crystal trajectories indicate that horizontal stratification of single crystals according to habit and level of origin occurred in this cloud. Both Queen Air and Lear data support this, with the exception of aggregated crystals. These were able to attain significant fall velocities and were observed in other lower regions of the cloud. The analysis indicates that, with the exception of aggregates, the only crystals originating within 45 km of the ridge crest which were able to be utilized in the precipitation process were those originating below the -12°C level. Dendrites were unable to reach the surface despite their larger sizes. From the trajectory analysis, it is evident that under conditions similar to November 24, unless the cloud system extends well beyond 100 km upwind, there is little interaction between clouds and precipitation at the ground.

CHAPTER V NOVEMBER 26, 1979 CASE STUDY

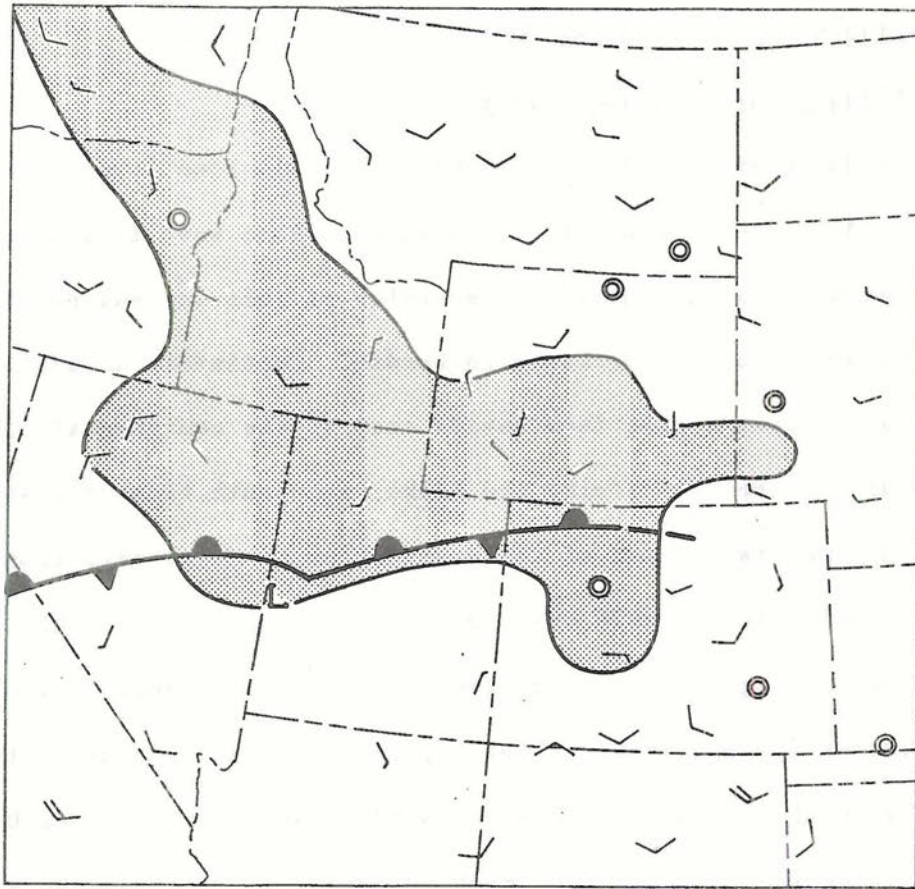
5.1 Major Synoptic Features

Conditions Prior to Mesoanalysis

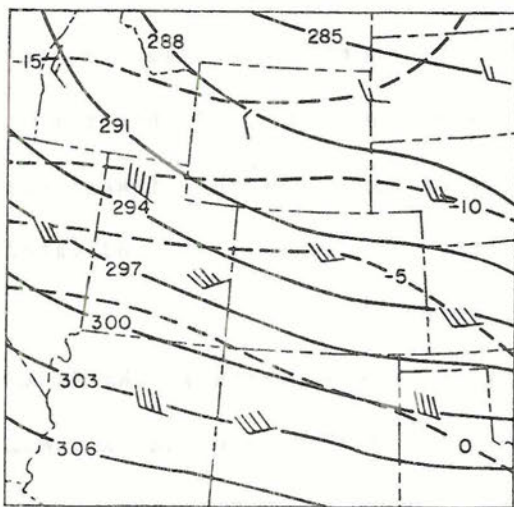
On November 26, 1979, a strong baroclinic zone located over northern Nevada and Utah was associated with a short wave trough and surface low pressure system. At 12Z, the center of this low was positioned east of Ely, Nevada on the Nevada-Utah border. Continuous snowfall was reported in a wide area from Nevada east to the continental divide, northward to central Wyoming and Idaho, and south to northcentral Colorado and Utah. East of the surface low, a stationary front extended across Utah into the COSE experimental area just north of Craig and Steamboat Springs, and then eastward to the Front Range. Figure 40 illustrates the positions of the important surface features at 12Z.

At 70 KPa, cold advection was evident north and west of Utah but a significant ageostrophic component to the flow over Colorado modified the advective pattern. Grand Junction, Colorado winds indicate that slight warm advection might be occurring. The major portion of this zone was north of the surface front. In the core of this zone of baroclinicity, windspeeds exceeded 20 m/s (see Figure 40). Within the baroclinic zone north of the front, between 85-50 KPa the airmass was very moist. Dewpoint depressions at three mandatory levels indicated for Lander and Salt Lake City never exceeded 1°C.

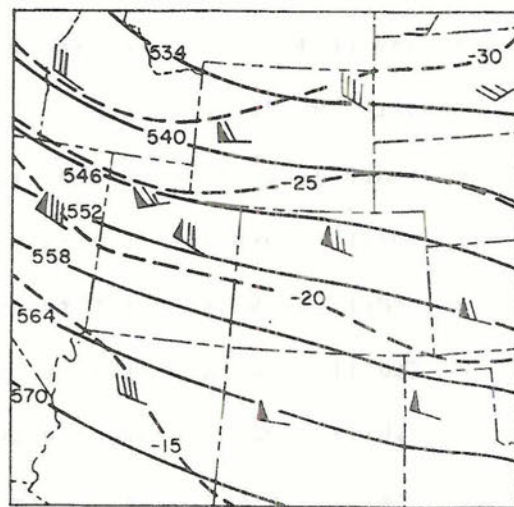
The intense baroclinic zone maintained its strength at the 50 KPa level where core windspeeds reached 45 m/s. Northward of the maximum wind core, cold air advection was evident, although not as strong as at 70 KPa (Figure 40).



Surface



70 KPa



50 KPa

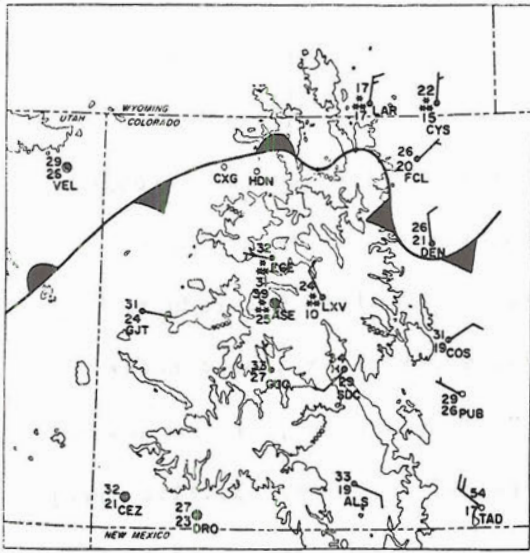
Figure 40. Major synoptic features at 12Z on November 26, 1979. Heights are in decameters, temperatures in $^{\circ}\text{C}$.

Evolution of the Surface Front

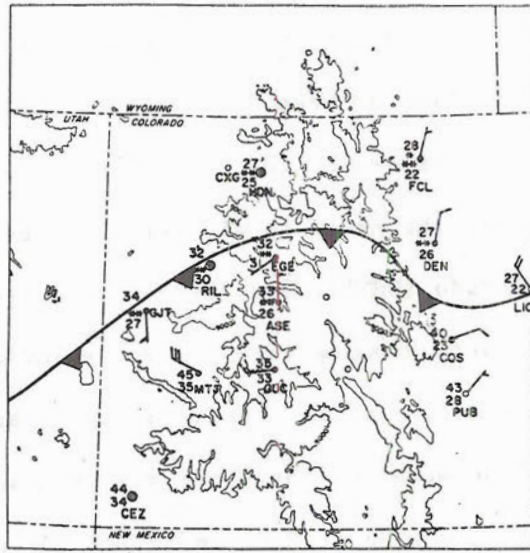
At 16Z (Figure 41) the surface front remained stationary along a SW-NE line between Hanksville, Utah (HVE) and Craig, Colorado (CXG), then eastward to the Front Range. The presence of a lee side trough caused the front to dip south on the Great Plains as far as Denver, Colorado (DEN). Reports over a large area of northern Colorado and southern Wyoming were generally indicating moderate, but continuous snowfall. In the immediate experimental area all precipitation gauges on the mountain above the valley base reported heavy precipitation ranging from 0.23 to 0.08 cm/hr. Winds at mid-ridge were estimated at 6 m/s. The highest values of precipitation occurred between 16-18Z on the mountain summit, corresponding to the time at and immediately after frontal passage.

The cold front continued to move southward at 18Z (Figure 41). Heavy snowfall continued throughout the hour on the summit of the Park Range with values of precipitation varying from 0.18 to 0.36 cm/hr at various locations across the barrier. Light snow continued to fall at Hayden.

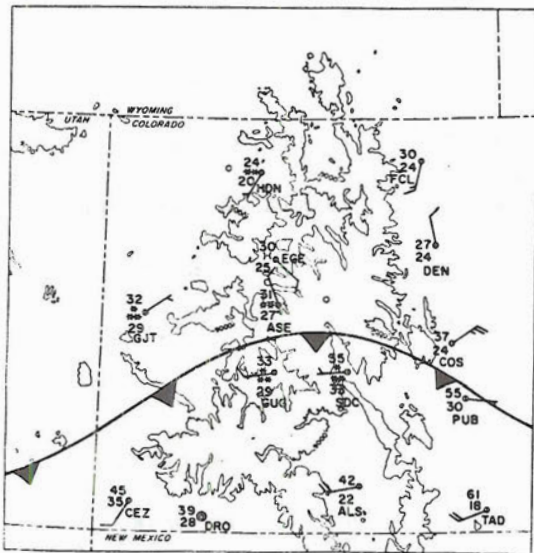
At 19Z, the Queen Air and Lear Flights were launched from Front Range airports. The Lear arrived at 1927Z and remained in the area until 2017Z. Due to the strong westerly winds at mid-levels the Queen Air arrived at 2030Z and remained in the experimental area for one hour. The mesoanalysis of the Park Range cloud in the following section is a composite of data taken during this period. Aircraft soundings taken over Hayden during this period are shown in Figure 42. At 19Z, the front had pushed south of Eagle and Grand Junction, Colorado with snow reported increasing in these communities. In the experimental area,



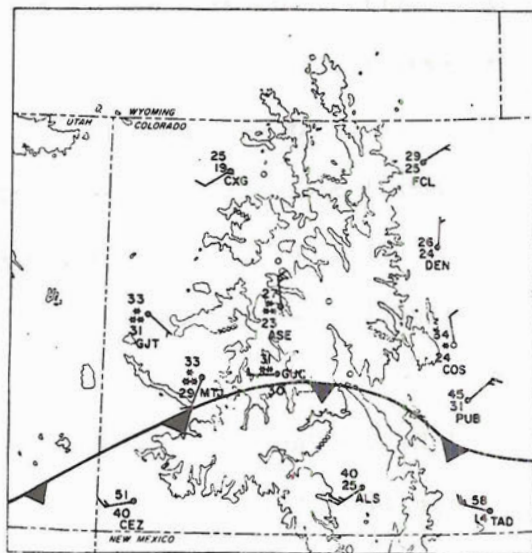
16Z



18Z

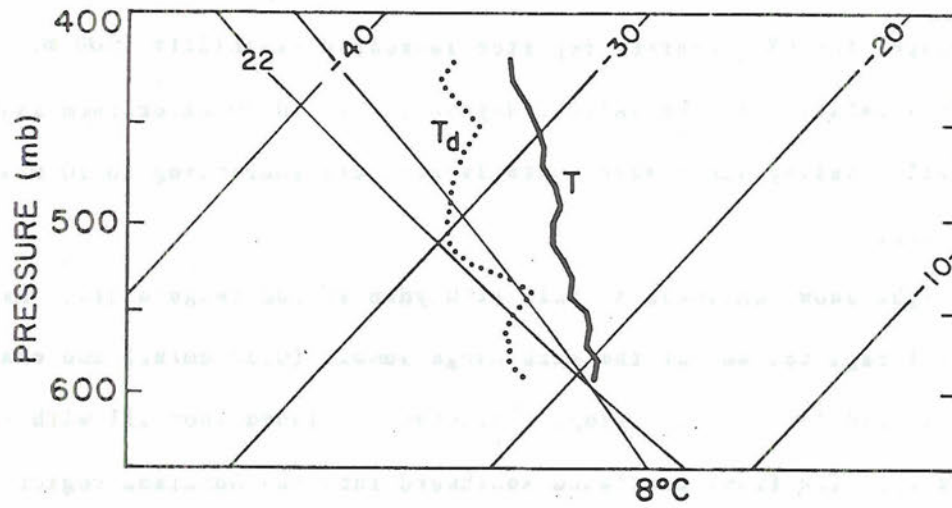


20Z

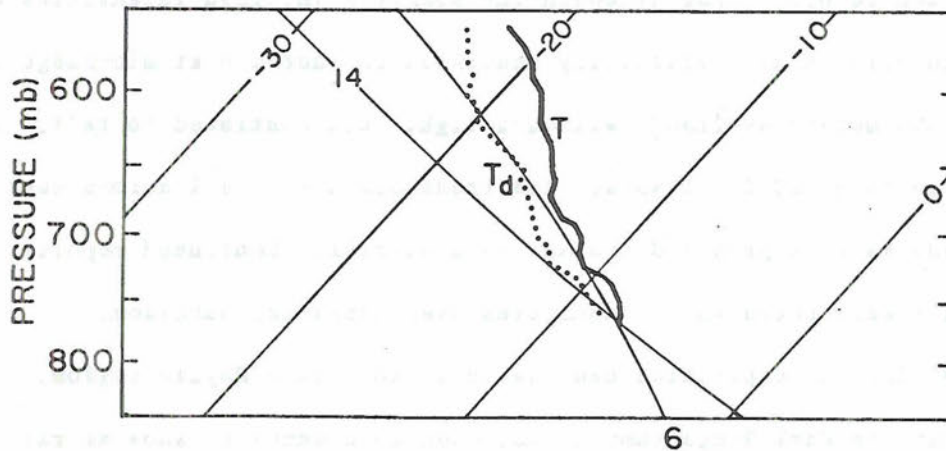


22Z

Figure 41. Evolution of the surface front during the November 26, 1979 storm.



Lear Sounding (1930-1935 Z)



Queen Air Sounding (2106-2122 Z)

Figure 42. Aircraft soundings taken during the November 26, 1979 storm over Hayden, Colorado.

snowfall continued to be heavy on the barrier (0.10-0.30 cm/hr). At mid-ridge, the CSU observer reported increased visibility (100 m), but steady snowfall. In the valley, Hayden continued to experience light snowfall. Valley winds were westerly at 3 m/s increasing to 10 m/s at ridge top.

Light snow continued to fall at Hayden at 20Z (Figure 41). Maximum snowfall reported was at the Park Range summit (0.36 cm/hr) and observations at mid-level on the ridge indicated continued snowfall with less intensity. The front continued southward into the Gunnison region of central Colorado. Moderate continuous snowfall was reported at all stations in the vicinity of the front and south to the San Juan Massif in Southern Colorado.

By 21Z, precipitation on the immediate lee of the Park Range had decreased to 0.03 cm/hr although the summit maintained intensities of 0.13 to 0.18 cm/hr. Visibility continued to increase at mid-ridge to about 300 meters by 2130Z, although light snow continued to fall. Hayden also reported light snow. The front began to stall across central Colorado as it approached the San Juan barrier. Continued reports of snowfall were noted in the mountains near Aspen and Gunnison.

At 22Z, precipitation had ceased in the Craig/Hayden region, although the Park Range summit continued to accumulate snow at rates of 0.10-0.18 cm/hr. The observer at Thunderhead Lodge reported light snow and fog, indicating cloud base was below mid-ridge. By 2245Z, cloud base had risen to the level of the lodge and snow diminished in intensity. Snow continued to fall lightly during the next hour at the summit, although the cloud layer had become thin enough to allow the moon to appear occasionally. The surface front remained north of the San

snowfall continued to be heavy on the barrier (0.10-0.30 cm/hr). At mid-ridge, the CSU observer reported increased visibility (100 m), but steady snowfall. In the valley, Hayden continued to experience light snowfall. Valley winds were westerly at 3 m/s increasing to 10 m/s at ridge top.

Light snow continued to fall at Hayden at 20Z (Figure 41). Maximum snowfall reported was at the Park Range summit (0.36 cm/hr) and observations at mid-level on the ridge indicated continued snowfall with less intensity. The front continued southward into the Gunnison region of central Colorado. Moderate continuous snowfall was reported at all stations in the vicinity of the front and south to the San Juan Massif in Southern Colorado.

By 21Z, precipitation on the immediate lee of the Park Range had decreased to 0.03 cm/hr although the summit maintained intensities of 0.13 to 0.18 cm/hr. Visibility continued to increase at mid-ridge to about 300 meters by 2130Z, although light snow continued to fall. Hayden also reported light snow. The front began to stall across central Colorado as it approached the San Juan barrier. Continued reports of snowfall were noted in the mountains near Aspen and Gunnison.

At 22Z, precipitation had ceased in the Craig/Hayden region, although the Park Range summit continued to accumulate snow at rates of 0.10-0.18 cm/hr. The observer at Thunderhead Lodge reported light snow and fog, indicating cloud base was below mid-ridge. By 2245Z, cloud base had risen to the level of the lodge and snow diminished in intensity. Snow continued to fall lightly during the next hour at the summit, although the cloud layer had become thin enough to allow the moon

to appear occasionally. The surface front remained north of the San Juan Mountains moving slightly southward east of the divide.

Post Analysis Conditions

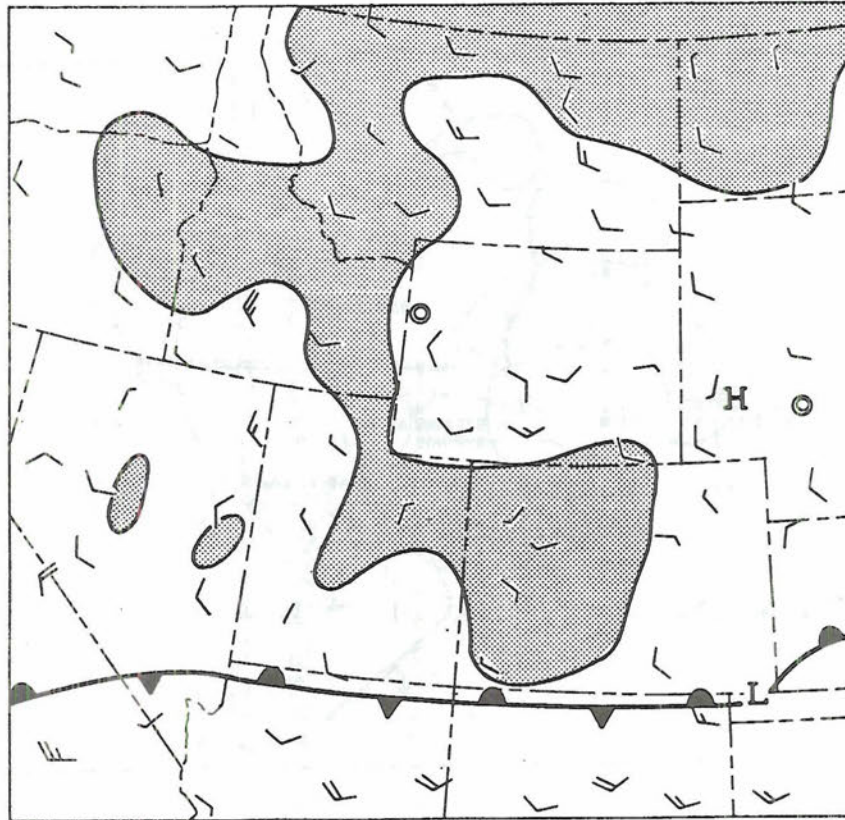
By 00Z on November 27, the surface front had weakened considerably and moved south of the San Juan Mountains (Figure 43). Snowshowers were still being reported at Southern Colorado stations. Light snow continued to fall on the summit of the Park Range. Precipitation was in the form of light snow.

At 70 KPa, the entire state came under influence of cold advection. Temperatures dropped 4°C from the previous 12Z measurement. Winds decrease slightly in intensity and veered slightly to WNW at 10 m/s. Weak cold air advection continued at 50 KPa with temperatures decreasing about 2°C over the 12 hour period.

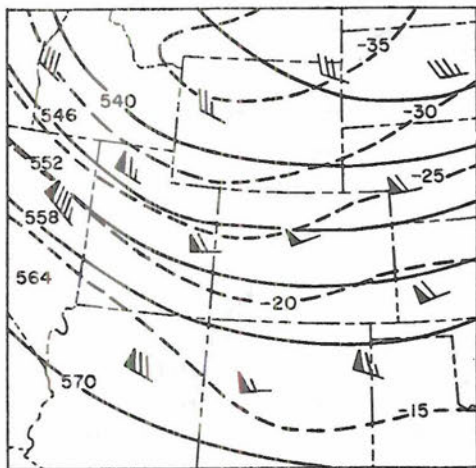
5.2 Flight Track Descriptions

Both aircraft flew in the experimental area during the period 1930Z to 2130Z. The NCAR Queen Air entered the area at 4300 meters msl from the south, reaching Rabbit Ears Pass at 2036Z (Figure 44). The aircraft then descended to 4200 meters msl and proceeded west along $40^{\circ}30'N$ to the Hayden vortac. A descent and ascent sounding were completed between 4200 meters and 2300 meters msl over the vortac. The plane then proceeded east along $40^{\circ}30'N$ in a gentle climb from 4200 meters at Hayden to 5000 meters at Hebron, exiting the area at 2129Z.

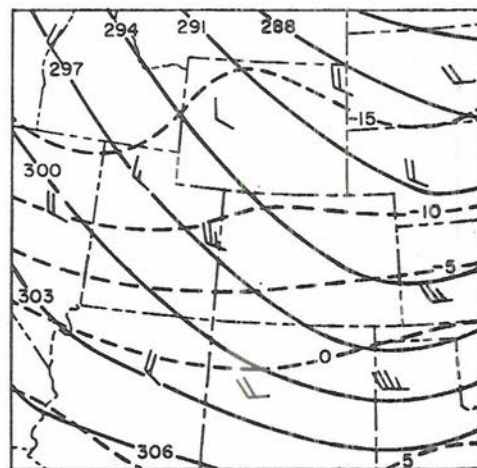
The Lear Jet entered the area at 1927Z from the east along $40^{\circ}30'N$ at an altitude of 6800 meters msl (Figure 44). The aircraft descended to 4350 meters msl on the approach to the Hayden vortac, then proceeded 29 kilometers southeast. The remainder of the flight consisted of five arcs from 10° to 110° centered on the Hayden vortac. The five arcs were



Surface



50 KPa



70 KPa

Figure 43. Major synoptic features at 00Z on November 27, 1979. Heights are in decameters, temperatures in $^{\circ}\text{C}$.

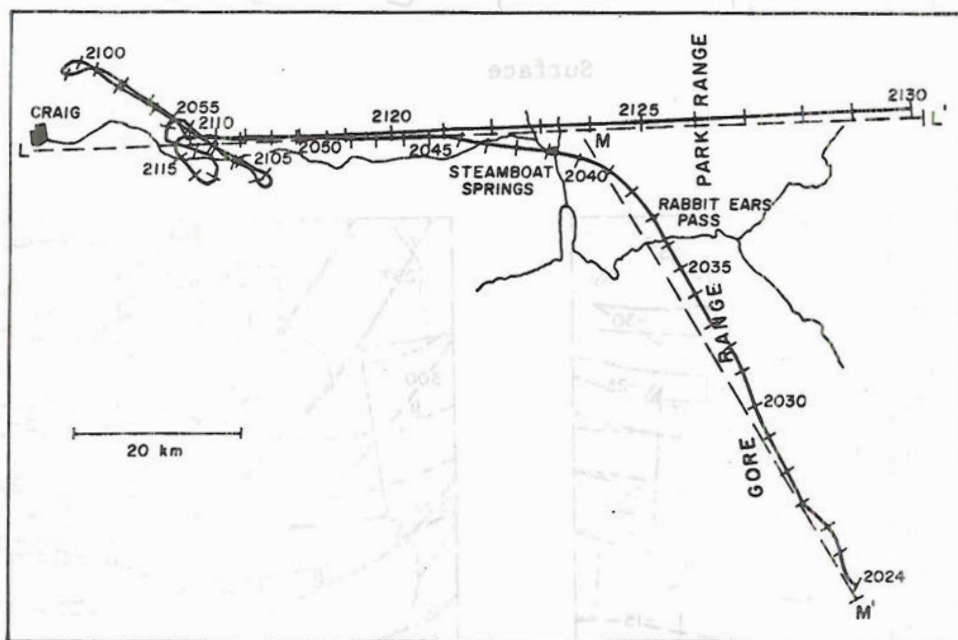
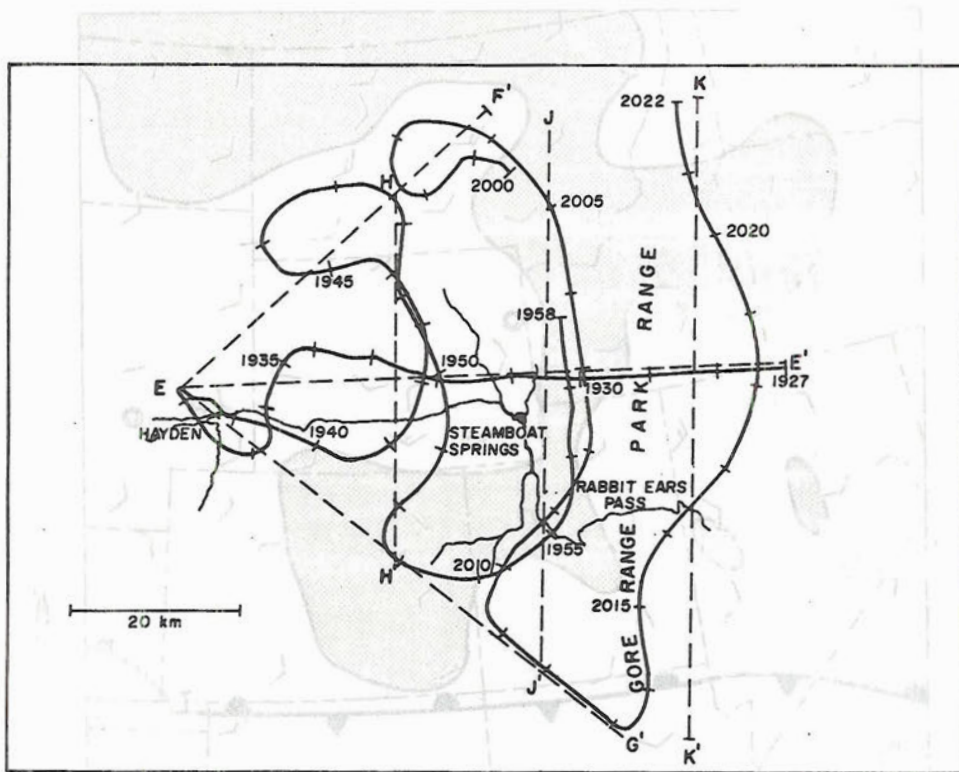


Figure 44. Queen Air and Lear flight tracks for November 26, 1979. The Lear track is the top figure.

flown at 29 kilometers (4350 and 4950 meters msl), 48 kilometers (4700 and 5300 meters msl), and 68 kilometers (5300 meters msl) from the vortex. The Lear then returned to Loveland, Colorado leaving the area at 2022Z.

Data for the Queen Air flight are represented on four cross-sections (Figures 45-48). The topography indicated on the cross-sections is taken along lines LL' and MM' on Figure 44.

Lear flight data are represented on six cross-sections (Figures 49-54). Topography for the cross-sections is taken along lines EE', EF', EG', HH', JJ' and KK' on Figure 44. Data structure for both Queen Air and Lear cross-sections is similar to that presented in the November 24, 1979 case study. The small letters below the base of the temperature scale are used to indicate the precise location of microphysical data presented in the following section.

5.3 Cloud Physical and Microphysical Characteristics

The aircraft penetrations of the November 26 cloud system occurred during the latter period of the storm about three hours after frontal passage. Cold air advection and very strong west-northwesterly winds were prevalent during the period. The cloud system extended from approximately 72 KPa (-10°C) to 42 KPa (-35°C). Cloud top was estimated from Doppler radar data and visual observations of the Lear observer. Cloud base was observed to rise throughout the period. A weak evaporation zone was observed over the east slope. Except for this narrow zone, the cloud extended to the Front Range. No convection was observed at any time in the cloud system. Soundings indicate the system was stably stratified.

Snow fell throughout the valley and on the barrier during the entire period but diminished in intensity with time after frontal

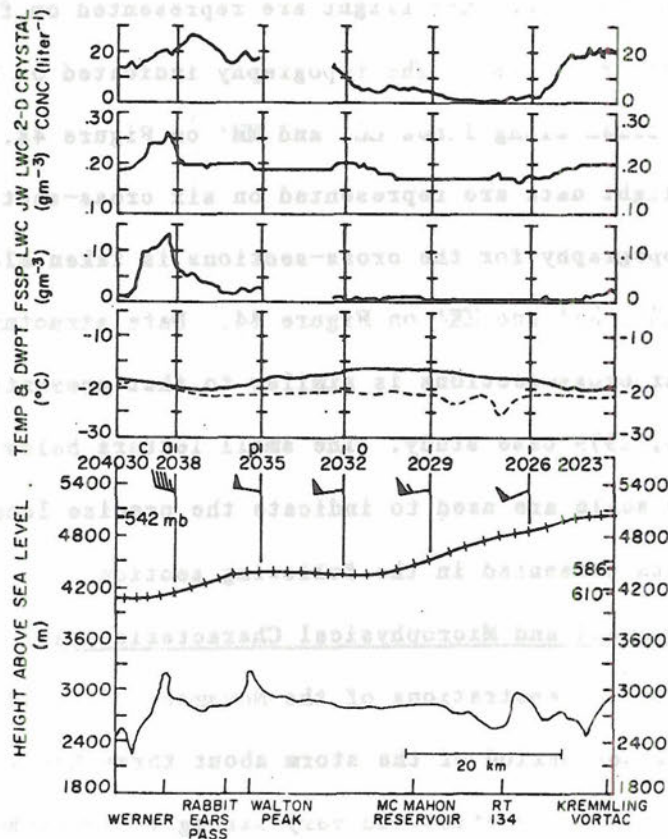


Figure 45. Vertical cross-section along line MM' on Figure 44 showing state, wind and microphysical data collected by the Queen Air on November 26, 1979. Data were averaged over ten second periods.

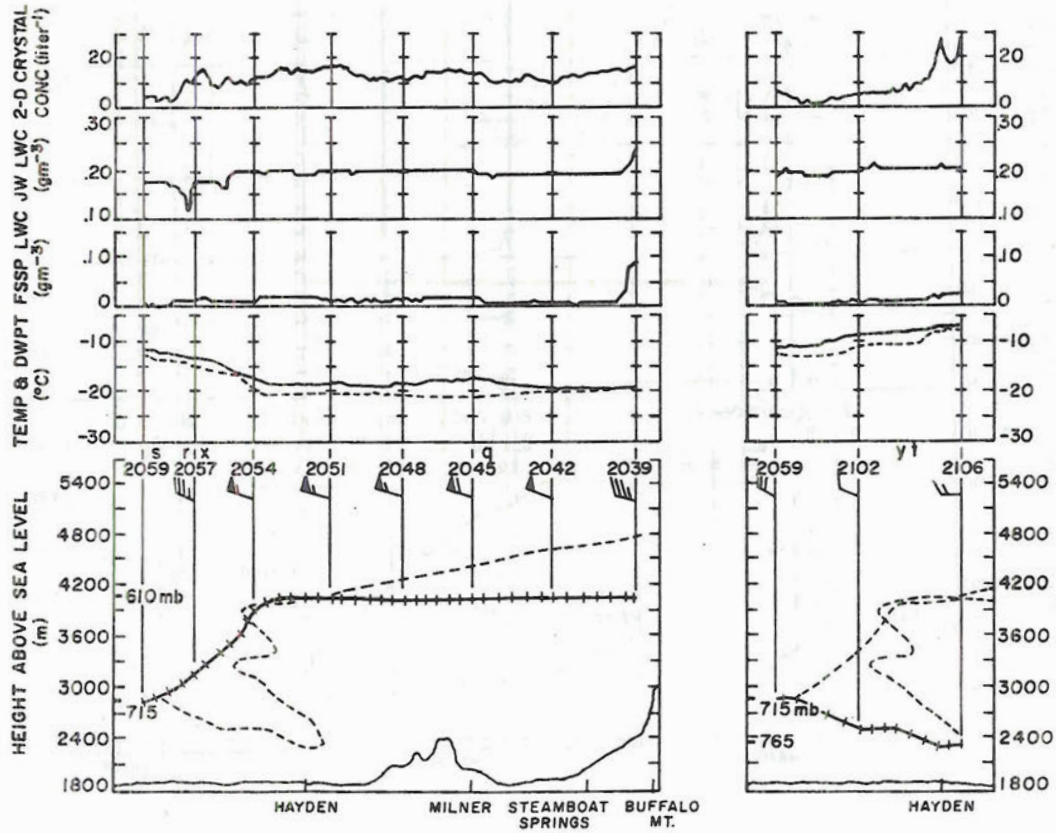


Figure 46. Vertical cross-sections along line LL' on Figure 44 showing state, wind and microphysical data collected by the Queen Air on November 26, 1979. Data were averaged over ten second periods.

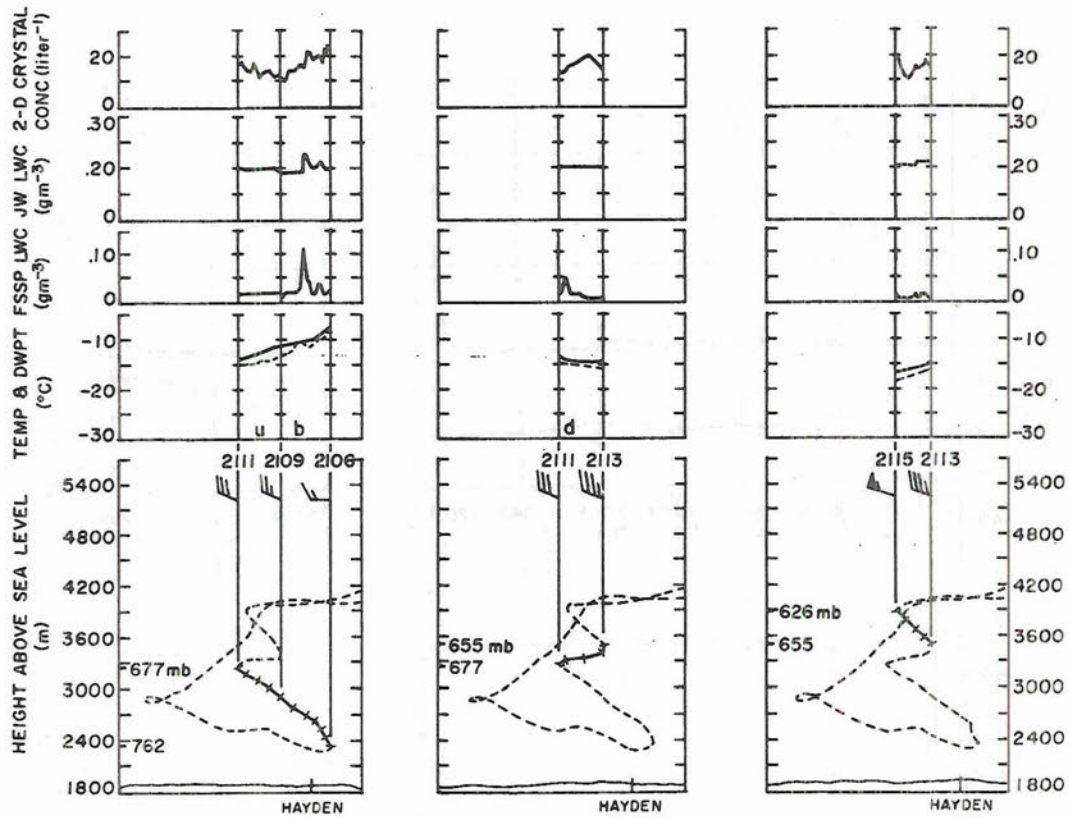


Figure 47. Vertical cross-sections along line LL' on Figure 44 showing state, wind and microphysical data collected by the Queen Air on November 26, 1979. Data were averaged over ten second periods.

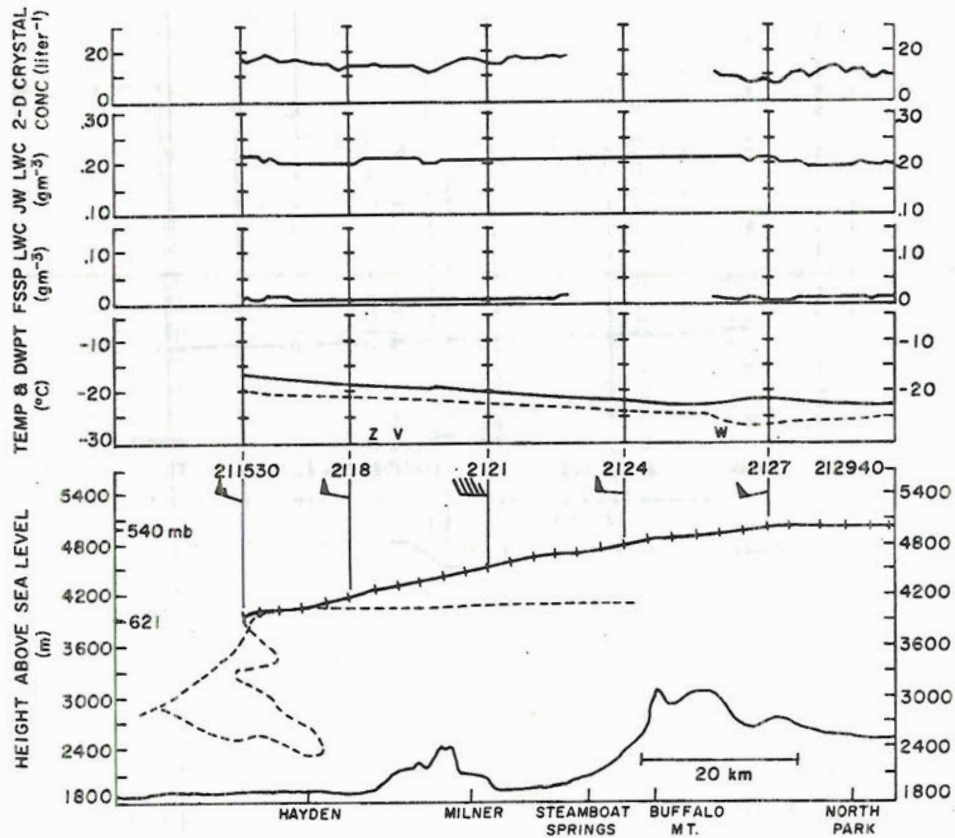


Figure 48. Vertical cross-section along line LL' on Figure 44 showing state, wind and microphysical data collected by the Queen Air on November 26, 1979. Data were averaged over ten second periods.

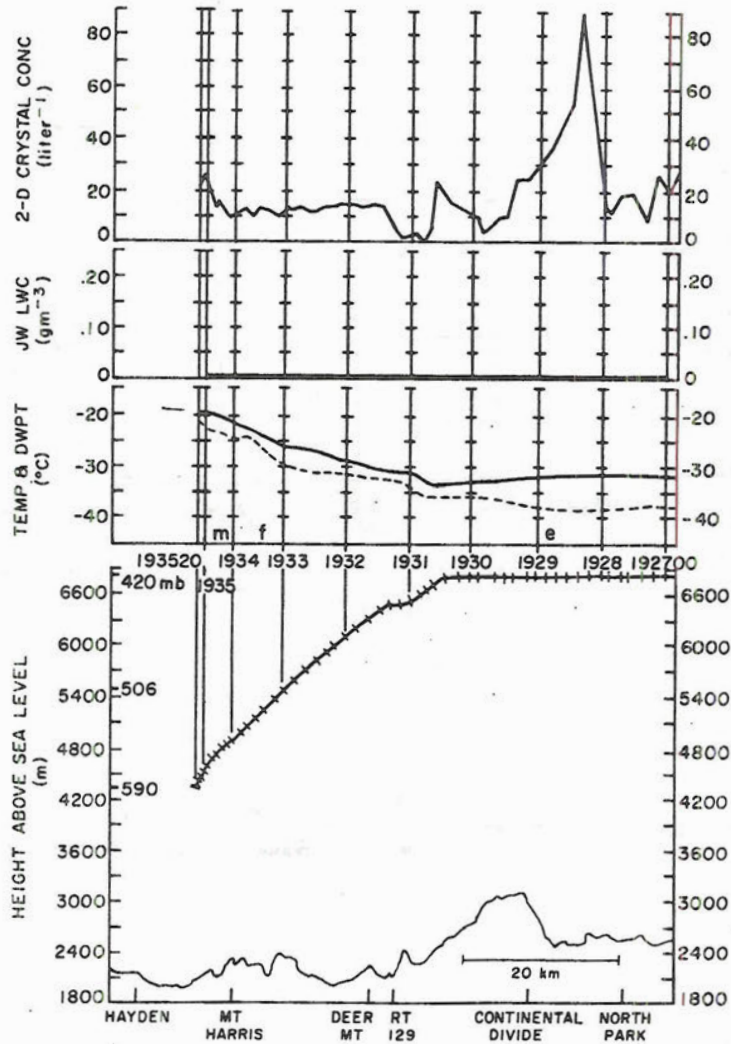


Figure 49. Vertical cross-section along line EE' on Figure 44 showing state and microphysical data collected by the Learjet on November 26, 1979. Data were averaged over ten second periods.

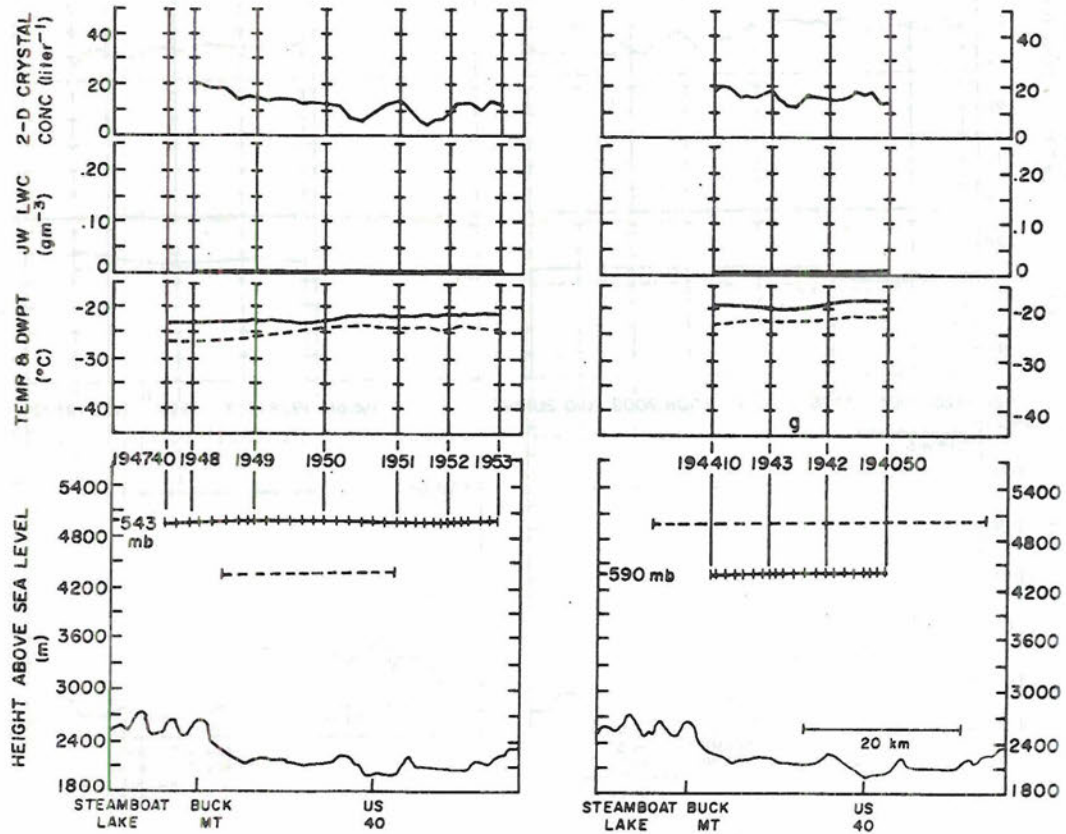


Figure 50. Vertical cross-sections along line HH' on Figure 44 showing state and microphysical data collected by the Learjet on November 26, 1979. Data were averaged over ten second periods.

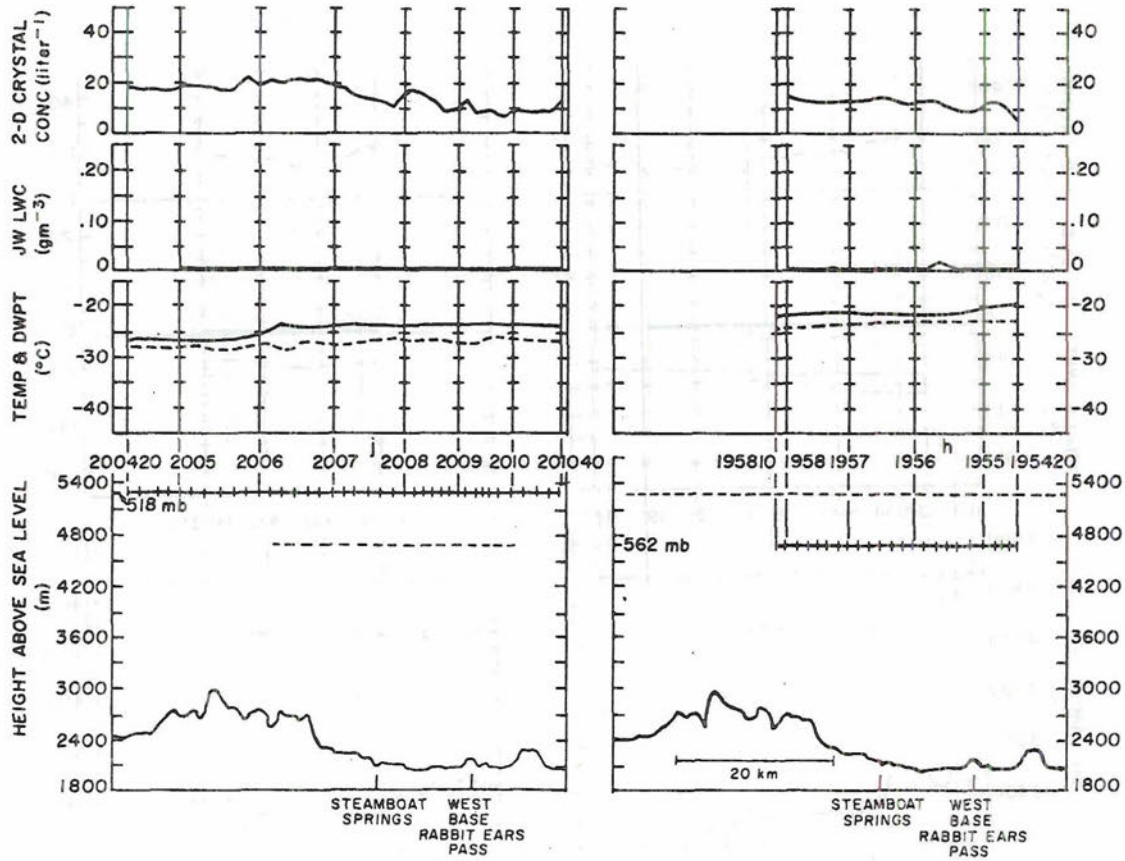


Figure 51. Vertical cross-sections along line JJ' on Figure 44 showing state and microphysical data collected by the Learjet on November 26, 1979. Data were averaged over ten second periods.

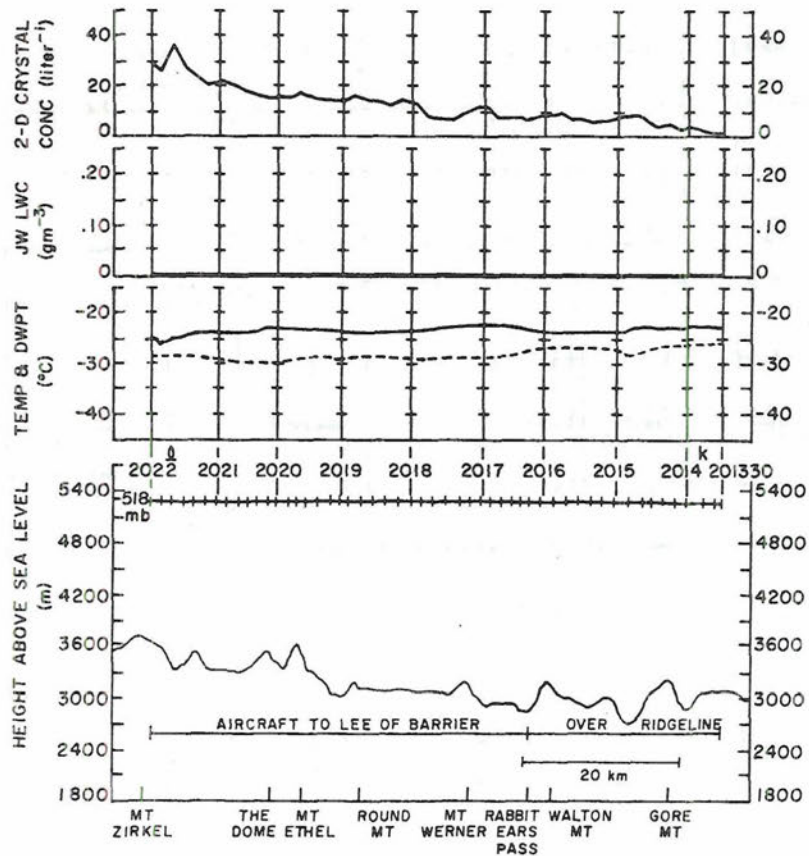


Figure 52. Vertical cross-section along line KK' on Figure 44 showing state and microphysical data collected by the Learjet on November 26, 1979. Data were averaged over ten second periods.

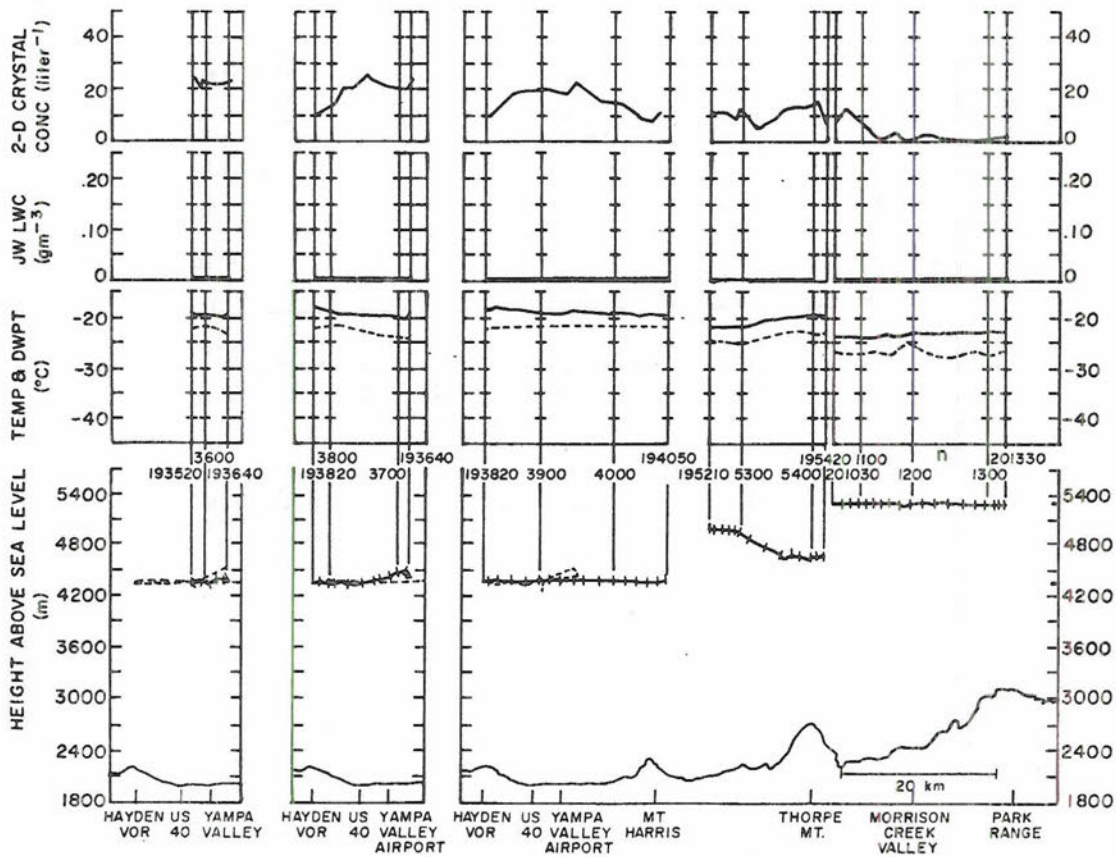


Figure 53. Vertical cross-sections along line EG' on Figure 44 showing state and microphysical data collected by the Learjet on November 26, 1979. Data were averaged over ten second periods.

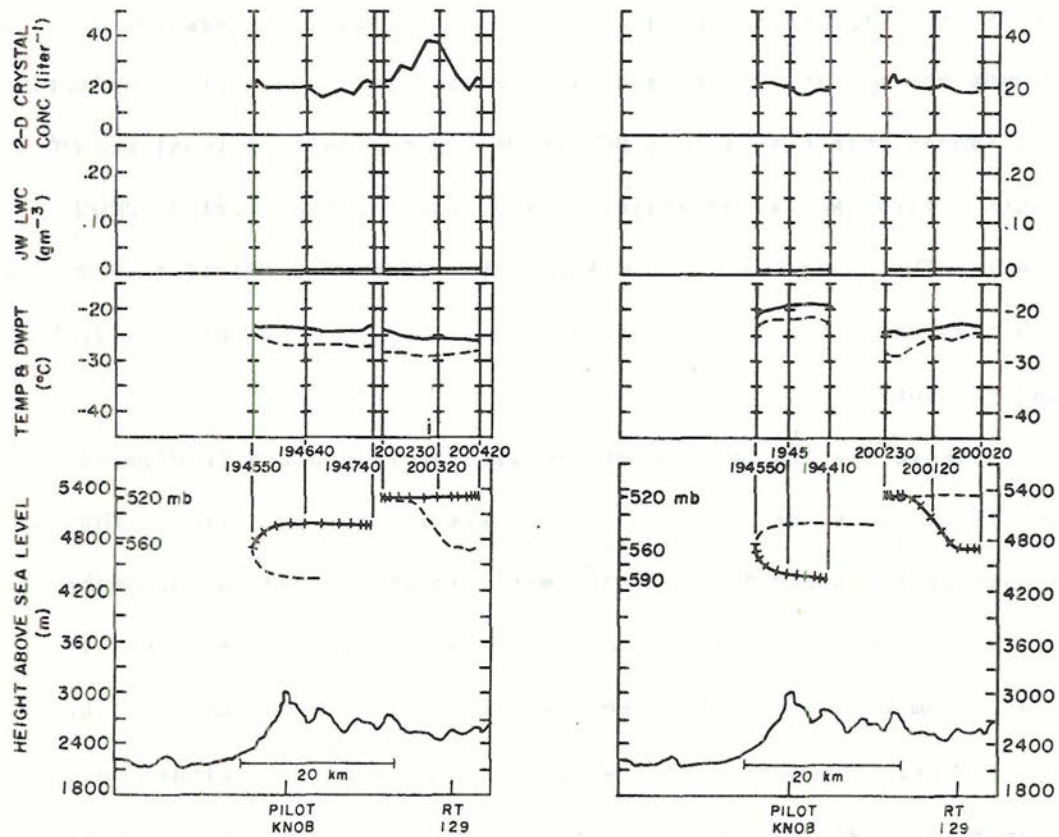


Figure 54. Vertical cross-sections along line EF' on Figure 44 showing state and microphysical data collected by the Learjet on November 26, 1979. Data were averaged over ten second periods.

passage. Maximum snowfall rates were observed at the barrier crest. Little evidence of riming or aggregation was reported by ground observers. Crystal replicas show occasional light aggregation of columns but mostly single crystals. Precipitation consisted primarily of columnar crystals early (1900-2000Z) in the observational period and plates toward the latter stages of the observational period (2000-2100Z). The change in habit was probably related to cloud base rising with time and cooling as colder air continued to move into the Park Range region.

Data in the following sections will be referenced to Figures 45-54, the flight cross-sections in a manner similar to that used in Chapter 4. Because of the scarcity of liquid water in this cloud, a reasonable statistical estimate of the JW bias for this flight could not be determined. Comparison of FSSP zero values with JW values indicate that the bias is near 0.18 g/m^3 . The JW bias of 0.18 g/m^3 is included on the November 26, 1979 flight track cross-sections. In the text, JW values quoted will have the bias subtracted out.

5.31 Cloud Liquid Water and Droplet Spectra

The locations of cloud liquid water in the November 26 cloud were very similar to that of the previous case study, but the quantities were substantially less. The primary zone of liquid water was found directly windward of the barrier in a narrow region over the western slopes. The maximum value recorded was 0.13 g/m^3 (a, Figure 45) observed at a temperature of -19°C . Virtually no liquid water was observed at any other location in the cloud except for a very narrow zone upwind of Mt. Harris near Hayden (b, Figure 47). This zone was probably associated with local topographic lifting. Liquid water contents in this region

reached a peak of 0.11 g/m^3 and maintained 0.02 g/m^3 over a six minute ascent through the lower portion of the cloud.

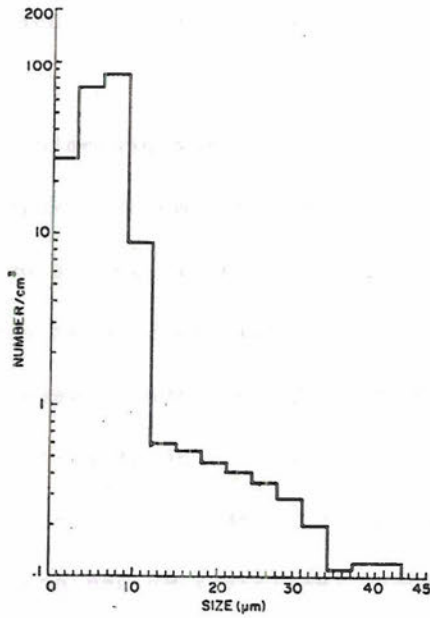
FSSP droplet spectra in these regions of the cloud are presented in Figure 55. The spectra were constructed from 10 second samples. Mean droplet diameters were less than $10 \text{ }\mu\text{m}$ in all cases. The largest droplets were $36\text{-}39 \text{ }\mu\text{m}$ in concentrations of 0.1 cm^{-3} . Maximum droplet concentrations were between $185\text{-}240 \text{ cm}^{-3}$ in the primary zone and between $165\text{-}210 \text{ cm}^{-3}$ in the upwind zone near Mt. Harris. These concentrations are a factor of 4 larger than that observed in the November 24 case. In the November 24 situation, the source air above the inversion had droplet spectra more characteristic of modified maritime air masses. Clearly, on November 26, the source air was more continental, accounting for the significant differences in the spectra.

5.32 Ice Crystal Structure and Crystal Size Spectra

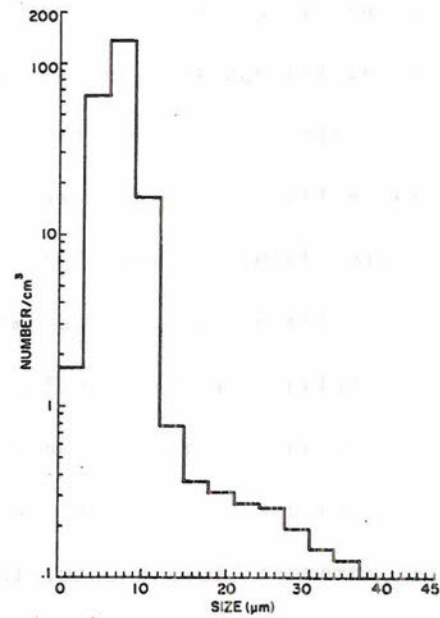
Data collected by the 2-D probe accompanying the discussion which follows are displayed in Figures 56-58. Crystal diameter size spectra for 2-D data are shown in Figures 59-60. The shorthand notation utilized in section 4.3 of the previous case study for referencing these figures will also be applied in this section. The data in these figures can be cross-referenced with the flight cross-sections (Figures 45-54) for location and comparisons with state and microphysical data.

Lear Flight

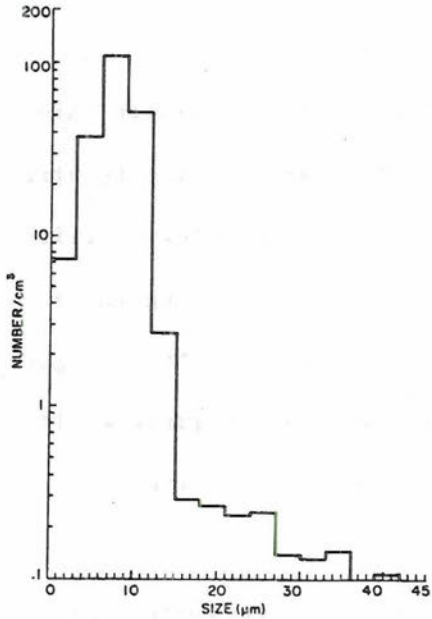
The Lear Jet probe of the November 26 cloud system covered only the upper portions of the cloud at temperatures below -18°C . Crystal image size and structure were largely homogeneous throughout the flight although concentrations varied between $1\text{-}40/\text{liter}$. A singular exception to these concentrations occurred as the aircraft approached the barrier



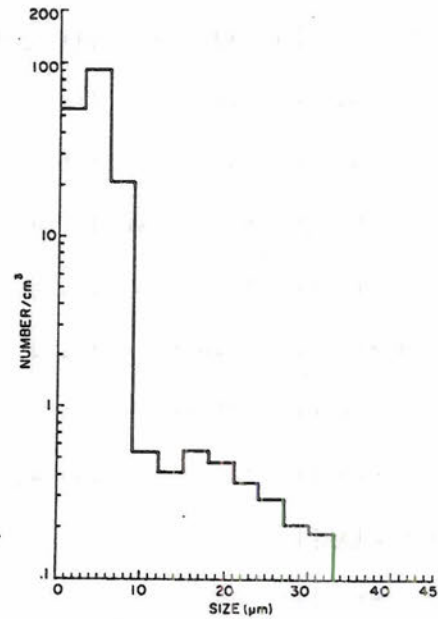
Time=203800 (figure 45,a)
 SV=198.2 cm³ ST=10 sec
 ND=36657 CD=185.0 cm⁻³



Time=203900 (figure 45,c)
 SV=240.1 cm³ ST=10 sec
 ND=49981 CD=240.1 cm⁻³



Time=210800 (figure 47,b)
 SV=162.3 cm³ ST=10 sec
 ND=34061 CD=209.9 cm⁻³



Time=211130 (figure 47,d)
 SV=169.6 cm³ ST=10 sec
 ND=28219 CD=166.4 cm⁻³

Figure 55. FSSP droplet spectra, November 26, 1979. The notation at the base of the diagrams include sample volume (SV), sample time (ST), number of droplets (ND) and concentration (CD).



Figure 56. 2-D probe images from the November 26, 1979 Lear flight. The reference at the bottom right of each image line refers to the precise location of the image on the flight track cross-sections.

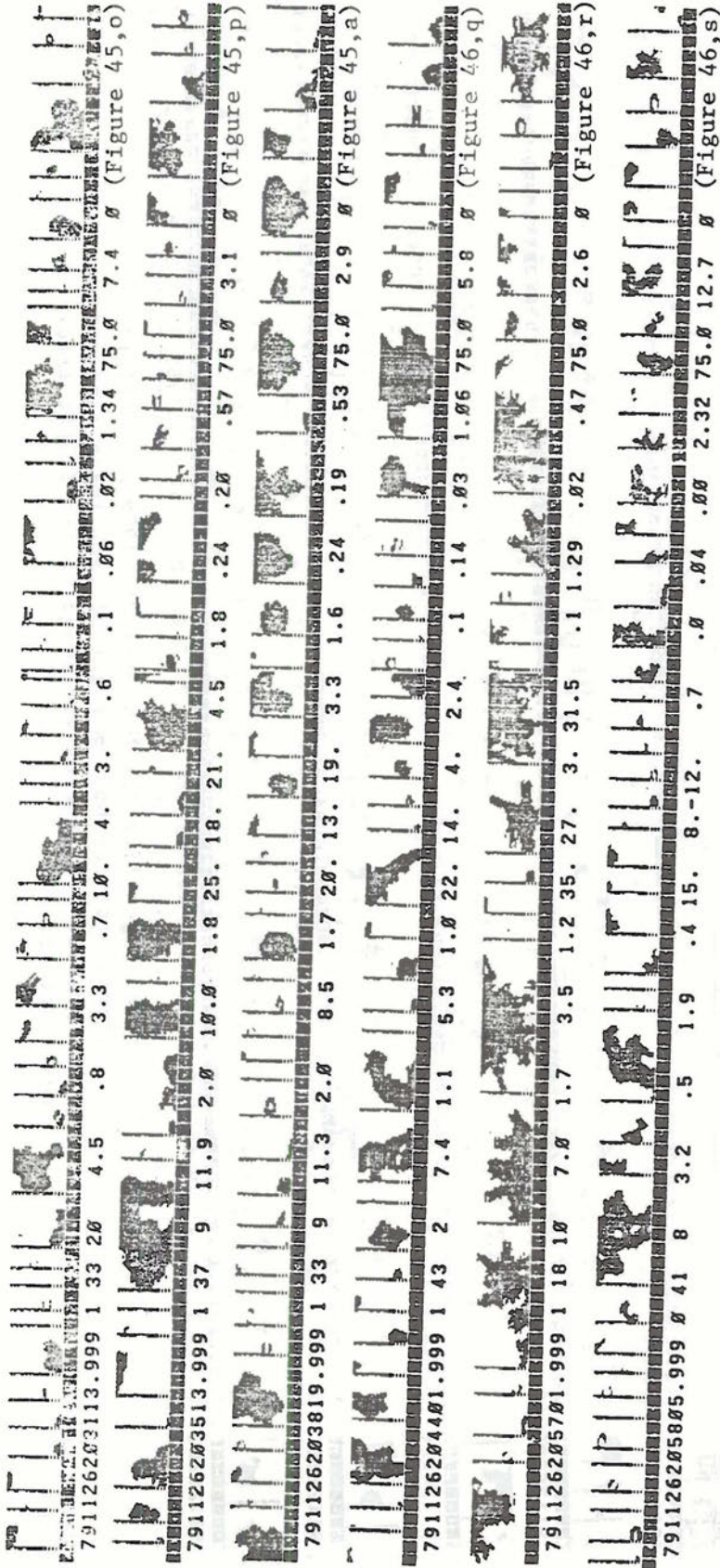


Figure 57. 2-D probe images from the November 26, 1979 Queen Air flight. The reference at the bottom right of each image line refers to the precise location of the image on the flight track cross-sections.

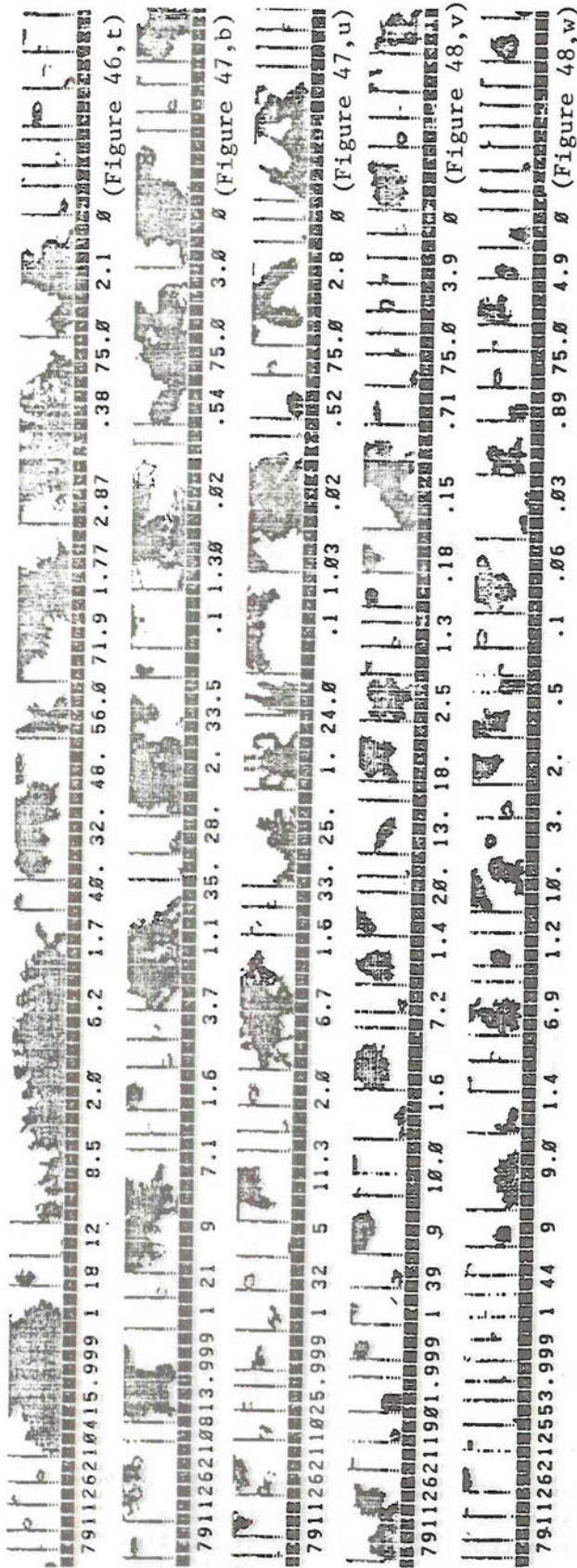
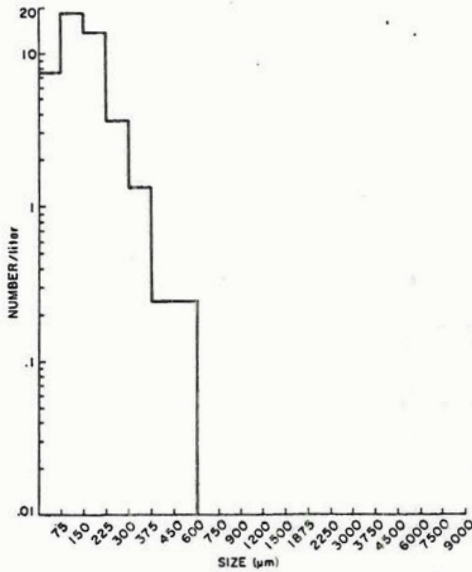
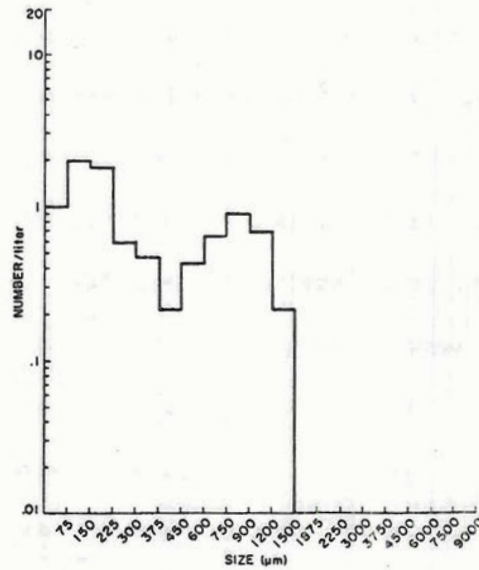


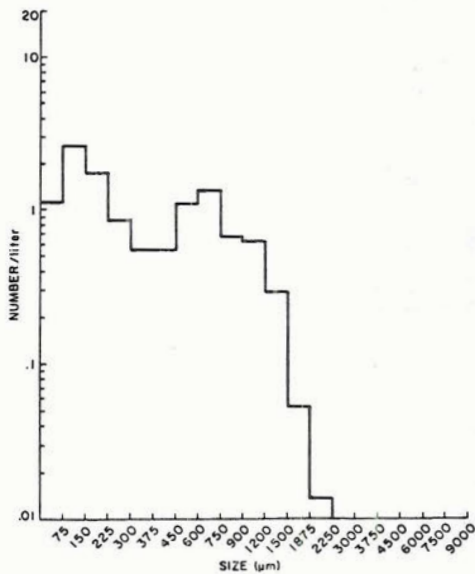
Figure 58. 2-D probe images from the November 26, 1979 Queen Air flight. The reference at the bottom right of each image line refers to the precise location of the image on the flight track cross-sections.



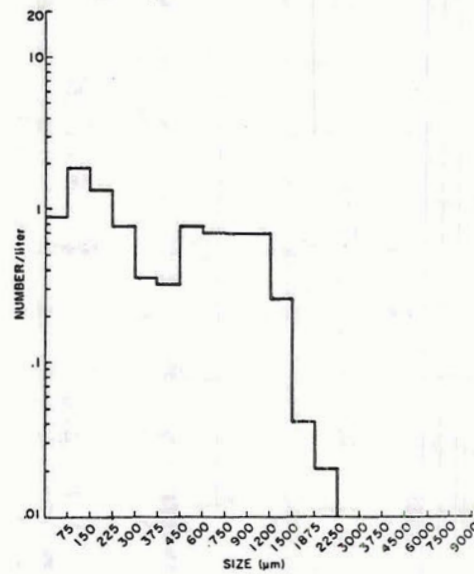
Time=192800-59 (Fig. 49,e)
 SO=50.9 lit⁻¹ RA=44.1 lit⁻¹
 TS=365



Time=193400-59 (Fig. 49,m)
 SO=12.5 lit⁻¹ RA=8.9 lit⁻¹
 TS=245

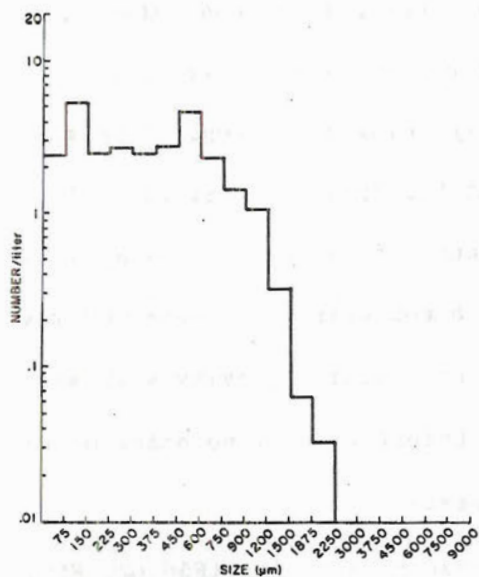


Time=194200-59 (Fig. 50,g)
 SO=15.5 lit⁻¹ RA=11.7 lit⁻¹
 TS=861

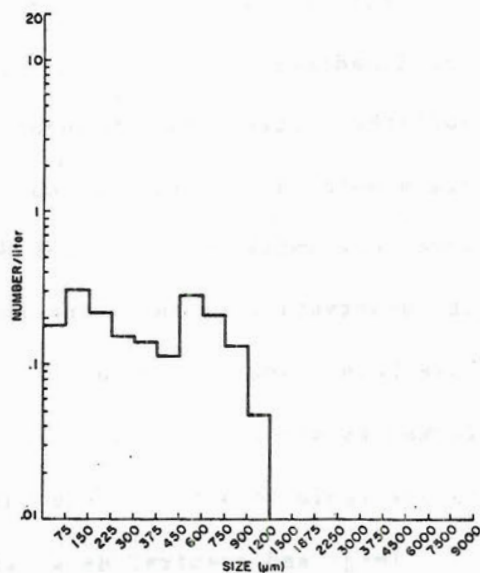


Time=195500-59 (Fig. 51,h)
 SO=12.7 lit⁻¹ RA=8.7 lit⁻¹
 TS=826

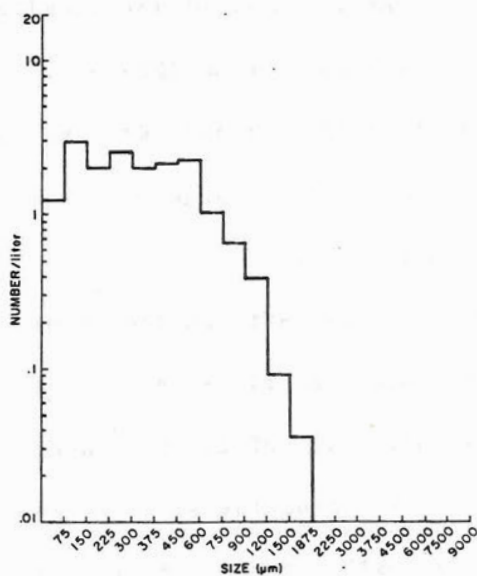
Figure 59. 2-D crystal size spectra taken during the November 26, 1979 Lear flight. Abbreviations refer to the concentrations determined by the shadow-or method (SO), the concentrations with the reject criteria applied (RA), and the total number of crystals in the sample (TS).



Time=200300-59 (Fig.54,i)
 SO=32.9 lit⁻¹ RA=23.0 lit⁻¹
 TS=867



Time=201200-59 (Fig.53,n)
 SO=1.7 lit⁻¹ RA=1.8 lit⁻¹
 TS=946



Time=202100-59 (Fig.52,1)
 SO=20.5 lit⁻¹ RA=17.6 lit⁻¹
 TS=945

Figure 60. 2-D crystal size spectra taken during the November 26, 1979 Lear flight. Abbreviations refer to the concentrations determined by the shadow-or method (SO), the concentrations with the reject criteria applied (RA), and the total number of crystals in the sample (TS).

from the east and entered the COSE area. For a 10 second interval to the immediate lee of the Range, crystal concentrations averaged 90/liter. This zone was about 300 meters below cloud top. Crystal sizes both in this region and throughout the traverse near cloud top were very small (F56, L1; F59, S1). Because of the close proximity of the observation to the mountain, the high concentrations observed may have been associated with a penetration of a stable gravity wave which formed as air flowed over the barrier. Unfortunately, no other evidence is available to substantiate this hypothesis.

Image and spectral data along the descent sounding (F56, L2; F59, S2) at the -25°C level indicate a broadening of the size spectrum so that the largest images reach 1500 μm size, 900 μm larger than those at the higher -32°C level. At the base of the sounding (-19°C), the maximum image dimensions exceeded 2000 μm (F59, S3). Throughout the four arcs lying entirely west of the barrier, crystal concentrations remained close to 20/liter and very little change occurred in the image shapes or sizes (F56, L4-L6; F59, S4; F60, S1).

On the final arc, the aircraft crossed ridgeline to the lee of the Range and then returned over the ridge in the vicinity of the Zirkel Mountains, the highest mountains of the Park Range. Crystal concentrations were less than 5/liter over the southern part of the ridge. Image sizes were consistently smaller than other regions of the cloud (F56, L7; F59, S27). As the Lear continued northward, concentrations increased steadily, even when the aircraft was in the lee of the barrier. At the point where the aircraft turned northwest and crossed ridgeline to the windward side, crystal concentrations reached 40/liter. Image sizes were larger (F56, L8; F60, S3) at this end of the Range.

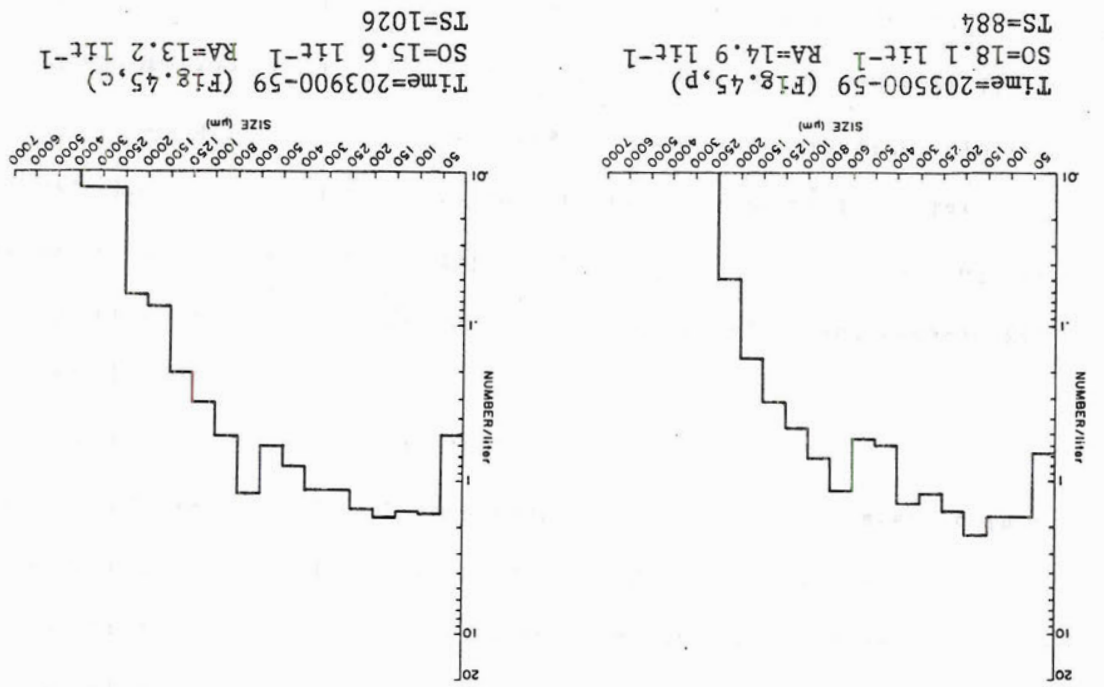
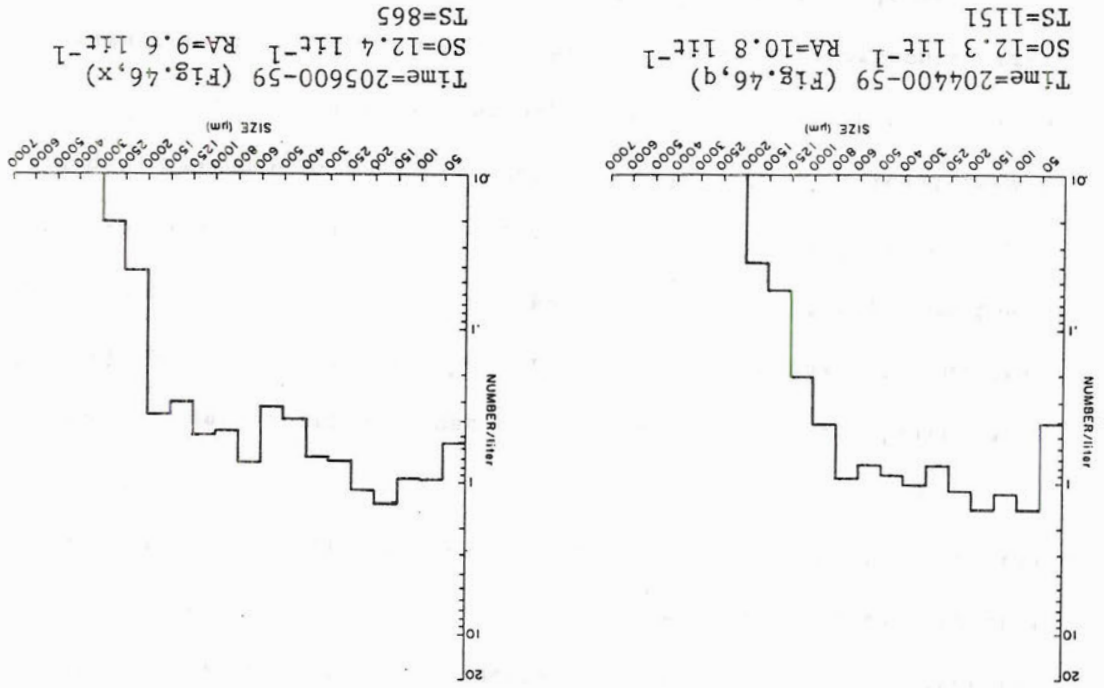
Throughout the flight, no evidence of aggregation or riming occurred in the images. Crystals at temperatures colder than -18°C were virtually all single. No liquid water was observed by the JW. Increases in concentration of ice crystals seem largely related to the proximity of the observation to the barrier.

Queen Air Flight

The Queen Air entered the COSE area from the south and crossed the Park Range at a narrow angle. While the aircraft was to the lee of the barrier, crystals were small and concentrations averaged 1-3/liter (F57,L1-2; F61,S1). As the plane crossed to the windward side, crystal concentrations increased to 20/liter. This region coincided with the zone of higher liquid water content. Apparently, little interaction between the crystals and droplets occurred because there was no evidence of riming or aggregation on the images. Because of the small mean droplet sizes, the collision efficiency of the droplets with the crystals was low. Crystal sizes were not substantially different in this region (F57,L3; F61,S2).

Crystal concentrations along the westbound leg of the flight at -18°C remained steady at approximately 12/liter. Images were entirely single crystals with no identifiable habits (F57,L4; F61,S3). On the descent sounding, as the aircraft passed through the -15°C level, crystal habits switched primarily to dendrites (F57,L5). At lower levels below -12°C (F57,L6), dendrites hardly appeared indicating that, as in the November 24 case, these crystals had approximately horizontal trajectories. In the dendritic zone, crystals were slightly larger (F61,S4) with concentrations averaging 10/liter.

Figure 61. 2-D crystal size spectra taken during the November 26, 1979 Queen Air flight. Abbreviations refer to the concentrations determined by the shadow-or method (SO), the concentrations with the reject criteria applied (RA), and the total number of crystals in the sample (TS).

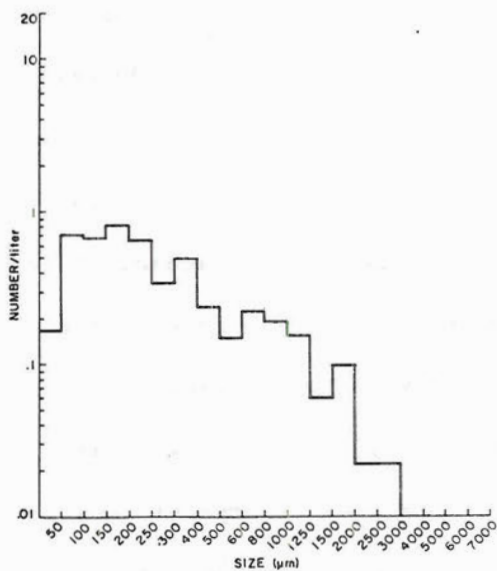


Once the aircraft descended below the dendritic zone, crystal concentrations dropped to between 1-5/liter (F62,S1). These concentrations persisted to the base of the sounding. On the eastern end of the lowest approach, upwind of the small barrier east of Hayden, concentrations increased continuously to 20/liter (F62,S2). The first evidence of crystal aggregation occurred in this region (F58,L1). Temperatures were between -3 and -5°C at the time. Aggregates were small, usually 2 or 3 crystals, based on image structure. Again, many small crystals were evident at these warm temperatures. Concentrations of crystals smaller than $300\ \mu\text{m}$ were on the order of 1-4/liter between the -6°C and -10°C levels throughout the ascent sounding (F62,S3). Evidence of aggregation also persisted to about the -10°C level (F58,L2). Aggregates appeared only on the eastern ascent when the aircraft was closer to the small ridgeline near Hayden, but not on the western ascent. Because of the proximity to the ridgeline during the ascent it is probable that the small barrier, by producing additional lift, was acting indirectly to enhance the precipitation process in this area.

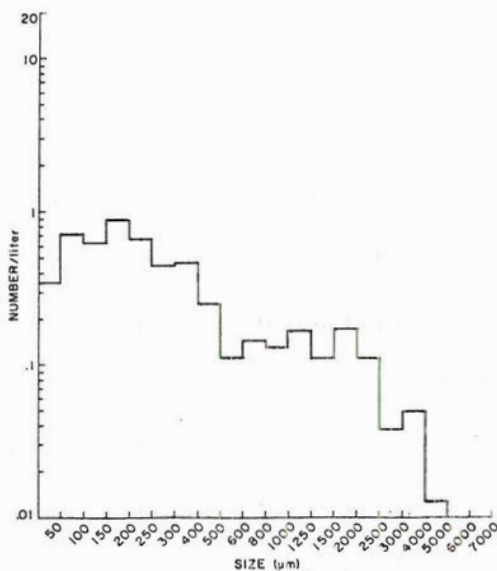
As the plane climbed through -12°C , dendrites again appeared in quantity, persisting until the plane passed through -15°C (F58,L3). Above that level, crystals were smaller, single, and in concentrations averaging 15/liter. This was true throughout the remainder of the flight (F58,L4-5; F62,S4).

5.4 Condensate Production and Production Rates in November 26 Cloud

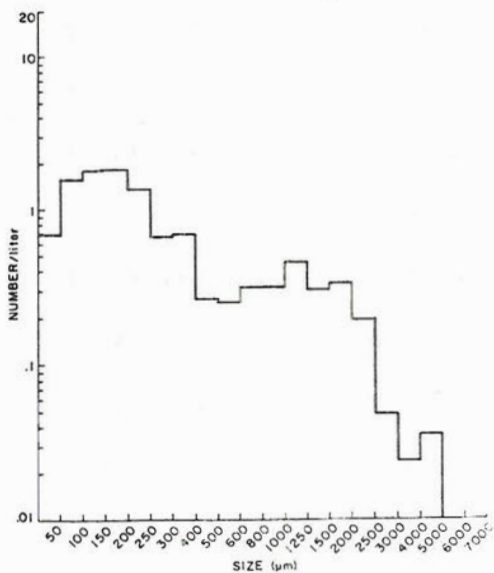
Aircraft and rawinsonde soundings taken on November 26, 1979 were used as input to the airflow model to determine condensate production and production rates in the cloud system. The streamline analysis for this case is shown in Figure 63. As in the previous case, air parcels



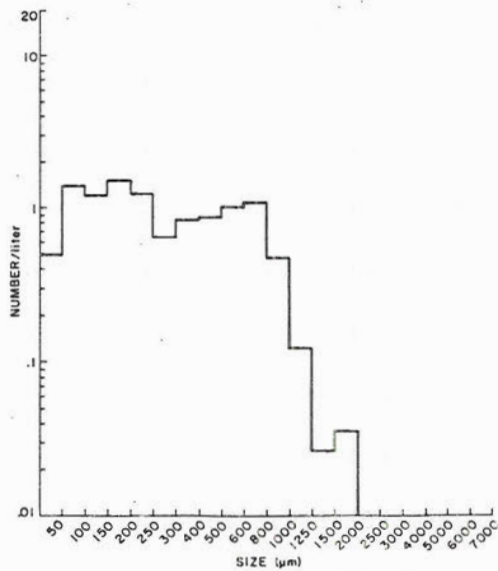
Time=205800-59 (Fig.46,s)
 SO=5.3 lit⁻¹ Ra=5.0 lit⁻¹
 TS=897



Time=210300-59 (Fig.46,y)
 SO=7.1 lit⁻¹ RA=5.5 lit⁻¹
 TS=875



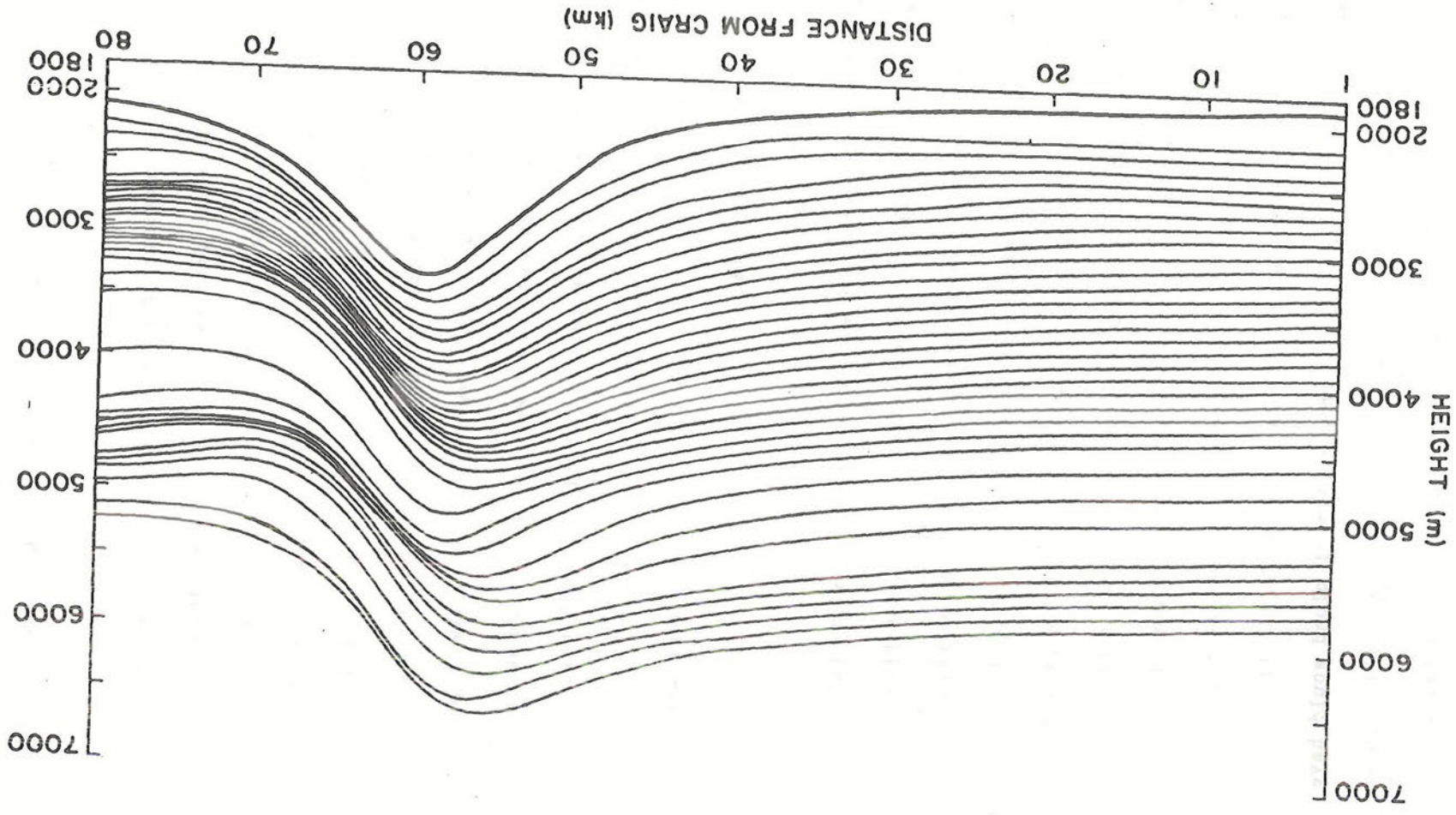
Time=210800-59 (Fig.47,b)
 SO=13.0 lit⁻¹ Ra=11.1 lit⁻¹
 TS=922



Time=211800-59 (Fig.48,z)
 SO=12.5 lit⁻¹ RA=10.8 lit⁻¹
 TS=1210

Figure 62. 2-D crystal size spectra taken during the November 26, 1979 Queen Air flight. Abbreviations refer to the concentrations determined by the shadow-or method (SO), the concentrations with the reject criteria applied (RA), and the total number of crystals in the sample (TS).

Figure 63. Model determined streamlines for the November 26, 1979 cloud system.



were initiated 60 km west of the ridge with aircraft data and advected eastward.

The maximum total condensate produced in this case occurred just above the top of the ridge and decreased continuously at higher cloud levels (Figure 64). The maximum value predicted was 1.0 g/m^3 at the barrier crest. Condensate production rates again indicate that the most probable location for cloud liquid water is in a narrow zone over the windward slopes. The maximum amount of liquid water observed was $.12 \text{ g/m}^3$ (Figure 45). The predicted condensate production in the approximate same location in the simulated cloud was 0.70 g/m^3 . These data indicate that this cloud system operated at better than 83% efficiency in converting available condensate to the ice phase. In fact, except in this narrow zone, the efficiency at which this cloud converted available condensate to ice approached 100%.

5.5 Doppler Radar Observations

The first Doppler radar observations during the COSE II project were taken during the November 26 storm. Three five minute periods of data were available during the time that the aircraft mesoanalysis was conducted. Mean vertical velocity profiles were obtained by averaging the data over each five minute period. Doppler vertical velocities quoted here represent the fall velocities of the crystals plus the vertical velocity of the air so that $w_D = w + V_T$ where w_D = doppler vertical velocity. The data are displayed in Figure 66. For the most part, crystals at temperatures colder than -20°C have average positive (upward) w_D . The largest (1000 μm) crystals in this region of cloud would have fall velocities of 0.40 m/s (platelike crystals) to 0.80 m/s (columnar crystals). Since the radar integrated over the entire spectra, average

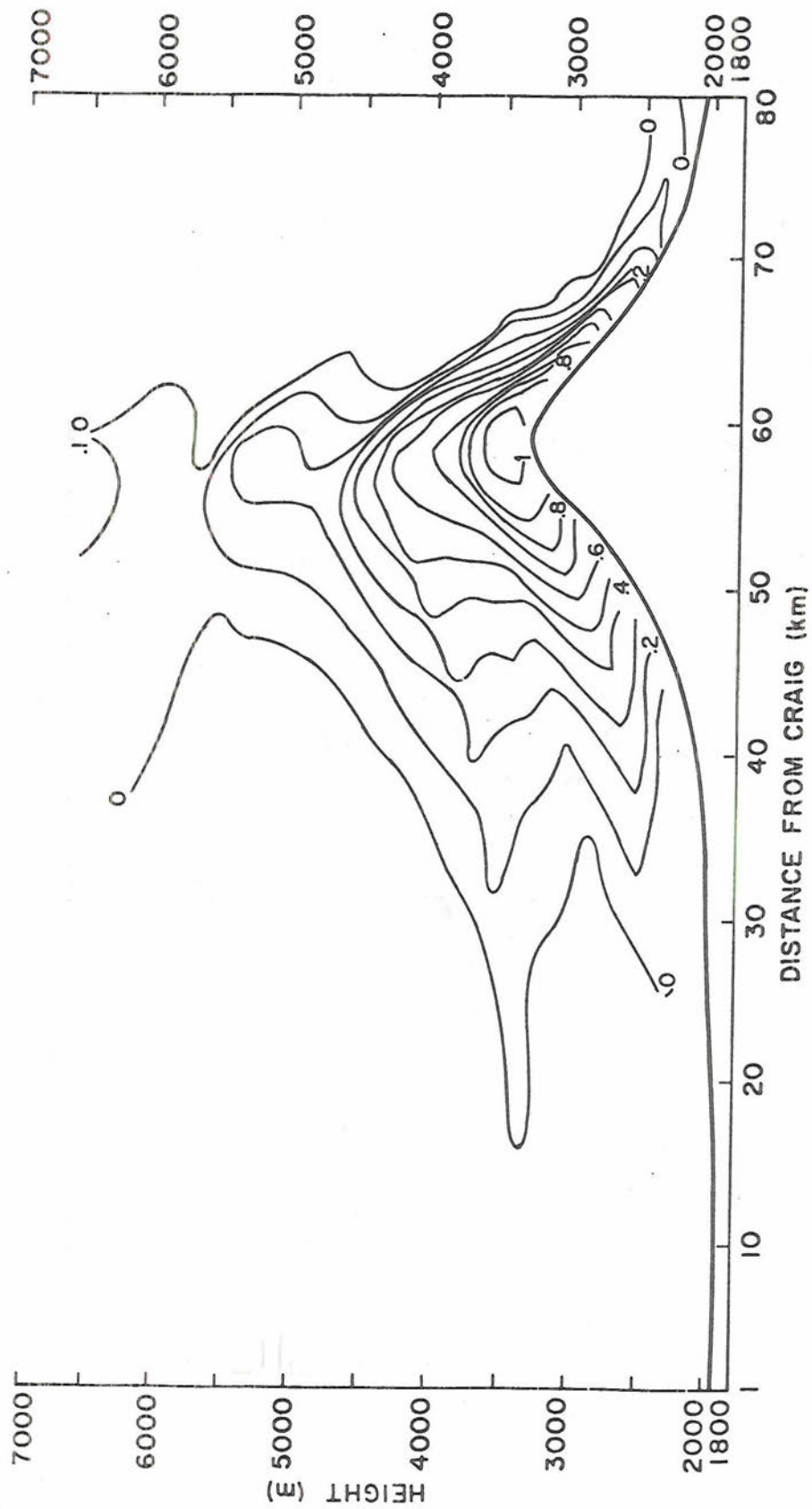


Figure 64. Steady-state potential condensate production in the $^{-3}$ November 26, 1979 cloud system. Isopleths are in gm^{-3} .

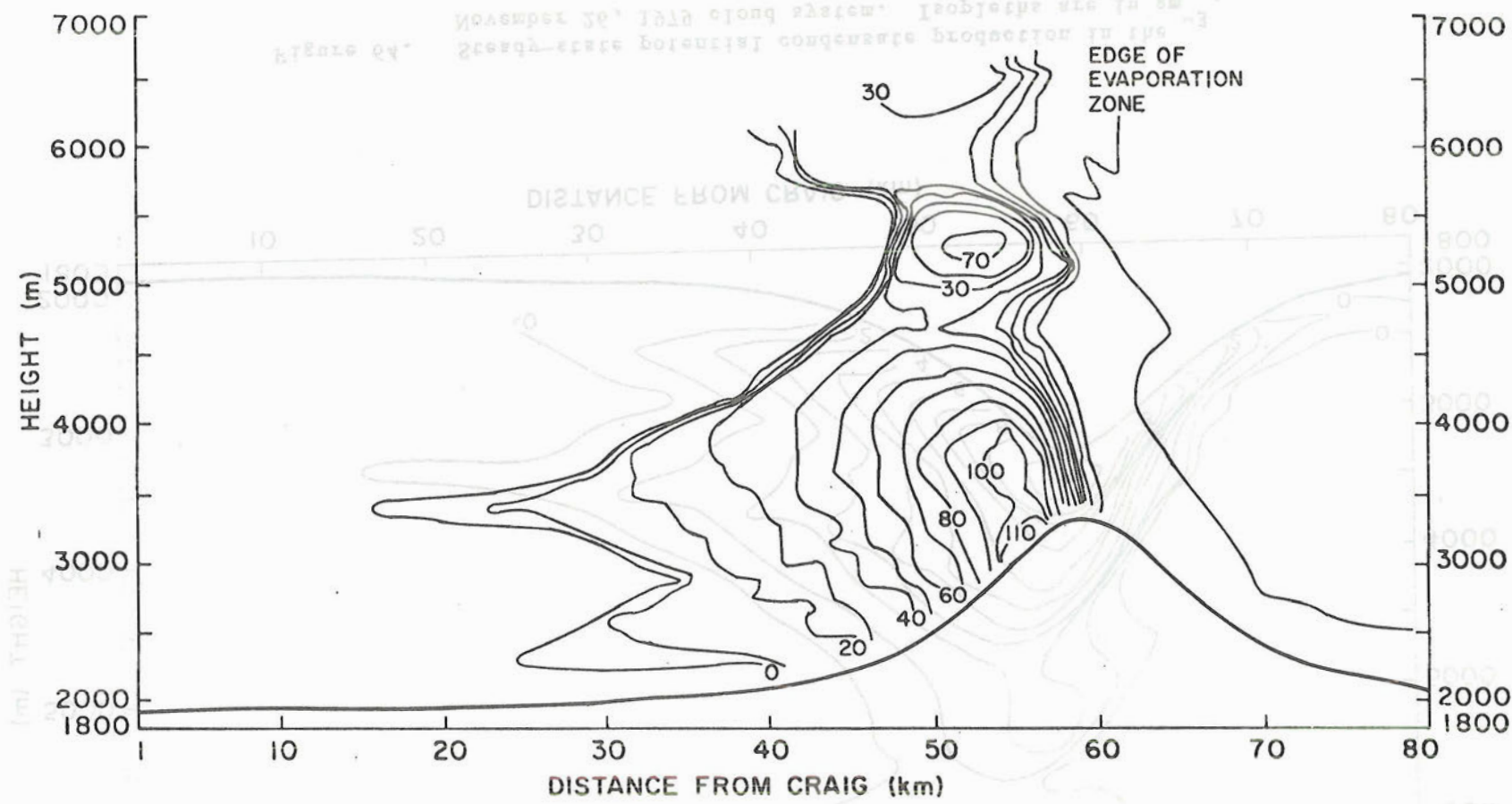


Figure 65. Potential condensate production rates in the November 26, 1979 cloud system. Isopleths are in units of $10^5 \text{ gm}^{-3} \text{ s}^{-1}$.

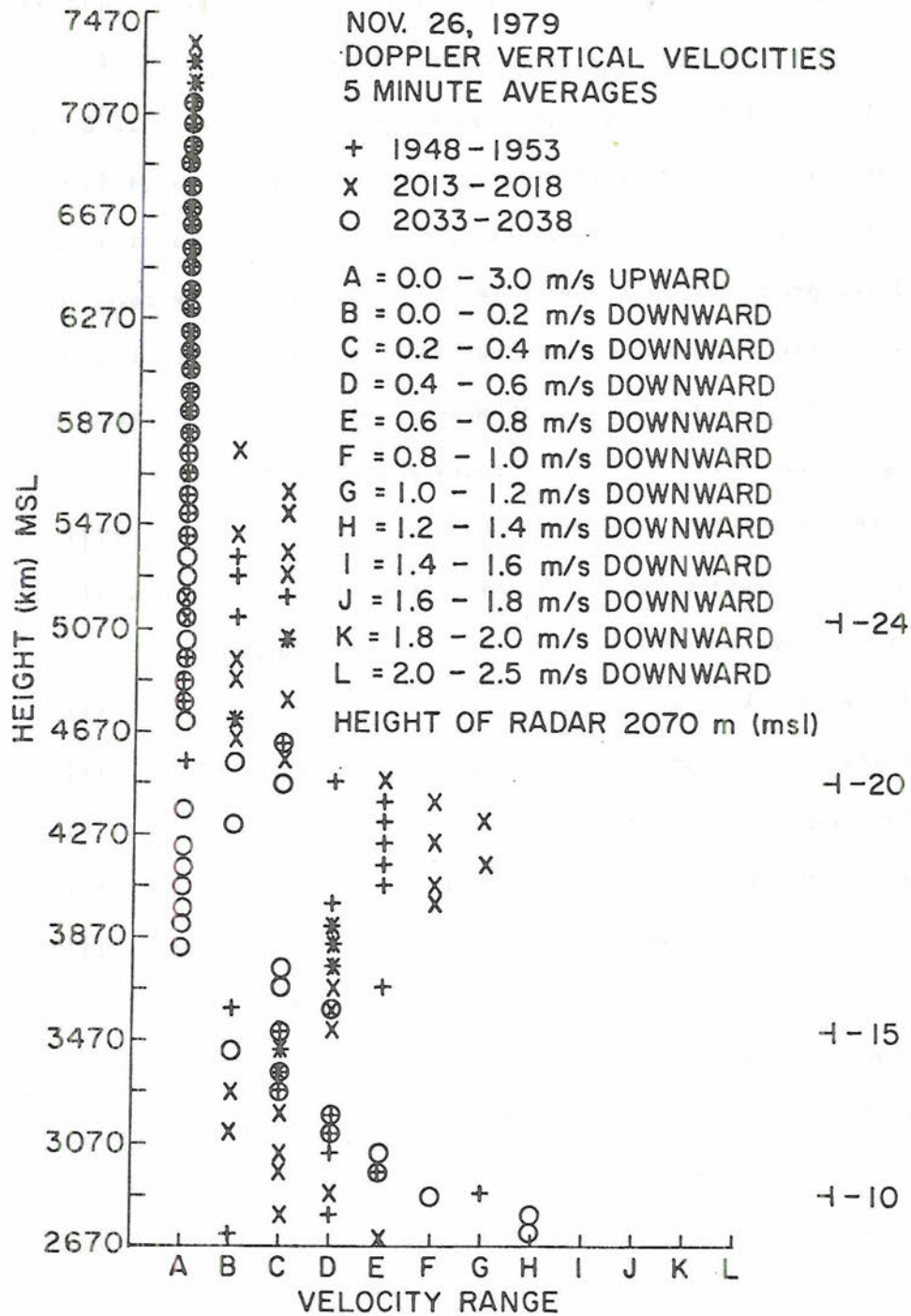


Figure 66. Doppler radar determined vertical velocities (w_D) on November 26, 1979. Data were averaged over five minute periods.

fall velocities would be smaller than these values. Still, the Doppler spectra indicates ambient air upward vertical velocities of at least 0.40-0.50 m/s over the radar at temperatures colder than -20°C . Between -20°C and -15°C the vertical velocity profiles show a large degree of variability with time and at times downward w_D values substantially exceed the predicted fall velocities of crystals with average sizes and habits similar to those observed in that vicinity of the cloud by the Learjet. For instance, over a 50 minute period at -18°C (4150 meters) w_D ranges from upward to 1.1 m/s downward. This large variability occurs throughout most of the depth between -18°C and the ground except in a 200 meter zone between 3250-3450 meters. It is maximum 600 meters above the ground and at 2000 meters above the ground.

The most likely mechanism for this large variability is that it is dynamically induced by interaction between the airflow and locally complex topography. The topography in the immediate vicinity of the radar was quite complicated. The radar location was directly in the lee of a 500 meter hill which extends 7 km. In addition the radar is just windward of the main barrier. Significant topography also exists to the north and south at greater distances. Airflow from virtually any direction would interact with these features to produce both standing and transient wave motion. Fall velocities of crystals embedded in this flow would reflect this air motion behavior. This is one explanation of why some velocities exceed predicted terminal velocities of observed crystals.

The most important point which can be derived from this limited set of data is that complicated time-dependent dynamic processes do exist even in these relatively simple cloud systems which can substantially

alter crystal trajectories. Crystal trajectories such as those calculated in section 4.5 at best represent mean steady-state conditions and should be considered with the knowledge that variations in space (topography) and time (airflow characteristics) may substantially alter the actual path the crystals take.

5.6 Summary of the November 26 Case Study

On November 26, 1979, a strong baroclinic zone with an associated surface front approached the Park Range region of Colorado. Frontal passage in the COSE area occurred three hours before the aircraft mesoanalysis. Strong west-northwesterly winds persisted at all levels during the flights.

The cloud system on November 26 extended through a 30 KPa depth to 42 KPa (-33°C). Observations by the Queen Air indicate that the primary zone of liquid water existed in a narrow region over the windward slopes of the barrier. Liquid water contents at the -19°C level in this zone were measured at or below 0.13 g/m^3 . A second small zone existed upwind of the small ridgeline east of Hayden. In the lowest portion of the cloud liquid water contents rose briefly to 0.11 g/m^3 but were generally in the vicinity of 0.02 g/m^3 . Droplet spectra indicated that this cloud, in contrast to the previous case study, was more continental in nature. Mean droplet diameters ranged from 6-9 μm in concentrations of approximately $200/\text{cm}^3$.

Riming was not observed in this cloud system. Precipitation particles were largely single crystals although small aggregates were observed at low levels in the cloud and in the crystal replicas.

The difference in the activity of the aggregation process in the two case studies seems to be associated with the presence of liquid

water or at least a sufficiently large condensate supply rate. Aggregation occurred on November 24, 1979 at much colder temperatures than November 26, 1979, particularly in regions where some cloud water was present.

Theoretical calculations of condensate production rates again indicate that the production of significant liquid water in this cloud is limited to a narrow zone over the windward slopes. The observations agree very well with the predicted location. Comparison between theoretical values and measurements indicate that the cloud system operated at better than 83% efficiency in converting available condensate to the ice phase in the region of maximum condensate production and near 100% everywhere else.

Although crystal trajectories were not explicitly calculated for this case, a simple review of the differences between November 24 and 26 can give an intuitive idea of how the trajectories might differ. In general, the horizontal winds were stronger on November 26. In addition, the supersaturation above ice was generally less. Calculated airflow vertical velocities were slightly higher for the November 26 case. These three factors combine to force trajectories higher and, because of the high wind speeds, more horizontal. However, although these differences will alter the trajectories so that they will differ somewhat from November 24, the conclusions drawn for that case will still apply. From the Doppler analysis, it is also apparent that actual trajectories are complicated by time-dependent dynamic processes which result in the airflow due to variations in topography and airflow characteristics.

CHAPTER VI SUMMARY AND CONCLUSIONS

6.1 Summary and Conclusions

Two case studies of stably stratified storm systems over the Park Range of northern Colorado have been documented in this thesis. The microphysical processes associated with the growth and development of cloud and precipitation particles in each system have been described based on observations taken by aircraft, Doppler radar, rawinsondes and ground based instrumentation. The observations taken by the two COSE aircraft were compared with the results of a two-dimensional steady state model of condensate production and production rates developed for stable flow over an ideal barrier. Trajectories of crystals were determined for one storm to determine the level of origin of crystals which interact in precipitation processes. The model was also used to test the feasibility of converting small upwind zones of liquid water to crystals which can then interact with droplets in the primary zone in the riming process. The major results and conclusions which can be drawn concerning stably stratified orographic storms based on this research are the following:

Cloud Liquid Water

- 1) The majority of cloud liquid water in stably stratified orographic storms exists in a narrow zone over the windward slopes of the primary barrier. During both storms aircraft observations confirmed the presence of cloud water in this location. Model results indicate that this zone extends vertically over the slope with maximum liquid water contents near the surface. On both days the model predicted location of the zone was in excellent agreement with aircraft observations.

Comparison of predicted total condensate with observed liquid water contents indicates that the efficiency with which potential condensate is converted to the ice phase varies considerably within the zone. It is emphasized that this efficiency is not related to precipitation efficiency. However, for weather modification purposes, it represents a more meaningful number. On the two days studied, the efficiency varied from 14% (24 Nov) to 83% (26 Nov). Outside of the narrow zone, the conversion efficiency to the ice phase in both systems approached 100%.

It should be noted that efficiency calculations of this sort are limited because of the two-dimensional steady state assumptions inherent in the calculation of available condensate. Such things as dry air entrainment, turbulent mixing, and three-dimensional flow variations all serve to modify these numbers in the actual cloud system.

- 2) Droplet spectra in stable orographic cloud systems vary substantially depending on the air mass source region. On November 24, the overrunning air mass had modified maritime characteristics. One possibility for these characteristics was the decoupling of the airmass from the boundary layer during its transit in cloud over the underlying cold airmass. If the air had sufficient time within the precipitating system its aerosol properties could have been modified to produce the observed droplet spectra. Mean droplet diameters were near $15\mu\text{m}$, droplet concentrations were $60/\text{cm}^3$ and maximum liquid water contents near $0.42 \text{ g}/\text{m}^3$. On November 26, the air mass

- behind the cold front had continental characteristics. Mean droplet sizes were 6-9 μm , droplet concentrations, 200/cm³ and liquid water contents 0.13 g/m³.
- 3) Secondary zones of liquid water exist upwind of the primary barrier in regions of enhanced upward motion generated by smaller upwind topography. The existence of this secondary zone upwind of a small ridge east of Hayden was confirmed on both days by the Queen Air. Liquid water contents in the zone were measured at 0.05-0.10 g/m³. The utilization of upwind zones such as these in this and other locations in the northern Rockies may prove to be the best strategy for seeding this type of storm.
 - 4) Model results indicate that maximum liquid water contents in stably stratified systems occur near the surface just below the crest of the barrier. One effective way to determine these liquid water contents may be to utilize rime ice measurements on the slopes.

Crystal Growth and Fallout

- 1) Model results indicate that single crystals in storms with moderate or strong wind speeds normal to the mountain have essentially horizontal trajectories. This result was supported by aircraft observations within the dendritic growth zone. Dendrites, although very common between -15^oC and -12^oC, seldom appeared below this level in the images. The exception was aggregated crystals, which appear at all levels below the initial level of aggregation due to their higher fall velocities. Also, crystals embedded in airflow crossing

complex topography have their trajectories substantially modified by wave motion induced in the airflow as it interacts with the terrain.

- 2) The aggregation process was significantly enhanced in regions where some liquid water was present, particularly at temperatures above -12°C .
- 3) Within 60 km of the primary barrier model results indicate that there is virtually no interaction between crystals produced in upper levels of the cloud and those falling on the ground as precipitation. Estimates of trajectories indicate that cloud systems of this type would have to extend well beyond 100 km upwind before any significant interaction between cloud top and precipitation at the barrier were to occur.
- 4) Model results indicate that the only single crystals produced within 60 km of the ridge which reached the ground in the Nov 24 storm were those produced below -12°C . 2-D images indicate that aggregates of crystals from higher levels also have fall velocities large enough that they could reach the ground. 2-D data indicates that the difference in precipitation values between mountain and valley stations seems largely the result of the enhancement of the riming and particularly the aggregation process over the windward slopes. Because of this, the presence of the liquid water in this zone is necessary to maintain an efficient precipitation process at the barrier.
- 5) Model results indicate that crystals which are initiated in upwind liquid water zones either reach the primary zone of

cloud water as small crystals capable of interacting in aggregation and riming processes or fall out as single crystal precipitation. If situations can be found with two barriers located in such a manner so that crystals initiated by the diffusional growth process in the liquid water zone generated by the first barrier can survive to interact with the liquid water zone at the second in the aggregation and riming processes, effective utilization of cloud water from both ridges can be accomplished. This situation is quite idealistic, since transport and dispersion of seeding materials is so poorly understood. Still it remains one possible method of utilizing additional cloud water from these locations.

- 6) Significant ($> 1/\text{liter}$) quantities of crystals smaller than $300\mu\text{m}$ were present at temperatures between -6 and -10°C in both cloud systems. There was no direct physical evidence of a known multiplication process in these systems. Even so, these concentrations exceed theoretical concentrations of ice nuclei active at those temperatures by several orders of magnitude. The total concentration of crystals in both cloud systems showed little dependence on cloud temperature.

System Dynamics

- 1) The existence of an inversion above ridgetop upstream of a mountain when 70 KPa winds are strong has been associated with the presence of strong downslope winds on the lee side of the range (Scheetz et al., 1976). Observations of downslope motion and rapid evaporation of nearly all cloud water and ice

on November 24 support this idea. The inversion in this case was located at 65 KPa.

- 2) Complicated time dependent airflow processes exist in these systems due to variations and topography in airflow characteristics. These processes are probably manifested in wave motion of both transient and standing nature and can at times significantly affect crystal trajectories and cloud microphysical processes.
- 3) While convective elements are present in some orographic cloud systems in the Park Range area, they should not have occurred and in fact were not observed during these two case studies.

6.2 Implications of the Results for Weather Modification

Model and observational evidence of stably stratified storms indicates that most of the liquid water associated with this system is located directly over the windward slopes of the primary barrier. In many cases, a considerable amount of this liquid water evaporates as it advects to the lee of the barrier. Because of the close proximity of the maximum generation and evaporation zones in the cloud, it is highly unlikely that the initiation of enhanced crystal development in the liquid water zone directly over the primary barrier would lead to the development of precipitation sized ice particles capable of reaching the ground before evaporating. Because of this, seeding this zone would have little effect on increasing total barrier precipitation. On the other hand, it has been shown that the aggregation process and certainly the riming process, is significantly enhanced in cloud water zones.

Since particles interacting in these processes have the most potential to become precipitation because of their high fall velocities, the

presence of a cloud water zone at the primary barrier produces a significant positive effect on the total precipitation formation process. Conversion of the cloud water to ice particles at the primary barrier would decrease the potential for riming and aggregation and probably produce a net decrease in total precipitation.

A second more attractive possibility is to increase crystal concentrations entering the liquid water zone. This would enhance the aggregation and riming process, resulting in net increases in total barrier precipitation. To accomplish this, the first of a set of barriers would be seeded. The upwind barrier liquid water zone would be depleted by the production and growth of small ice crystals. These would then advect nearly horizontally to the primary zone at the downwind barrier and interact with the cloud liquid water in that zone. The net result would be depletion of the liquid water in both zones and production of precipitation sized particles at the primary zone.

This seeding approach would require sufficient technology to assure that concentrations of seeding material entering the secondary zone upwind would not exceed values necessary to deplete that zone. Otherwise, remaining seeding material will be advected into the primary zone where it will produce ice crystals too small to precipitate.

In the case of multiple barriers this problem is less pronounced. Seeding the first of a series of barriers would probably always produce a downwind positive effect if the cloud system extends across all the barriers and lee side evaporation zones are not significant.

In conclusion, modification of stably stratified orographic storms occurring over a single mountain range would probably be detrimental to the precipitation process at that barrier. Seeding the single barrier

cloud system would enhance the diffusional growth process at the expense of the riming and aggregation processes. Because of the short trajectory time to the lee side evaporation zone, fewer crystals would develop sufficiently to precipitation sizes. However, seeding the first of a multiple barrier range would produce a total net increase in precipitation, most of it falling at downwind barriers as crystals interact in cloud water zones in the riming and aggregation processes.

6.3 Implications of the Results for Flight Operations

Over recent years several aircraft accidents have occurred in mountainous terrain due to rapid icing and turbulence. On November 24, the NCAR Queen Air encountered considerable icing as it crossed the windward slopes of the Park Range. Just prior to the icing episode, the plane was forced to lower its altitude to gain airspeed on the lee side of the Range as strong downslope motion persisted along the barrier's east face. Small aircraft flying in cloud conditions similar to November 24 in the vicinity of these active icing zones could encounter serious difficulty maintaining altitude, particularly if the aircraft is already flying near minimums as it approaches the barrier. On west to east flights, ice loading, followed directly by strong downslope motion, could force the aircraft to dangerously low altitudes before safe passage across the barrier. East to west flights could result in the aircraft entering the icing zone at too low an altitude in a region where the cloud could extend close to the ground. Flights parallel to the barrier over windward slopes should not be attempted by anything but high performance aircraft because of long residence times in the icing zone. Forecasting this type of a cloud system involves identification of an inversion at mid-levels, a moderate to strong westerly component

to the winds at mid-levels in a situation where moist air is overrunning a cold air mass situated in the mountain valleys. This situation typically occurs as organized synoptic systems which the Colorado Rockies from the northwest after a previous air intrusion.

6.4 Recommendations for

This research cloud system occurring in the northern Colorado Rocky stratified orographic cloud. Similar analyses should be done on the other types of cloud systems identified by Lee (1980). In this study, reflectivity information was not yet available from k, ku and x-band radars to integrate additional temporal and spatial information concerning the structure of the cloud. Future research on these cloud systems, particularly those with a convective component, should incorporate as much of this data as is available. In future field projects more emphasis must be placed on flight track design to maximize information concerning cloud structure near the barrier. The addition of instrumentation for determining cloud liquid water content, such as the recently developed Bureau of Water and Power Resources microwave radiometers, would also be extremely valuable. More emphasis should be placed on obtaining continuous ground information concerning snowfall characteristics and intensities.

Concerning stably stratified cloud systems, research should be conducted to determine the nature of the interaction between the microphysical processes occurring in locations where two barriers are close together. Dynamic interactions in airflow passing over more complex topography than a single ideal mountain should also be investigated. Better definition of the general transient structure of orographic cloud systems and airflow should be attempted both from observations and

to the winds at mid-levels in a situation where moist air is overrunning a cold air mass situated in the mountain valleys. This situation typically occurs as organized synoptic systems approach the Colorado Rockies from the northwest after a previously strong cold air intrusion.

6.4 Recommendations for Future Research

This research emphasized one type of cloud system occurring in the northern Colorado Rockies, the stably stratified orographic cloud. Similar analyses should be done on the other types of cloud systems identified by Lee (1980). In this study, reflectivity information was not yet available from k, ku and x-band radars to integrate additional temporal and spatial information concerning the structure of the cloud. Future research on these cloud systems, particularly those with a convective component, should incorporate as much of this data as is available. In future field projects more emphasis must be placed on flight track design to maximize information concerning cloud structure near the barrier. The addition of instrumentation for determining cloud liquid water content, such as the recently developed Bureau of Reclamation microwave radiometers, would also be extremely valuable. More emphasis should be placed on obtaining continuous ground information concerning snowfall characteristics and intensities.

Concerning stably stratified cloud systems, research should be conducted to determine the nature of the interaction between the microphysical processes occurring in locations where two barriers are close together. Dynamic interactions in airflow passing over more complex topography than a single ideal mountain should also be investigated. Better definition of the general transient structure of orographic cloud

systems and airflow should be attempted both from observations and modelling.

The importance of the aggregation process has been demonstrated in this thesis. Development and verification of models of aggregation, combined with better observations concerning the conditions which favor aggregation would lead to a better understanding of the total precipitation process in mountain cloud systems.

CHAPTER VII REFERENCES

- Bashkirova, G. M. and T. A. Pershina, 1964: On the Mass of Snow Crystals and Their Fall Velocity. *Trudy Glav. Geofiz. Observ.*, 165, 90-100.
- Baumgardner, D., 1980: A Critical Analysis and Comparison of Four Water Droplet Measuring Instruments. Master's Thesis, Atmospheric Science Department, University of Wyoming, Laramie, Wyoming.
- Brown, R. C. and L. G. Post, 1978: Airborne Research Instrumentation System IV Operation Guide. Research Systems Facility, National Center for Atmospheric Research, Boulder, Colorado.
- Brown, S. R., 1970: Terminal Velocities of Ice Crystals. Atmos. Science Paper #170, Colorado State University, Fort Collins, Colorado.
- Brown, S. R. and D. Rottner, 1974: The Use of a Computer Model in the Analysis of Orographic Weather Modification Experiments. 4th National Conference on Planned and Inadvertant Weather Modification, Fort Lauderdale, Florida, Nov. 18-21, 1974, pp. 473-477.
- Brownscombe, J. L. and J. Hallot, 1967: Experimental and Field Studies of Precipitation Particles Formed by the Freezing of Supercooled Water. *Quart. J. Roy. Meteor. Soc.*, 93(396), 455-473.
- Byers, H. R., 1965: Elements of Cloud Physics, University of Chicago Press, pp. 109-127.
- Chappell, C. F. and D. R. Smith, 1976: Simulation of Cold Cloud Precipitation in a Three-Dimensional Mesoscale Model. NOAA Tech. Report.
- Chappell, C. F., D. R. Smith, E. C. Nickerson and E. L. Magaziner, 1979: A Numerical Simulation of Cloud Seeding over the San Juan Mountains. 7th Conference on Inadvertant and Planned Weather Modification, Banff, Alberta, Oct. 8-12, 1979, pp. 80-81.
- Cooper, W. A. and C. P. R. Saunders, 1980: Winter Storms over the San Juan Mountains, Part II: Microphysical Processes. *J. Appl. Meteor.*, 19, 927-941.
- Cooper, W. A. and J. D. Marwitz, 1980: Winter Storms over the San Juan Mountains, Part III: Seeding Potential. *J. Appl. Meteor.*, 19, 942-949.
- Cooper, W. A., 1977: Cloud Physics Investigations by the University of Wyoming in HIPLEX 1977, Dept. of Atmospheric Science, Univ. of Wyoming, Laramie, Wyoming. Report No. AS 119, 320 pp.
- Corby, G. A., 1954: The Airflow over Mountains. *Quart. Jour. Roy. Met. Soc.*, 80, Oct. 1954, pp. 491-521.

- Cornford, S. G., 1965: Fall Speeds of Precipitation Elements. Quart. Jour. Roy. Met. Soc., 91, 91-94.
- Cotton, W. R., 1970: A Numerical Simulation of Precipitation Development in Supercooled Cumuli. Report # 17 to the National Science Foundation, Department of Meteorology, The Pennsylvania State University, University Park, PA. 16802.
- Cotton, W. R., 1972: Numerical Simulation of Precipitation Development in Supercooled Cumuli, Part II. Mon. Wea. Rev., 100, 764-784.
- Davis, C. I., 1974: Ice Nucleating Characteristics of Various AgI Aerosols. Ph.D. Dissertation, Dept. of Atmos. Resources and Mechanical Eng., College of Engineering, University of Wyoming, Laramie, Wyoming, 259 pp.
- Davis, C. I. and A. H. Auer, Jr., 1974: Use of Isolated Orographic Clouds to Establish the Accuracy of Diffusional Ice Crystal Growth Equations. Conf. on Cloud Physics October 21, 1974, Tucson, AZ, pp. 141-147.
- Derickson, R. G., 1974: Three Dimensional Modelling of Cold Orographic Cloud Systems. National Conference on Cloud Physics, Tucson, AZ, Oct. 21-24, 1974, pp. 473-477.
- Elliott, R., R. W.W. Shaffer, A. Court, and J. F. Hannaford, 1978: Randomized Cloud Seeding in the San Juan Mountains, Colorado. J. Appl. Meteor. 17, 1298-1318.
- Fraser, A. B., R. C. Easter and P. V. Hobbs, 1973: A Theoretical Study of the Flow of Air and Fallout of Solid Precipitation over Mountainous Terrain, Part II: Microphysics. J. Atmos. Sci. 30, 813-823.
- Frossling, N., 1938: UBER die Verdunstung Fallender Tropfen. Gerlands Beitr, Geophysik 52, 170-216.
- Fukuta, N., M. N. Plooster, Y. Palk, L. F. Evans, A. Gorove and T. L. Wang, 1973: The Engineering, Microphysical, and Dynamical Aspects of Precipitation Management. Final Report to U.S. Bureau of Reclamation, Contract 14-16-D-7048, 150 pp.
- Heymsfield, A. J. and J. L. Parrish, 1979: Techniques Employed in the Processing of Particle Size Spectra and State Parameter Data Obtained with the T-28 Aircraft Platform. NCAR Technical Note/ TN-137+1A, May 1979.
- Hindman, E. E. and L. O. Grant, 1981: Utility of Mountaintop Rime-Ice Measurements. Preprints 2nd Conf. Mt. Meteor., 10-13 Nov. 1981, Steamboat Springs, CO, Amer. Meteor. Soc, Boston, in press.
- Hobbs, P. V. and J. D. Locatelli, 1974: Fallspeeds and Masses of Solid Precipitation Particles. J. Geophys. Res. 79, 15, 2185-2197.

- Hobbs, P. V., 1975a: The Nature of Winter Clouds and Precipitation in the Cascade Mountains and Their Modification by Artificial Seeding, Part I: Natural Conditions. J. Appl. Meteor. 14, 753-804.
- Hobbs, P. V., 1975b: The Nature of Winter Clouds and Precipitation in the Cascade Mountains and Their Modification by Artificial Seeding, Part III: Case Studies of the Effects of Seeding. J. Appl. Meteor. 14, 819-858.
- Hobbs, P. V. and L. F. Radke, 1975: The Nature of Winter Clouds and Precipitation in the Cascade Mountains and Their Modification by Artificial Seeding, Part II: Techniques for the Physical Evaluation of Seeding. J. Appl. Meteor. 14, 805-818.
- Hobbs, P. V., L. F. Radke, J. R. Fleming and D. G. Atkinson, 1975: Airborne Ice Nucleus and Cloud Microstructure Measurements in Natural and Artificially Seeded Situations over the San Juan Mountains of Colorado. Research Report X, Contributions from the Cloud Physics Group, Dept. of Atmos. Sciences, University of Washington, Seattle, Washington.
- Hobbs, P. V., R. C. Easter, and A. B. Fraser, 1973: A Theoretical Study of the Flow of Air and Fallout of Solid Precipitation over Mountainous Terrain, Part II: Microphysics. J. Atmos. Sci. 30, 813-823.
- Holmbue, J. and H. Klieforth, 1957: Investigations of Mountain Lee Waves and the Air Flow over the Sierra Nevadas. Dept. of Meteor., Univ. of California, Final Report, Contract No. AF 19(604)-728, 1957.
- Jayaweera, K.O.L.F. and B. J. Mason, 1965: The Behavior of Freely Falling Cylinders and Cones in a Viscous Fluid. J. Fluid. Mech. 22, 709-720.
- Jayaweera, K.O.L.F. and B. J. Mason, 1966: The Falling Motion of Loaded Cylinders and Disks Simulating Snow Crystals. Quart. J. Roy. Meteor. Soc. 92, 151-156.
- Jayaweera, K.O.L.F. and R. E. Cottis, 1969: Fall Velocities of Platelike and Columnar Ice Crystals. Quart. J. Roy. Meteor. Soc. 95, 703-709.
- Jayaweera, K. and B. F. Ryan, 1972: Terminal Velocities of Ice Crystals. Quart. Jour. Roy. Meteor. Soc. 98, 193-197.
- Kajikawa, M., 1971: A Model Experimental Study on the Falling Velocity of Ice Crystals. Jour. of the Met. Soc. of Japan 49, 367-375.
- Kajikawa, M., 1972: Measurement of Falling Velocity of Individual Snow Crystals. Jour. of the Met. Soc. of Japan 50, 577.
- Kajikawa, M., 1973: Laboratory Measurement of Falling Velocity of Individual Ice Crystals. Jour. of the Met. Soc. of Japan 51, 4, 263-272.

- Kajikawa, M., 1975a: Experimental Formula of Falling Velocity of Snow Crystals. Jour. of the Met. Soc. of Japan 53, 4, 267-275.
- Kajikawa, M., 1975b: Measurement of Falling Velocity of Individual Graupel Particles. Jour. of the Met. Soc. of Japan 53, 6, 476-481.
- Knollenberg, R. G., 1976: Three New Instruments for Cloud Physics Measurements: the 2-D Spectrometer, The Forward Scattering Spectrometer Probe, and the Active Scattering Aerosol Spectrometer. Preprints, International Conference on Cloud Physics, Boulder, CO, Amer. Meteor. Soc. 554-561.
- Langleben, M. P., 1954: The Terminal Velocity of Snowflakes. Jour. Roy. Meteor. Soc. 80, No. 340.
- Lavoie, R. L., 1968: A Mesoscale Numerical Model and Lake Effect Storms. Ph.D. Dissertation, Pennsylvania State University, University Park, PA. 102 pp.
- Lee, R. R., 1980: Wintertime Cloud Systems over the Colorado Rockies: Three Case Studies. Atmospheric Science Paper #331, Dept. of Atmospheric Science, Colorado State University, Ft. Collins, CO.
- List, R. and R. S. Schemenauer, 1971: Free Fall Behavior of Planar Snow Crystals, Conical Graupel and Small Hail. Jour. Appl. Sci. 28, 110-115.
- Litvinov, I. V., 1956: Determination of the Steady-State Velocity of Falling Snow Particles. IZV. Akad. Nauk SSSR. Geophysical Series, 1956, 7, 853-856.
- Magono, C., 1951: On the Fall Velocity of Snowflakes. J. Meteor. 8, 199-200.
- Magono, C., 1954: On the Falling Velocity of Solid Precipitation Elements. Science Reports of the Yokohama National University, Sec. I, No. 3, 33-40.
- Magono, C., 1957: On Snowflakes. 6th Weather Radar Conference, Cambridge, Mass., MAR 26-28, 1957, 31-36.
- Marwitz, J. D., R. E. Stewart, T. S. Karacostas and B. E. Martner, 1978: Cloud Physics Studies in SCPP during 1977-78. Research Report #AS 122, Dept. of Atmos. Sci., University of Wyoming, Laramie, WY 82071.
- Marwitz, J. D., R. E. Stewart, T. S. Karacostas and B. E. Martner, 1978: Cloud Physics Studies in SCPP during 1978-79. Research Report #AS 123, Dept. of Atmos. Sci., University of Wyoming, Laramie, WY 82071.
- Marwitz, J. D., 1980: Winter Storms over the San Juan Mountains, Part I: Dynamical Processes. J. Appl. Meteor. 19, 913-926.

- Middleton, J. R., 1971: A Numerical Model of Ice Crystal Growth Within a Predicted Cap Cloud Environment. Report No. AR101, Dept. of Atmos. Res., College of Engineering, University of Wyoming, Laramie, WY.
- Nakaya, U. and T. Terada, 1935: Simultaneous Observations of the Mass, Falling Velocity and Form of Individual Snow Crystals. J. Fac. Sci. Hokkaido Imp. Univ., 11,1, No. 7.
- Nakaya, U., 1954: Snow Crystals. Harvard University Press, Cambridge, Mass., 510 pp.
- Nickerson, E. C. and G. L. Magaziner, 1976: The Numerical Simulation of Orographically Induced Non-Precipitating Clouds. NOAA Tech. Report.
- Nickerson, E. C., C. F. Chappell and G. L. Magaziner, 1976: Effects of Seeding on the Dynamics of Cold Orographic Clouds. 2nd International W.M.O. Conference on Weather Modification, Boulder, CO. Aug 2-6, 1976, 123-130.
- Plooster, M. N. and N. Fukuta, 1975: A Numerical Model of Precipitation from Seeded and Unseeded Cold Orographic Clouds. J. Appl. Meteor. 14, 859-867.
- Plooster, M. N. and L. Vardiman, 1976: Orographic Snowfall Prediction with a Numerical Model. 2nd International W.M.O. Conference on Weather Modification, Boulder, CO. Aug. 2-6, 1976, 131-134.
- Podzimek, J., 1965: Movement of Ice Particles in the Atmosphere. Proceedings of the International Conference on Cloud Physics Tokyo, 224-230.
- Podzimek, J., 1968: Aerodynamic Conditions of Ice Crystal Aggregation. Proceedings of the International Conference on Cloud Physics, Toronto, 296-299.
- Podzimek, J., 1969: The Growth of Ice Crystal in Mixed Clouds. Docent Thesis, Charles University, Prague, Czechoslovakia.
- Queney, P., 1947: Theory of Perturbations in Stratified Currents with Application to Airflow over Mountain Barriers. Univ. of Chicago Press, Misc. Reports, No. 23, 1947, 81 pp.
- Queney, P., 1948: The Problem of Airflow over Mountains: A Summary of Theoretical Studies. Bul. Amer. Met. Soc., 20, 16-26, 1948.
- Rhea, J. O., P. Willis and L. G. Davis, 1969: Park Range Atmospheric Water Resources Program. Final Report to the U.S. Dept. of Interior, Contract No. 14-06-D-5640, Bureau of Reclamation, Denver, CO.

- Scheetz, V. R., J. F. Henz and R. A. Maddox, 1976: Colorado Severe Downslope Windstorms, Final Report to Techniques Development Laboratory, Systems Development Office, National Weather Service., Prepared by G.R.D. Corporation, Denv
- Scorer, R. S., 1949: Theory of Waves in the Lee of Mountains. Quart. J. Roy. Meteor. Soc. 75, 41-56.
- Smith, R.B., 1979: The Influence of Mountains on the Atmosphere, Advances in Geophysics, Volume 21, Academic Press, pp 87-127
- Stringham, G. E., 1965: Behavior of Geometric Particles Falling in Quiescent Viscous Fluids. Ph.D. Dissertation, Colorado State University, Denver, CO, 143 pp.
- Willis, P. T., 1970: A Parameterized Numerical Model of Orographic Precipitation. E. G. C. Contract No. 14-06-D-5640, Prepared for U.S. Dept. of Interior, Bureau of Reclamation, Denver, CO.
- Wilmarth, W. W., N. E. Hawk and R. L. Harvey, 1964: Steady and Unsteady Motions and Wakes of Freely Falling Disks. Phys. Fluids 7, 197-208.
- Young, K. C., 1974: A Numerical Simulation of Orographic Precipitation, Part I: Description of the Model Microphysics and Numerical Techniques. J. Atmos. Sci. 31, 1735-1748.
- Young, K. C., 1974: A Numerical Simulation of Orographic Precipitation, Part II: Comparison of Natural and AgI Seeded Conditions. J. Atmos. Sci. 31, 1749-1767.
- Zikmunda, J. and G. Vali, 1972: Fall Patterns and Fall Velocities of Rimed Ice Crystals. Jour. Appl. Sci. 29, 1334-1347.
- Zikmundova, J., 1968: On Evaporation of Water Drops. Proceedings of the International Conference on Cloud Physics, Toronto, Ontario, Canada, 364 .

The first part of the report deals with the general situation of the country and the progress of the work done during the year. It is followed by a detailed account of the various projects and the results achieved.

The second part of the report deals with the financial statement of the organization for the year. It shows the income and expenditure and the balance sheet at the end of the year.

The third part of the report deals with the administrative and general matters. It includes a list of the members of the organization and a statement of the work done by the various committees and sub-committees.

The fourth part of the report deals with the future prospects of the organization. It discusses the various problems that are likely to arise in the future and the steps that are being taken to meet them.

The fifth part of the report deals with the conclusions and recommendations. It summarizes the main findings of the report and suggests the steps that should be taken to improve the work of the organization.

The sixth part of the report deals with the appendixes. It includes a list of the various documents and reports that have been referred to in the main text of the report.